LIBRARY OF THE UNIVERSITY OF ADELAIDE
5/6/70

KINETICS OF FORMATION OF MONOAZIDOFERRIC ION

by

PETER ALLAN TREGLOAN, B.Sc. (Hons.) (Adelaide)

A THESIS

submitted to the University of Adelaide

in partial fulfilment of the requirements

for the Degree of

Doctor of Philosophy

Department of Physical and Inorganic Chemistry,

The University of Adelaide

September, 1969

This thesis contains no material previously submitted for any degree or diploma in any University, and, to the best of my knowledge and belief, contains no material previously published or written by another person, except where due reference is made in the text.

P. A. TRELOAR

1969

ABSTRACT

A study has been made of the kinetics of formation of the monoazidoferric ion in aqueous solution at ionic strength 0.5M over a wide range of temperatures and hydrogen ion concentrations. Where necessary for the complete treatment of the kinetic data, the thermodynamics of the complex ion formation and ligand hydrolysis have been measured or checked. Computer programs were written for the complete temperature and concentration dependence analysis of the considerable raw kinetic data required for an accurate analysis of such a system.

The formation is found to take place via a number of parallel reaction paths and the rate constants and activation parameters for these paths have been determined. The relative values of those parameters, and their relation to reactions in other ferric/ligand systems is discussed.

An analogous set of measurements have been made using deuterium oxide as solvent.

A stopped flow apparatus has been designed, built and tested, based on experience gained with other apparatus used in the study of the moderately fast reaction kinetics involved in this work, and full details of the apparatus are given.

ACKNOWLEDGEMENTS

My thanks go to my supervisor, Dr. G. S. Laurence, for encouragement, advice and companionship throughout the period of this work.

I also wish to express my appreciation to Professor D. O. Jordan, in whose department this work was conducted, especially for the use of the Beckman 190B Microcalorimeter, and to Professor D. R. Stranks, other members of the staff, and my fellow graduate students, for their counsel and friendship.

To my wife, who accepted the lot of being married to a post-graduate student, goes my gratitude and sympathy.

TABLE OF CONTENTS

LIBRARY OF THE UNIVERSITY OF ADELAIDE
1.

CHAPTER I

INTRODUCTION

The field of substitution reactions of metal complexes is large and one which is reviewed regularly (65E, 65S, 66L, 67B, 66S, 67Bn, 68L, 69M). This work has been primarily concerned with the analysis of substitution by ligands of a solvent molecule in the labile solvation shell of a metal ion. The purpose of this Introduction is therefore merely to set this work in the very general context of transition metal substitution reactions, the rather more narrow field of fast metal substitution reactions, and the substitution kinetics of the aquated ferric ion in particular.

In a discussion of the mechanisms of such reactions the obvious mechanistic distinction concerns the relative degree of importance of the loss of the leaving group and attachment of the entering group in the attainment of that configuration of reactant molecules of highest potential energy, the transition state, which provides the major energetic barrier to be overcome in conversion of reactants to products. Is an intermediate formed during this process or is the mechanism a concerted one? Detection of an intermediate of increased or decreased coordination is probably the best test of mechanism, but such intermediates may be very short lived and are seldom observed. Examination of the effects of a systematic variation of entering and leaving groups in a related group of

reactions, on the reaction rate is the usual basis of the decision on mechanism.

It might almost be expected that square planar complexes are best suited to reaction by associative pathways; the metal is exposed above and below the ligand plane for attack by an incoming group, and for low spin d^8 systems a vacant p_z orbital of relatively low energy is available which can help accommodate electrons of the incoming ligand. There is considerable evidence that for Pt (II), the most widely studied of such systems, activation is indeed associative. The rate law is described by a two term function:

$$\text{Rate} = k_1(MA_3X) + k_2(MA_3X)(Y) \qquad 1.1$$

where M is the central metal, X is the leaving group, Y is the entering group and A is a nonreactive ligand. The constant k_1 is constant for reactions with various Y in the same solvent and corresponds to the slow replacement of X by solvent, followed by a faster conversion of this product to MA_3Y; k_2 corresponds to the direct replacement of X by Y. Changing the system to solvents and ligands of various coordinating strengths markedly affects the values and relative importance of the two paths in a way that would be expected for an associative mechanism. Rates can be reduced considerably by blocking the attack position above and below the ligand plane by large nonreacting ligands, especially if placed

cis to the leaving group. Values of the entropy of activation are large and negative, suggesting considerable ordering of the reactants in the transition state. The entering group reactivity bears a considerable resemblance to the 'trans' labilising effect order, and this has been rationalised in terms of a trigonal bipyramidal intermediate, since, in that intermediate, the trans and entering groups occupy identical positions with respect to the leaving group. Several stable five coordinate Pt (II) complexes are known, so that the evidence seems strongly in favour of an associative mechanism.

Of the non labile octahedral complexes, those of Co (III), especially the pentammines, and Cr (III) have received most attention, and experimental observations seem to indicate that a dissociative mechanism operates for their substitution. No direct interchange of ligands is observed except when either the entering or leaving group is the solvent.

The strength of the leaving group-to-metal bond, calculated from heats of formation or visible spectra seems to correlate qualitatively with the rate of reaction, suggesting that loss of this group is the major factor in the mechanism. Large inert ligand groups can affect the solvent structure and stabilisation by solvation of the leaving group, to slow loss of this group; for larger inert groups, promotion of the rate is observed and this is considered due to the relief of steric strain in the complex. If the leaving group is only weakly held, and the reaction is not

strongly endothermic, a linear free energy plot of $\Delta G^{\ddagger}$ vs ΔG° should have a slope of 1.0 for a dissociative mechanism; this has been observed. The stereochemistry of substitution should give information on the mode and direction of ligand insertion; retention of configuration and activity has been observed and suggests dissociation via a tetragonal pyramidal structure. In nonaqueous solvents the ligand concentration dependence is suggestive of ion pair formation which is more prevalent in solvents of low dielectric constant; at high concentrations of anion, all of the metal complex may be present as outer sphere aggregates and reaction may be observed at similar rates for a variety of anions. By catalysing leaving group loss with Hg (II) or HNO_2 a reactive five coordinate intermediate may be produced, the characteristics of which can be examined by kinetic competition between solvent molecules and anions for the reactive site. If the metal complex is anionic, preventing ion pair formation at high anion ligand concentrations, ligand concentration behaviour which can also be explained in terms of a reactive five coordinate intermediate is observed.

Insertion of OH^- into the coordination sphere of the complex is regarded as a special case; rates are much greater than for any other ligands and the proposed mechanism is via the conjugate base of the metal complex.

The essential elements of the substitution kinetics of these complexes therefore are embodied in the reaction scheme:

$$\begin{array}{lcl} (A)\ M L_5 X & \rightleftharpoons^{+Y} & M L_5 X.Y \quad (B) \\ \uparrow\downarrow\ -X & & \uparrow\downarrow\ -X \\ (C)\ M L_5 & \rightleftharpoons^{+Y} & M L_5 Y \quad (D) \end{array}$$

The relative contributions of the paths ABD and ACD will, of course, vary from system to system, but in general:

$$k = K_{AB}k_{BD} + \frac{k_{AC}k_{CD}}{k_{CA} + k_{CD}(Y)} \qquad 1.2$$

where k is the observed forward rate constant, K_{AB} is the equilibrium constant of formation for the ion pair B, k_{BD} is the rate constant for the reaction involving the conversion of configuration B to configuration D, etc.

Using fast reaction techniques, especially those of temperature-jump, electric field-jump, ultrasonic absorption, and nuclear magnetic resonance, it has been possible to systematically study a wide range of other metal ion/ligand interactions in solution; the systems generally studied correspond to the substitution of a solvent molecule in the primary coordination shell of the metal ion by a ligand, or the dissociation of that monocomplex. The data is almost entirely restricted to interactions in water, although data is slowly accumulating for other solvents.

In a study of the ultrasonic absorption of solutions of alkali metal ions with a number of strong multidentate ligands, a

relaxation considered to correspond to the transformation of an ion pair and a possibly tetradentate aquated complex was observed (63E). Rates were around 10^8 sec^{-1} and found to be slowest for Li^+ ($5x10^7 sec^{-1}$) and fastest for Cs^+ ($5x10^8 sec^{-1}$). The rates of complex formation are only just slower than that for diffusion of the reactants together to form the ion pair and some slight variations attributed to the steric properties of the ligands in solution were noted. The rates of complex dissociation, however, showed a much greater variation with ligand than did the association; the rate of inner sphere substitution was found to be considerably less affected by ionic strength than the ion pair formation.

For the alkaline earth ions, the substitution rates for Ca^{+2}, Sr^{+2} and Ba^{+2} are similar to those for the alkali metals (63E) and again show slightly faster rates for the larger ions. A correlation for the +1 and +2 ions of log k vs. 1/(ionic radius) confirms the electrostatic nature of the interactions (63Ei). Substitution rates for Mg^{+2} are, however, around 10^5 sec^{-1}, some 100 times slower than would be expected from the trend suggested from the larger alkaline earths, and it has been suggested that there may, for a given charge group, be some critical value of radius beyond which the simple electrostatic picture no longer holds (63D). It is interesting that the coordination number in water of Ba^{+2} has been determined by NMR methods as 5.7 and Ca^{+2} as 4.3 (66Ba); it is possible that the smaller size of Mg^{+2} allows it to fit into the tetrahedral water structure with a coordination number of 4, stabil-

ising its hydration shell. $BeSO_4$ shows a complex relaxation spectrum of six processes with relaxation times of 10^{-9} to 1 second; three of these were attributed to hydrolysis steps and three to stepwise formation of the ion pair and complex (59D). Reactions of Be^{+2} are slower again than those of Mg^{+2}, due to its very high charge density ($68B_H$).

Ultrasonic absorption coefficients of a number of 2:2 electrolytes, including alkaline earth and first row transition element sulphates were measured by Eigen (57E) over a wide range of frequencies. The spectra showed two distinct absorption maxima, both of which could be attributed to specific ionic interactions; it was suggested that after the aquated ions had approached close enough by a diffusion process, these specific interactions, with longer relaxation times, became important. The mechanism proposed for complex formation is the now well known:

$$M^{+2}_{aq} + L^{-2}_{aq} \rightleftharpoons M^{+2} \cdot O\begin{matrix}H\\H\end{matrix} \cdot O\begin{matrix}H\\H\end{matrix} \cdot L^{-2} \qquad 1.3$$

$$\rightleftharpoons M^{+2} \cdot O\begin{matrix}H\\H\end{matrix} \cdot L^{-2} \qquad 1.4$$

$$\rightleftharpoons (ML)_{aq} \qquad 1.5$$

Reaction 1.3 is diffusion controlled and the magnitude of the equilibrium constant is electrostatically determined. Reaction 1.4 is the

loss of water from the hydration sheath of the anion; the rate of this process was shown to be independent of the cation, but varied with the anion used and had values around $10^9 sec^{-1}$. Reaction 1.5 is the loss of coordinated water from the metal cation solvation shell, and varied between 10^4 and $10^7 sec^{-1}$ for the systems studied. The rate of water exchange from between hydrated transition metal ions and the bulk solvent determined using O^{17} NMR line broadening by Connick and coworkers (59Cn, 61C, 62S) is in reasonable agreement with the rates of reaction 1.5 above.

A large number of systems especially involving the divalent first row transition elements have now been studied, using various fast reaction techniques; a considerable amount of data was compiled and presented by Eigen and Wilkins (65E), and the general mechanism, of electrostatic preassociation followed by a rate determining step involving loss of coordinated water from the metal ion hydration shell, and corresponding, in fact, to path ABD in the reaction scheme proposed for nonlabile octahedral substitution reactions, will be referred to as the Eigen-Wilkins mechanism.

Whereas, in the nonlabile systems, the ionic preassociation has, in many cases, been measured (68Be), in labile systems, in most cases, it cannot be or has not been; the electrostatic model of Fuoss (58F) is that which has been generally used to estimate its magnitude. Despite objections which might be raised about the model on the grounds that it assumes the solvent medium to be a continuum; that its use requires the rather arbitrary choice of an interionic separation, taken

by most workers as 5Å (62H, 66M, 67A); and that, in general, no account is taken of any dielectric saturation of the interionic water which, around a highly charged ion, may be considerable (59L), the results produced generally provide good support for the mechanism of Eigen and Wilkins. It has been noted by some workers in labile and nonlabile systems (67D, 67S) that, after allowing for the pre-association, the substitution rate may differ from the independently determined water exchange rate by a factor which is roughly constant for similar systems; it has been suggested (67S) that, in the ion pair, the ligand occupies only one of a number of outer sphere sites and that, when a dissociative loss of coordinated solvent occurs, the chance of the ligand being in the ideal position for replacement is something less than one.

Taken as a group, rates of substitution of the divalent first row transition metal ions correlate qualitatively with the crystal field stabilisation expected for the various d orbital configurations (65H) and are insensitive to the incoming group. The notable features are the relative slowness of reaction of Ni(II) and V(II) (d^8 and d^3) rationalised by stabilisation due to the crystal field, and the very rapid rate for Cu(II) (d^9), presumably labilised due to the distortion of the Cu(II) octahedra to produce two weakly held axial water molecules which exchange rapidly with the equatorial ligands (63Eg). Ni(II) has been by far the most extensively studied system, and interest is extending to the effect of changing solvent on the solvent exchange rate (66B) and of the influence of coordinated groups

on the rate of loss of subsequent solvent molecules (67M); the chelation rate is generally held to be determined by the rate of loss of the first solvent molecule.

Of the triply charged ions, for Scandium, Yttrium and the lanthanides the rates of solvent exchange and ligand attachment are similar, but much faster than expected on a simple electrostatic argument of ionic radius and charge, and systematic studies through the series show a break in the complex formation rate at erbium or gadolinium (65G, 68G); this is paralleled by a break in some physical properties in solution, and is attributed to a change in coordination number of the ions through the series.

Aluminium, Gallium and Indium sulphate formation rates have been measured (68M) and these show a parallel path via the monohydroxy complex of the metal. The rate of complex formation after allowance for the ion pair formation is, for Al(III), very close to that for the water exchange rate (68F); for Ga(III), however, the complex rate is some thousand times slower than the exchange rate and, coupling this with the fact that the entropy of activation for the water exchange is -22 eu (Al(III) 28 e.u. (68F)), it has been suggested that Ga(III) and In(III) complex formations proceed via an associative pathway.

The rates of formation of the monothiocyanato complex of Vanadium (III) has been measured (67Ba, 68Kr) and the conclusion of both sets of workers, based on comparison with the Co(III), Cr(III), Rh(III) and Fe(III) thiocyanates, the opportunity for ligand involvement

through the unfilled d orbitals of V(III), and confirmed by a negative entropy of activation (-24 e.u.), was that an associative mechanism was involved.

It has been suggested (61E, 63R) that for small, highly charged and relatively easily hydrolysable ions such as Be(II), Al(III) and Fe(III), where, because of the high charge density at the cation, the rate of water exchange was expected to be relatively slow, a separate mechanism involving basic ligands might come into force. After the cation and ligand had formed an ion pair, a process of 'internal hydrolysis' was proposed, where a proton was transferred to the ligand from a coordinated water of the cation; the presence of the hydroxy group would then labilise the remaining water molecules to provide a faster route for entry of the ligand, which, once co-ordinated, would transfer the proton back to the hydroxy group. The mechanism bears a strong resemblance to the 'conjugate base' mechanism proposed for Cobalt(III) pentammine base hydrolyses (67B), and the labilisation of the remaining water presumably takes place by a similar process to that induced by the amido group. Certainly, the rates of reaction of $FeOH^{+2}$ with ligands is orders of magnitude faster than the reaction with Fe^{+3}_{aq}, whereas the rates of water exchange in the mono and dichloro complexes of Fe(III) increase by a factor of only about two for each chloride added (64B). A conjugate base mechanism has been proposed for the reaction of Ni(II) with polyamine ligands (66R).

The similarity in both rates and activation energies for reaction of Be^{+2} with HF, F^-, and SO_4^{-2} suggest that such a mechanism

does not operate in these systems (68Bn), and, as has been noted above, a simple dissociative mechanism is thought to apply for Al(III)/SO_4^{-2} (68M).

The data for Fe(III) reactions on which this mechanism was originally proposed are given in TABLE 1.1:

TABLE 1.1

RATE CONSTANTS FOR Fe^{+3} COMPLEX FORMATION (l/m/s)

Ligand	Fe^{+3}	$FeOH^{+2}$	Reference
Br^-	20	$3x10^4$	61M
Cl^-	9	10^4	59Co
SCN^-	127	10^4	58B
SO_4^{-2}	$3x10^3$	$3x10^5$	62Ze
F^-	$4x10^3$	-	60P

It can be seen that a qualitative correlation between ligand base strength and substitution rate, as would be expected for a conjugate base mechanism, certainly exists.

In 1963 Seewald and Sutin (63S) measured the rate of the formation of the monoazide complex at 25° and pointed out that, of the possible reaction paths for formation of the complex by a basic ligand:

$$Fe^{+3} + L^- \underset{}{\overset{k_1}{\rightleftharpoons}} FeL^{+2} + H_2O \qquad 1.6$$

$$FeOH^{+2} + L^- \underset{}{\overset{k_2}{\rightleftharpoons}} FeL^{+2} + OH^- \qquad 1.7$$

$$Fe + HL \underset{}{\overset{k_3}{\rightleftharpoons}} FeL^{+2} + H^+ + H_2O \qquad 1.8$$

$$FeOH + HL \underset{}{\overset{k_4}{\rightleftharpoons}} FeL^{+2} + H_2O \qquad 1.9$$

the two given by equation 1.6 and 1.9 were kinetically indistinguishable, and although a dependence of rate constant on ligand is observed if the acid independent pathway is considered to be path 1 as above, if for basic ligands it is assumed to be path 4, this dependence is reduced, as shown in TABLE 1.2:

TABLE 1.2

RATE CONSTANTS FOR Fe^{+3} COMPLEX FORMATION (1/m/s)

Ligand	Reaction via Fe^{+3}	Reaction via FeOH	Reference
Cl^-	9.4	1.1×10^4	59Co
Br^-	20	2.7×10^4	61M
SCN^-	127	1.0×10^4	58B
SO_4^{-2}	-	3×10^5	62D
SO_4^{-2}/HSO_4^-	(6.4×10^3)	(1.4×10^5)	62We
F^-/HF	(5.0×10^3)	(3.1×10^3)	60P
HF	11.4	-	60P
N_3^-/HN_3	(1.6×10^5)	(6.8×10^3)	63S
HN_3	4.0	-	63S

The pairs shown in parentheses were calculated assuming path 1 or path 4.

If the data for sulphate, fluoride and azide is considered to be via path 4, all of the rate constants for Fe^{+3} reactions are in the range 4 to 127 l/m/s and $FeOH^{+2}$ in the range $3x10^3$ to $3x10^5$ l/m/s. These were compared to the reported values of water exchange at Fe^{+3} of 280 l/m/s and $FeOH^{+2}$ of around $3x10^4$ l/m/s, and claimed to add support to the view proposed for other metal ions, that the rate of complex formation was primarily controlled by the rate of loss of a coordinated water molecule. The range of values covered by the data for various ligands is, however, still around 100 for Fe^{+3} and $FeOH^{+2}$, and testing the data against the lifetime of a coordinated solvent molecule as proposed in the Eigen-Wilkins mechanism gives values of the preassociation constant for, say, chloride, of 0.004 and 0.03 for interaction with Fe^{+3} and $FeOH^{+2}$.

The suggestion was made by Seewald and Sutin that, at lower acidities, reaction between $FeOH^{+2}$ and N_3^- may contribute to the observed rate, but that the scatter of their data made the magnitude of this contribution difficult to assess.

It was decided, therefore, that this work should involve the setting up of equipment and techniques suitable to accurately measure the kinetics of such reactions, and that a re-examination of the ferric/azide system, where no activation parameters had been determined, and where the possibility of measuring the rate parameters of a set of reaction pathways, closely related in size and shape of reactants, but differing in ligand basicity had been suggested, might enable a more specific statement on the mechanism of such systems, to be made.

While this work was in progress and preparation, a number of publications concerning anation in aquated ferric systems have appeared (66M, 67A, 67C, 68C, 69A), two of which, those of Accasina, Cavasino and d'Allesandro (67A) and Carlyle and Espenson (67C) have been concerned directly with measurements on the ferric/azide system, and these will be discussed where appropriate, later in this work. The appearance of these results has not been accompanied by any essential alteration to the arguments proposed by Seewald and Sutin, and made no difference to the methods used, results obtained, or conclusions drawn in this work, except that, where conflict was suggested, confirmation of the experimental values obtained was attempted, where practicable.

CHAPTER II

EQUILIBRIA

Because data was not available, or because of conflicting results in the literature for data which was available, it was decided to independently determine a number of thermodynamic quantities which were required for the kinetic analysis of the ferric-azide system.

MATERIALS.

Reagents used in both the kinetic and thermodynamic measurements were prepared from similar starting materials and standardised in the same way. All solutions were made up in demineralised water which had been distilled from alkaline permanganate, followed by distillation from acidified dichromate solution.

(i) Ferric perchlorate was prepared by recrystallisation of commercial (Fluka crystallised) reagent, once from 1M perchloric acid, and once from concentrated perchloric acid; the product was washed thoroughly with concentrated perchloric acid after each recrystallisation. A solution of this solid in water, on approximate standardisation by methods described below, was generally found to be more concentrated in ferric ion than acid; a calculated amount of concentrated perchloric acid was added to obtain a stock

solution of about 1M $Fe(ClO_4)_3$/1M $HClO_4$. An aliquot of this was diluted to a working stock solution of about 0.1M Fe/0.1M acid.

The ferric ion concentration was determined by reduction by stannous chloride and titration against permanganate (standardised with arsenious oxide) as described by Vogel (61V). Standardisation of the acid concentration was performed by titration of the ferric/acid solution with standard sodium hydroxide to a pH of 9, using a pH meter or phenolphthalein indicator as described by Milburn (55M); titrations using phenolphthalein were carried out with hot solutions to aid coagulation of the ferric hydroxide formed. Subtraction of the sodium hydroxide used to precipitate ferric hydroxide allowed the 'analytic' acid concentration, free from any contribution due to hydrolysis of ferric ion present, to be calculated.

Using these techniques, allowing for reproducibility of analyses, possible inaccuracies in standard solutions and tolerances on volumetric glassware used, concentrations of ferric solutions should be subject to an error of ± 0.5%. Concentration of acid in ferric solutions should be accurate to ± 5.0%.

(ii) Sodium azide solutions were prepared from commercial (B.D.H. laboratory reagent) material in two ways.

(a) Hydrazoic acid evolved from the addition of solid sodium

azide to 2N sulphuric acid, maintained at 50 - 80°C, was bubbled through standardised sodium hydroxide solution for 2 - 3 hours; the purified sodium azide solution obtained was gently boiled for about an hour to remove any excess hydrazoic acid. The concentration of azide in a sample run was found to be about 1% higher than expected from the initial sodium hydroxide concentration. Azide concentrations were determined by titration against standard silver nitrate solution, using potassium chromate or a potentiometric method to determine the end point.

Solutions of 0.1M sodium azide were used as stock, and their concentrations were subject to an error of ± 0.3%.

(b) Pure sodium azide was also prepared as described by Ellis and Hall (68E), by precipitation from a saturated solution of laboratory reagent azide with alcohol.

(iii) Perchloric acid solutions were prepared from concentrated A.R. reagent (G. Frederick Smith and Co. 70%, S.G. = 1.66), and standardised against sodium tetraborate to methyl red end point. Concentrations were subject to an error of ± 0.3%.

(iv) Sodium perchlorate solutions were prepared from two commercial products (B.D.H. low in chloride laboratory reagent, and Fluka), and standardised gravimetrically by drying aliquots

to constant weight at 110 - 120°C. Solution concentrations were subject to an error of ± 0.1%.

(v) Sodium bromide solutions were prepared as 0.1M stock from B.D.H. Analar reagent without further purification, and standardised by potentiometric titration against standard silver nitrate solution. Concentrations of bromide were considered accurate to within ± 0.3%.

(vi) Deuterium oxide was obtained from the Australian Institute of Nuclear Science and Engineering with a nominal isotope purity of 99.5% deuterium. Solutions of reagents were prepared for early experiments by concentrating aliquots of aqueous reagent by evaporation and making up to volume with 99.5% D_2O. Mass spectroscopic analysis of solvent distilled from solutions prepared in this way indicated a resultant D/H ratio of 94/6. For later measurements, concentrated aliquots were diluted with this 94% deuterated material, reconcentrated and then made to volume with 99% solvent to obtain a higher deuterium content.

FERRIC AZIDE ASSOCIATION.

The association of ferric ions with azide ions and hydrazoic acid has been investigated by a number of workers under a variety of conditions.

Using the method of continuous variations, with ((ferric) + (azide)) constant at 0.004M and 0.16M with a wide range of ionic strengths, Wallace and Dukes (61W) concluded that the reaction proposed earlier by Rices (45R) on the basis of specific conductivity measurements of ferric/hydrazoic acid mixtures, could be verified spectrophotometrically as

$$Fe^{+3} + HN_3 = FeN_3^{+2} + H^+ \qquad 2.1$$

ElShamy and Sherif (59E), however, while obtaining results for continuous variation experiments which verified the existence of a 1:1 complex at ((ferric)+(azide)) less than 0.01M, found that further increases produced a shift away from a 1:1 system, until at ((ferric)+(azide)) of 0.8M, the results suggested a predominant product of composition $Fe(N_3)_2^+$. These workers also conducted a series of investigations of ferric/azide interactions using specific conductivity, solution viscosity, and potentiometric titrations as probes to the chemistry (61E), and suggest evidence for the formation of complex ions of mole ratio 1:1 through to 1:6. Conditions for these experiments were ((ferric)+(azide)) less than 0.15M and with pH changing considerably over a series. No quan-

titative estimate of the relative abundance of the various species could be made.

Bunn, Dainton and Duckworth (61B) investigated ferric/azide interactions at ((ferric)+(azide)) around 0.02M, but with hydrazoic acid in excess by a factor of 10 - 50; they considered that under their conditions, the formation of complexes higher than 1:1 could be neglected. These workers also examined ferric/azide association in deuterium oxide as solvent under similar concentration conditions.

In 1967, Carlyle and Espenson (67C), because of discrepancies in a kinetic study of ferric/azide interactions, re-examined the equilibrium behaviour of the association. They performed two series of experiments, one comparable with the conditions of Bunn, Dainton and Duckworth, with hydrazoic acid in excess, and another in which ferric ion concentration was in excess. They obtained a value of the apparent equilibrium constant for the first series which was about 20% higher than their own value for the high iron series, and suggested, therefore, that the formation of the diazido complex was playing a significant part in their result at high azide concentrations.

We had been measuring the kinetics of formation of the ferric azide complex under conditions of ((ferric)+(azide)) of 0.015M, with ferric concentration in excess by a factor of 2, but were anxious that there should be no interference to the system by the formation of higher azido complexes. We therefore

instituted a series of spectrophotometric measurements of our own to determine the seriousness of the effect of higher complexes under our kinetic conditions.

Consider a reaction 'model' of the form

$$Fe^{+3} + HN_3 = FeN_3^{+2} + H^+ \qquad 2.2$$

with formation equilibrium constant K, so that at equilibrium

$$K = x.(H+x)/(a-x)(b-x) \qquad 2.3$$

where b is the initial concentration of the reactant in excess, and to a first approximation can be considered constant; a is the initial concentration of the other reactant, x is the concentration of product, FeN_3^{+2}. Conditions of the experiment can be chosen so that the hydrogen ion concentration, H, is essentially constant.

Now from Beers Law,

$$x = D/E \qquad 2.4$$

where D is the optical density, and E is the extinction coefficient referred to a particular path length cell.

So that

$$K = D/E.H/(a-D/E).b \qquad 2.5$$

This can be expanded and rearranged to give a variant of the well known Benesi-Hildebrand relation, which has been used in many guises for the spectrophotometric determination of equilibrium constants and extinction coefficients for a large number of systems, including other ferric/ligand interactions (55L, 61B, 61W, 65C, 67C, 68K):

$$a/D = H/E.K.b + 1/E \qquad 2.6$$

A plot of a/D vs H/b should be linear with intercept 1/E and slope 1/K.E.

For a complete analysis of the system, a number of other equilibria which take place must be considered.

$$Fe^{+3}_{aq} = FeOH^{+2} + H^{+} \qquad 2.7$$

$$2Fe^{+3}_{aq} = (FeOH)_2^{+4} + 2H^{+} \qquad 2.8$$

$$HN_3 = N_3^{-} + H^{+} \qquad 2.9$$

Although experimental conditions may be chosen to minimise hydrolysis via these paths, the expressions derived above refer to the 'free' concentrations of reactants ferric ion, hydrazoic acid and hydrogen

ion, and allowance should be made for them.

RESULTS AND DISCUSSION.

Two series of experiments were carried out, one with ferric ion in excess by a factor of 50 - 150, the other with hydrazoic acid in excess by a similar amount. The total concentrations of ((ferric)+(azide)) were low (0.02M - 0.06M), the hydrogen ion concentration was maintained at about 0.1M, and the total ionic strength of solutions at 0.50M with sodium perchlorate. Measurements were made at 460mμ on a Shimadzu Model QR50 spectrophotometer fitted with a cell housing through which water, thermostated to 25.0 ± 0.05°C, could be circulated. The 1 cm silica cells were calibrated for path length with potassium chromate, using the data of Haupt (52H), and were fitted with tightly sealing teflon stoppers. Optical densities measured in unstoppered cells were found to drift by around 5% during the 10 minute period required for thermostating and measurement, presumably due to evaporative loss of hydrazoic acid, which has a boiling point of 37°C.

Results of the equilibrium measurements, and data determined from them, are given in TABLE 2.1, and plotted in FIGURES 2.1 and 2.2; optical density readings are the mean of three measurements on the same solution, which, in general, agreed to ± 0.001. To correct the measured optical densities for any background absorption due

Table 2-1

2 page

TABLE 2.1

FERRIC/AZIDE ASSOCIATION AT 25°. IONIC STRENGTH 0.5M

(Concentrations in moles per litre)

EXCESS FERRIC SERIES

Sample No.	(Fe^{+3}_T)	(As_T)	(H^+_T)	O.D. corrected	ϵ/D_3 (x 10^{-3})	(H)/b
FE 01	0.0196	4.62×10^{-4}	0.101	0.207	2.23	5.28
02	0.0294		0.102	0.288	1.60	3.56
03	0.0490			0.422	1.09	2.17
04	0.0686			0.531	0.869	1.57
08	0.0199	4.60×10^{-4}	0.101	0.213	2.16	5.19
10	0.0298	4.61×10^{-4}		0.293	1.57	3.49
11	0.0497			0.431	1.07	2.13
12	0.0696			0.509	0.906	1.68
19	0.0407			0.370	1.25	2.58
20	0.0335			0.322	1.43	3.12
21	0.0263			0.268	1.72	3.96
22	0.0233			0.244	1.89	4.45
23	0.0213			0.225	2.05	4.86
24	0.0183			0.195	2.36	5.64
36	0.0655	4.60×10^{-4}		0.498	0.924	1.71
37	0.0405			0.365	1.26	2.59
38	0.0297			0.288	1.60	3.51
39	0.0183			0.193	2.38	5.65
42	0.0213	4.61×10^{-4}	0.100	0.221	2.09	4.80
43	0.0262			0.259	1.78	3.91
44	0.0334			0.316	1.46	3.08
45	0.0487			0.426	1.08	2.09

(contd.)

TABLE 2.1 (CONTINUED)

FERRIC/AZIDE ASSOCIATION AT 25°, IONIC STRENGTH 0.5M

EXCESS AZIDE SERIES

Sample No.	(Fe^{+3}_T)	(Az^-_T)	(H^+_T)	C.D. corrected	a/D ($\times 10^3$)	(H)/b
FQ 05	4.97×10^{-4}	0.0185	0.118	0.206	2.37	5.39
06		0.0278	0.128	0.292	1.67	3.60
07		0.0463	0.146	0.424	1.15	2.16
13		0.0185	0.119	0.219	2.23	5.43
14		0.0278	0.128	0.308	1.58	3.63
15		0.0461	0.147	0.438	1.11	2.19
25		0.0734	0.174	0.601	0.813	1.37
26		0.0568	0.157	0.511	0.952	1.77
27		0.0397	0.140	0.391	1.25	2.53
28		0.0258	0.126	0.279	1.75	3.89
29		0.0228	0.123	0.254	1.92	4.40
30		0.208	0.121	0.235	2.08	4.82
31		0.0185	0.119	0.211	2.31	5.42
32		0.0278	0.128	0.295	1.66	3.61
33		0.0327	0.133	0.342	1.43	3.07
46	4.35×10^{-4}	0.0734	0.173	0.611	0.794	1.36
47		0.0278	0.128	0.300	1.62	3.60
48		0.0208	0.121	0.238	2.04	4.81

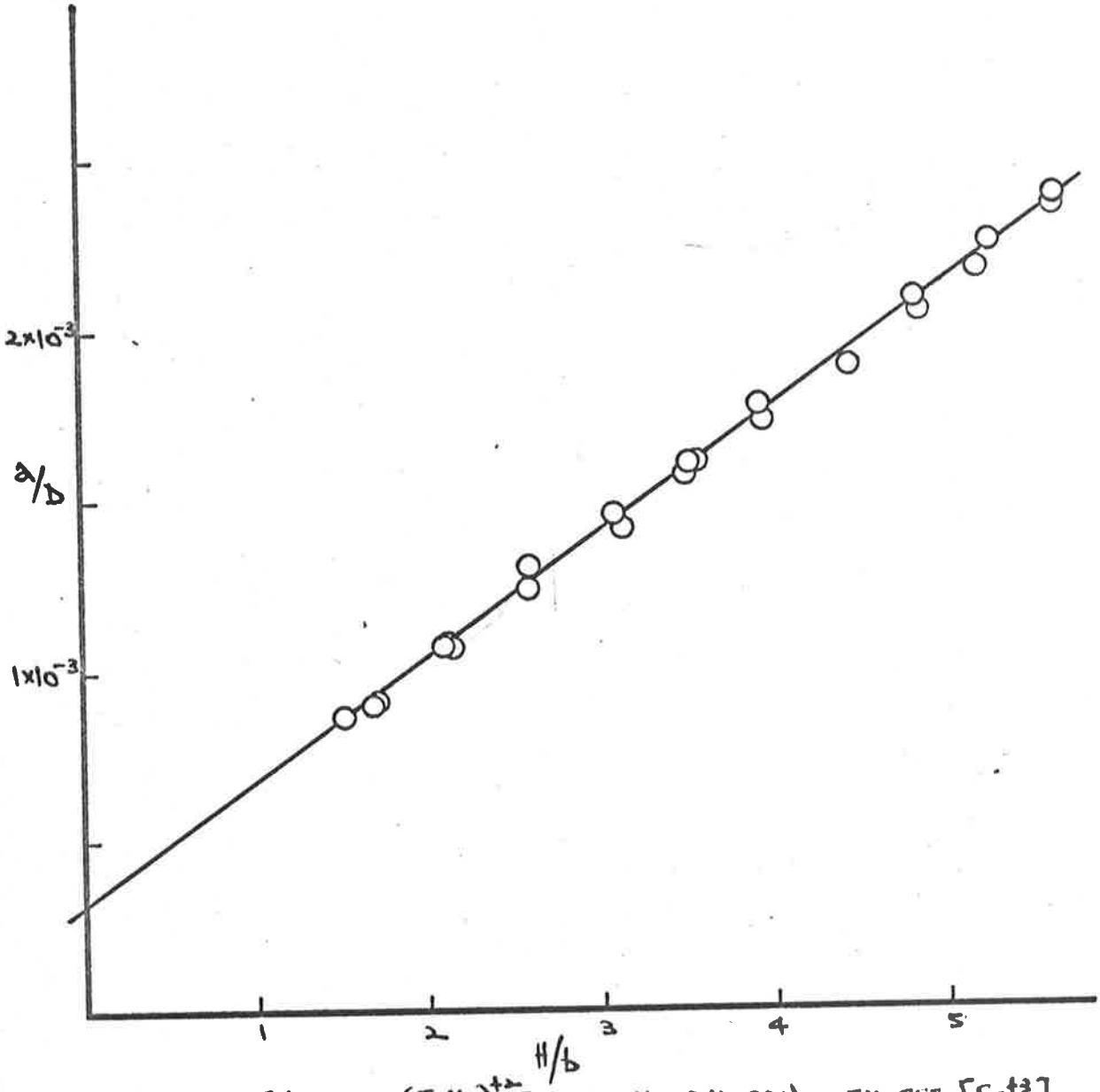

FIG. 2.1 $(FeN_3)^{+2}$ FORMATION EQUILIBRIA ; EXCESS $[Fe^{+3}]$

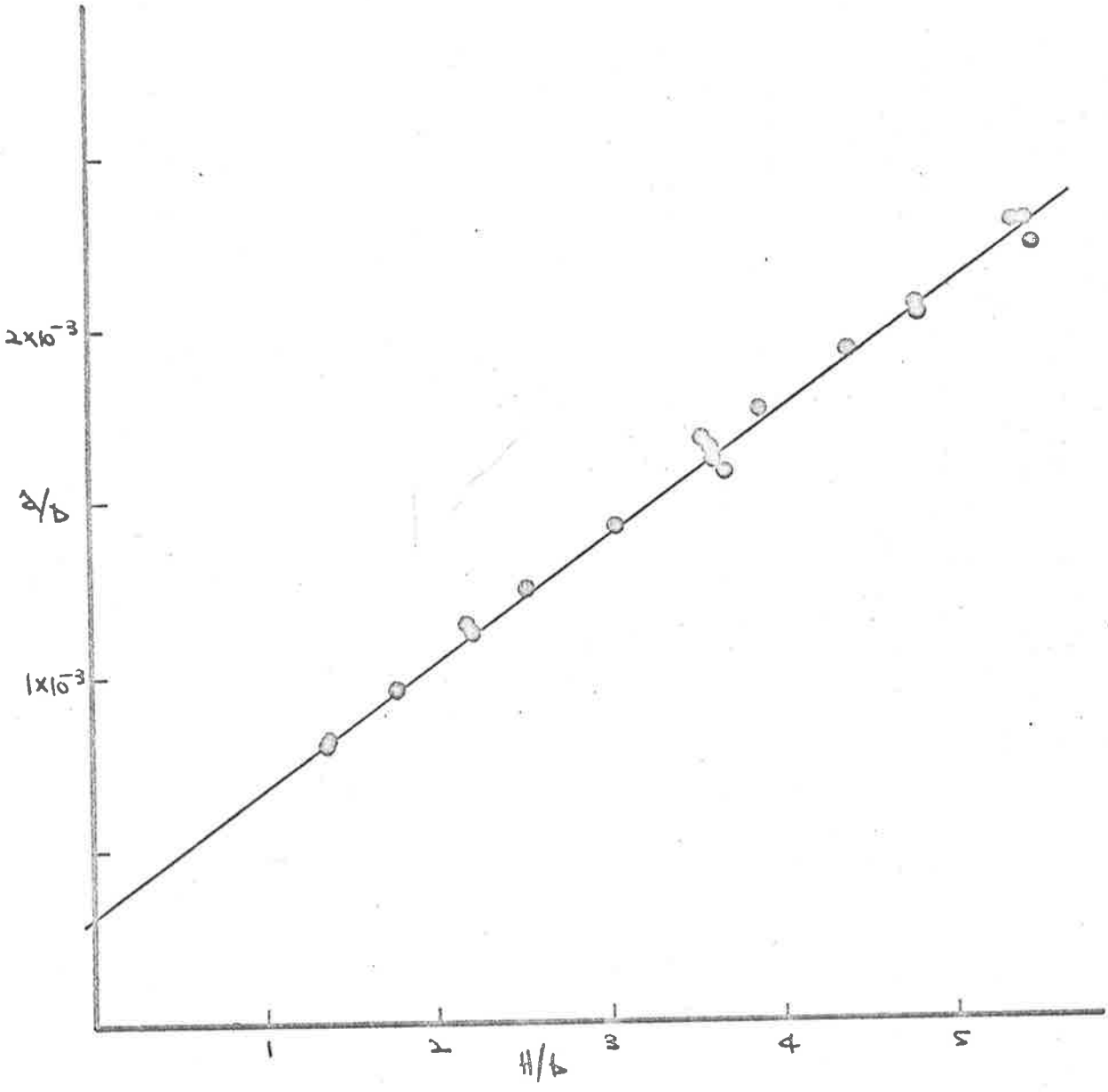

FIG. 2.2 $(FeN_3)^{+2}$ FORMATION EQUILIBRIA ; EXCESS $[HN_3]$

to Fe^{+3}_{aq} and $FeOH^{+2}$, the extinction coefficients of these species at 460mμ were determined using the data of Milburn (57M) to calculate concentrations. Results of these experiments are given in TABLE 2.2.

TABLE 2.2

DETERMINATION OF EXTINCTION COEFFICIENTS OF Fe^{+3}_{aq} AND $FeOH^{+2}$ AT 460mμ

Sample No.	(Fe^{+3}_{F})	$(FeOH^{+2})$	(H^{+})	O.D.
FQ34	0.0981	0.00160	0.1062	0.0465
FQ35	0.0179	0.00199	0.0229	0.0325
FQ40	0.0179	0.00199	0.0229	0.0290
FQ41	0.0981	0.00160	0.1062	0.0440

The values obtained from these measurements are $E_{Fe} = 0.24$ and $E_{FeOH} = 13.3$, subject to an error of ±10% and ±5% respectively; these values can be compared with those of Rabinowitch and Stockmayer (42R), 0.05 and 11 at 460mμ.

The results in TABLE 2.1 were analysed using computer program EQUIL, given in full in APPENDIX 1.1. Essentially, the program determines E and K from the intercept and least squares slope of a/D vs H/b, uses this result to correct H and b for the small contribution of product formed, then recalculates E and K

as before; incorporated is subroutine CONCS2 which corrects the reactant and product concentrations for any hydrolysis under the conditions defined by the data.

The results returned by EQUIL, together with those of other workers, are compiled in TABLE 2.3.

TABLE 2.3

FERRIC/AZIDE ASSOCIATION CONSTANTS AND EXTINCTION COEFFICIENTS AT 460mμ

(Data refer to 25°C; those data marked * have been corrected to 25° using the authors' own enthalpy data).

Reference	Conditions	K	E_{460}	Ionic Strength
This work	High Fe	0.84 ± 0.05	3270±140	0.5
	High HN_3	0.88 ± 0.08	3120±230	0.5
	High HN_3 (13,14 out)	0.83 ± 0.05	3240±200	0.5
	All points	0.86 ± 0.05	3200±140	0.5
	High Fe	0.71	3230	1.0
	High HN_3	0.74	3180	1.0
61B	High HN_3	0.89 ± 0.04	3380±200	0.5*
	High HN_3	0.76 ± 0.08	3380±200	1.0*
67C	High Fe	0.512±0.015	4400±160	1.0
	High HN_3	0.596±0.015	3570± 60	1.0
61W	High HN_3	0.75	3680	0.5*
	High HN_3	0.62	3680	1.0*

Values of K quoted in this work include standard errors in the extinction coefficient used in their calculation. Although differences between the high ferric and high azide series can be accounted for within the experimental error, this difference is made entirely negligible if two points of the high azide series, which are considerably affecting the result, are disregarded.

Agreement with Bunn, Dainton and Duckworth's result seems well within experimental error. Wallace and Dukes quote no experimental error, but the slope of the Benesi-Hildebrand function $1/K\varepsilon$, which can in general be much more accurately measured than the extrapolated intercept, gives a value of 2.66×10^{-4}, compared with our value of 2.67×10^{-4} calculated from all points.

Differences between Carlyle and Espenson's high and low azide results are well outside their quoted experimental error. The possibility that the effect of the second complex is much more important at higher ionic strengths than in our region of kinetic interest, 0.5M, was examined by making several measurements at 1.0M. These are given in TABLE 2.4 and the results included in TABLE 2.3. Because of the small number of measurements, no standard errors have been included; assuming that they are comparable to our data at ionic strength 0.5, there seems to be no measurable effect due to higher complexes. Agreement with Bunn, Dainton and Duckworth, and Wallace and Dukes, again appears

TABLE 2.4

FERRIC/AZIDE ASSOCIATION AT IONIC STRENGTH 1.0M

Sample No.	(Fe^{+3}_T)	(Az_T)	(H^+_T)	O.D. corrected	a/D	(H)/b
FQ9	0.0199	4.60×10^{-4}	0.101	0.178	2.58×10^{-3}	5.21
FQ16	0.0696	4.61×10^{-4}	0.112	0.444	1.04×10^{-3}	1.68
FQ17	4.97×10^{-4}	0.0184	0.119	0.185	2.63×10^{-3}	5.42
FQ18	4.97×10^{-4}	0.0461	0.147	0.390	1.25×10^{-3}	2.19

to be better than with Carlyle and Espenson.

The expression used by Carlyle and Espenson to treat their data

$$D/a = E - (D/a).\ H/Kb, \qquad 2.10$$

a rearrangement of the relation used to treat our data, has the advantage that K and E can be determined independently from the plot; it has the disadvantage that the measured quantity, D/a, is included in the ordinate and abscissa, and any errors in D are thus included in both. We have treated our experimental data using program EQUIL3, a modification of EQUIL, to evaluate the expression defined by EQUATION 2.10, and obtained the results in TABLE 2.5; they are essentially unchanged.

TABLE 2.5

OUTPUT FROM PROGRAM EQUIL3: DATA AT IONIC STRENGTH 0.5M

Conditions	K	E
High Fe	0.84 ± 0.03	3270 ± 100
High HN_3 (13, 14 out)	0.85 ± 0.05	3190 ± 130
All points	0.882 ± 0.03	3140 ± 90

In order to check that the experimental method was capable of detecting higher complex formation, the ferric/bromide association was examined. Lister and Rivington (55L) had suggested that higher complex formation did occur, and it was intended to perform a kinetic investigation on this system including activation parameters which, as yet, have not been measured. Using the same nomenclature as for the azide system above, optical density measurements for the system

$$Fe^{+3} + Br^{-} = FeBr^{+2} \qquad 2.11$$

should be described by

$$a/D = 1/E + 1/KEb. \qquad 2.12$$

Two series of measurements, one at high and one at low bromide concentration, were made in 4cm silica cells on the

Shimadzu QR50 at 405mμ, the reported peak of the complex absorption (55L); hydrogen ion concentration was 0.1M and the total ionic strength maintained at 0.5M. Because the absorption due to Fe^{+3}_{aq} and $FeOH^{+2}$ at this wavelength is quite significant compared with that due to complex formed, measurements were made with respect to a reference solution, identical to the reaction mixture except for the addition of bromide. Results are given in TABLE 2.6 and shown in FIGURE 2.3.

Because of the small optical density changes produced by complex formation, due to a concentration 'ceiling' imposed by the ionic strength limit, 0.5M, the extrapolation to obtain the intercept, 1/E, is extremely inaccurate, and any distinction between the measured equilibrium constant at high and low bromide impossible. The slope of the function, however, can be measured quite accurately, and it is obvious that the apparent equilibrium constant, extinction coefficient or both, have changed in moving from low to high bromide concentrations; formation of higher complexes must occur. Results are tabulated in TABLE 2.7 and a comparison with the ferric/azide system is included.

In order to obtain more accurate values for E, and therefore K, for the high ferric series, another set of experiments was performed at ionic strength 3.5M, so that higher ferric concentrations could be employed; hydrogen ion concentration was raised to 0.5M, and measurements made in 1cm cells at 405mμ.

Assuming that the intensity of the transition we were

TABLE 2.6

FERRIC/BROMIDE ASSOCIATION AT 25°, (H^+) = 0.10M, IONIC STRENGTH 0.5M, CELL PATH = 4.0cm.

Sample No.	(Fe^{+3}_T)	(Br^-)	O.D.	4a/D	1/b
GQ2	0.00993	0.00504	0.052	0.388	100.7
3	0.0149		0.078	0.259	67.2
4	0.0199		0.110	0.183	50.3
5	0.0298		0.151	0.134	33.6
6	0.0397		0.207	0.097	25.2
7	0.0596		0.317	0.064	16.8
8	0.00496	0.0126	0.076	0.261	79.3
9		0.0189	0.116	0.171	52.9
10		0.0252	0.147	0.135	39.7
11		0.0378	0.221	0.090	26.4
12		0.0504	0.297	0.067	19.8
13		0.0757	0.440	0.045	13.2

TABLE 2.7

FERRIC/BROMIDE ASSOCIATION

Conditions	KE	K	E
High Fe	260 ± 2	1000 ± 2000	0.26 ± 0.5
High Br	307 ± 4	310 ± 200	0.99 ± 0.7
c.f. ferric/amide association			
High Fe	275 ± 3		
High HN_3	273 ± 5		

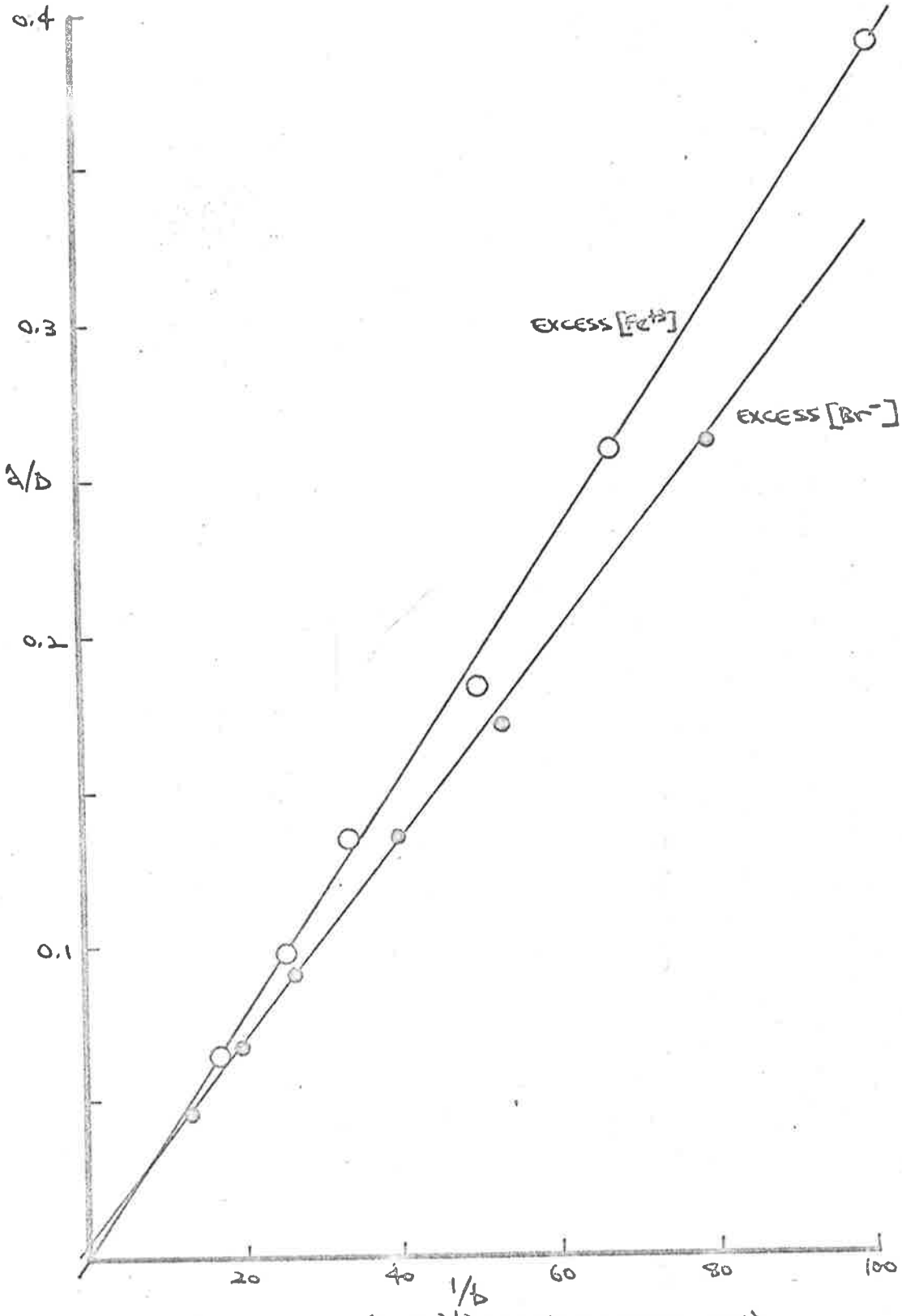

FIG. 12.3 $(FeBr)^{+2}$ FORMATION EQUILIBRIA.

observing would be unaffected by this change in environment, the value of E obtained was used to evaluate K at ionic strength 0.5M. There is evidence to suggest that, although the charge transfer bands to the solvent are markedly affected by environment, the d-d transitions and charge transfer transitions within metal complexes are not (55Li, 58S). The data for this series of measurements are given in TABLE 2.8 and the results in TABLE 2.9.

TABLE 2.8

FERRIC/BROMIDE ASSOCIATION AT 25°, (H^+) = 0.5M, IONIC STRENGTH = 3.5M, CELL PATH = 1.0cm.

Sample No.	(Fe^{+3}_T)	(Br^-_T)	O.D.	a/D	1/b
GQ14	0.496	0.00504	0.722	0.00699	2.01
15	0.248		0.505	0.0100	4.03
16	0.165		0.373	0.0135	6.07
17	0.124		0.301	0.0168	8.06
18	0.099		0.251	0.0200	10.07

TABLE 2.9

FERRIC/BROMIDE ASSOCIATION

Conditions	KE	E	K	Ionic strength
Very high Fe	614 ± 6	280 ± 95	2.21 ± 0.7	3.5
High Fe	assuming	280	0.94	0.5

This value of K is slightly more accurate than our earlier estimates and is in reasonable measurement with Lister and Rivington's value of 0.61 at ionic strength 1.2M. It is not possible to make any reliable estimate of the value of the equilibrium constant for the formation of the second bromo complex from our data.

There seems little doubt that the method should be capable of detecting higher complex formation in the ferric/azide system, should it occur; we have been unable to detect any. In the treatment of kinetic data, because we have also examined the formation of the ferric azide complex in deuterium oxide solvent, we have used the equilibrium data of Bunn, Dainton and Duckworth, which, although measured under conditions of excess ligand, seems to be substantiated by our own measurements under conditions of excess metal ion.

HYDRAZOIC ACID DISSOCIATION CONSTANT.

For analysis of the kinetic data, it was necessary to check that the values of pKa determined by Duckworth (60D) for hydrazoic acid and deuterohydrazoic acid, could be extrapolated to an ionic strength of 0.5M.

We determined the pKa of hydrazoic acid at several ionic strengths by performing pH titrations of perchloric acid (ca. 0.1M) solution against sodium azide solution (ca. 0.01M) in a vessel thermostatted at 25°C, using a Radiometer Model 4 pH meter. It can be shown that for a titration of H^+ and N_3^-, in the buffer region around the half titration point, the pH titration curve can be quite accurately described by

$$pH = pKa + \log \frac{B_T - (H_T - H_F)}{(H_T - H_F)} \qquad 2.13$$

where B_T refers to the total azide concentration, H_T to the total acid concentration, if none were used in reaction with azide, and H_F to the experimental free hydrogen ion concentration.

Results of a typical titration curve are given in TABLE 2.10 and shown in FIGURE 2.4; standard errors in the intercept were generally around 0.01. Results of experiments performed are shown compared with Duckworth's data, recalculated at 25°C using the enthalpy data of Gray (56G), in FIGURE 2.5. Agreement

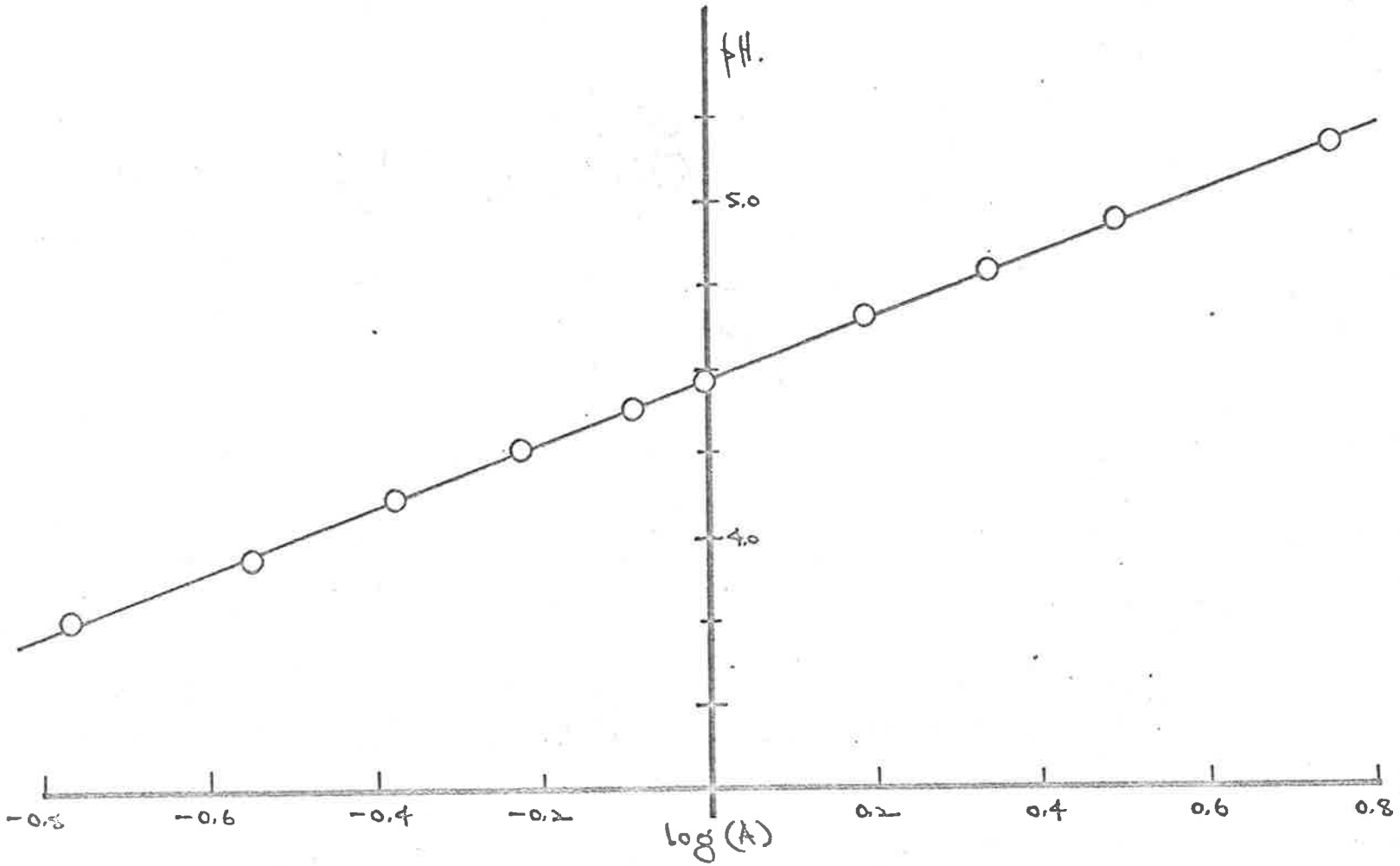

FIG. 2.4 DATA FROM A TYPICAL pK_A DETERMINATION ; TITRATION 10.

TABLE 2.10

DATA FOR TYPICAL pH TITRATION

Titration 10 : 0.1003M $HClO_4$ vs 25.00 ml 0.0101M NaN_3

ionic strength = 0.5, temperature = 25.0°C.

Vol. acid	pH	$\log \frac{B_T - (H_T - H_F)}{(H_T - H_F)}$
0.39	5.15	0.743
0.62	4.93	0.491
0.80	4.78	0.339
0.99	4.65	0.195
1.28	4.45	- 0.004
1.41	4.38	- 0.091
1.60	4.255	- 0.224
1.80	4.115	- 0.375
2.01	3.93	- 0.551
2.21	3.755	- 0.767

is quite good, and the extrapolated value was used in the treatment of the kinetic data.

Because the results of Duckworth for the dependence of pKa on the square root of ionic strength for deuterohydrazoic acid were a much better straight line than for hydrazoic acid, no extra measurements were made for this system.

The pKa of hydrazoic acid was also measured at 7.8°C using a single buffer mixture; the value obtained was 4.63.

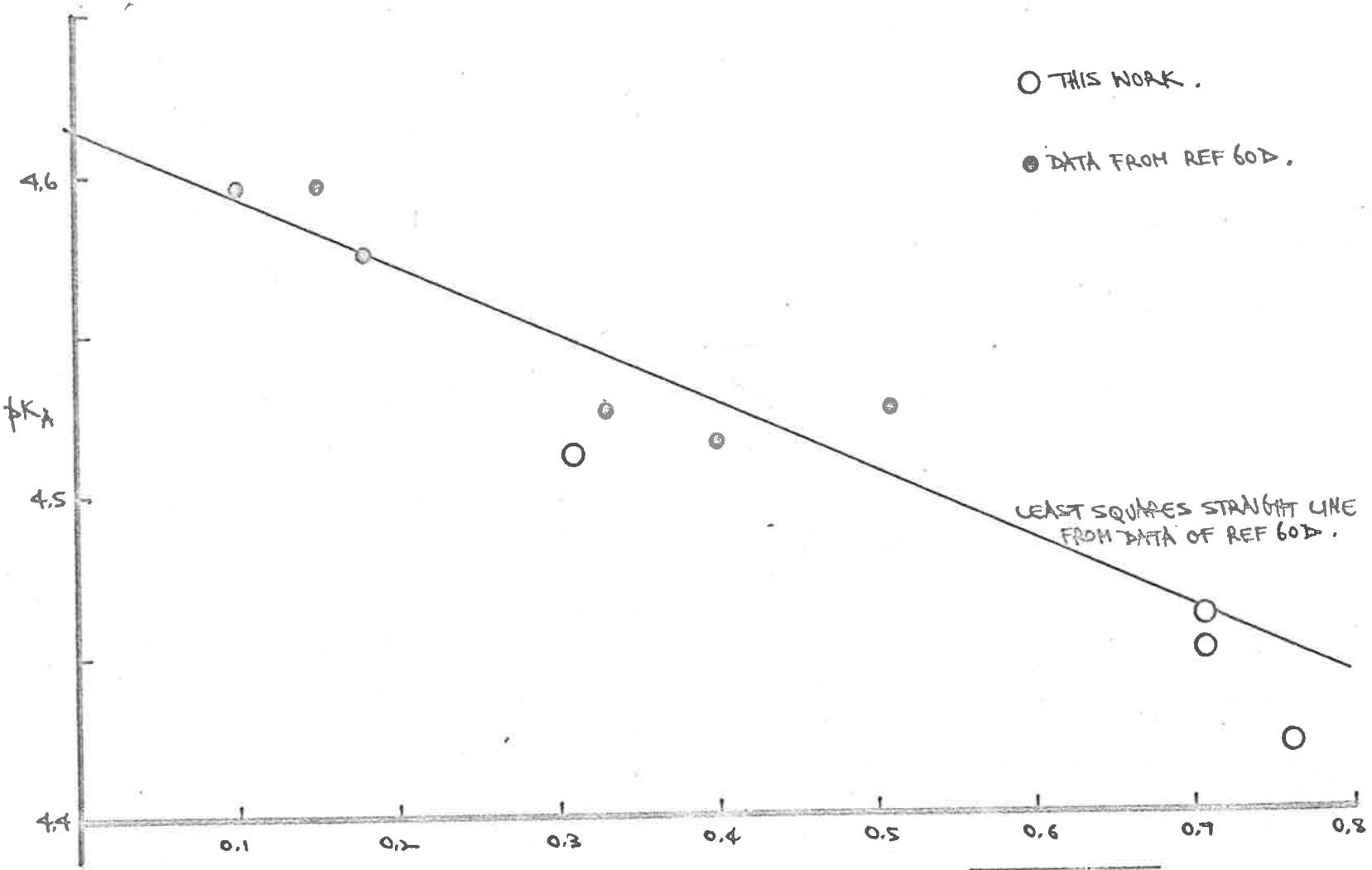

FIG. 2.5 DEPENDENCE OF pK_A OF HYDRAZOIC ACID ON $\sqrt{\text{IONIC STRENGTH}}$.

Considerable difficulty was encountered in some measurements because of impurities of up to 1% carbonate in the B.D.H. sodium perchlorate used to maintain the ionic strength. All results reported above used Fluka sodium perchlorate which gave no measurable buffer effect due to carbonate impurities.

HEAT OF NEUTRALISATION OF AZIDE ION IN H_2O AND D_2O.

The heat of neutralisation of the azide ion in water, i.e. the enthalpy change for the reaction

$$H^+aq + N_3^-aq = HN_3aq, \qquad 2.14$$

ΔH_a, was remeasured to check the experimental technique, then the corresponding quantity for reaction in deuterium oxide as solvent, ΔH_d was determined.

Considerable time was spent in the design and construction of a small volume calorimeter in which to make the measurements; it is shown in FIGURE 2.6. The temperature rise when excess thermostatted reactant B was run from the side vessel into an aliquot of thermostatted reactant A in the calorimeter, and thoroughly mixed, was sensed by a thermistor bridge/amplifier and recorded on a fast response pen recorder. The equilibrium mixture was then brought back to bath temperature, and an accurately known amount of electrical energy used to heat the solution by a

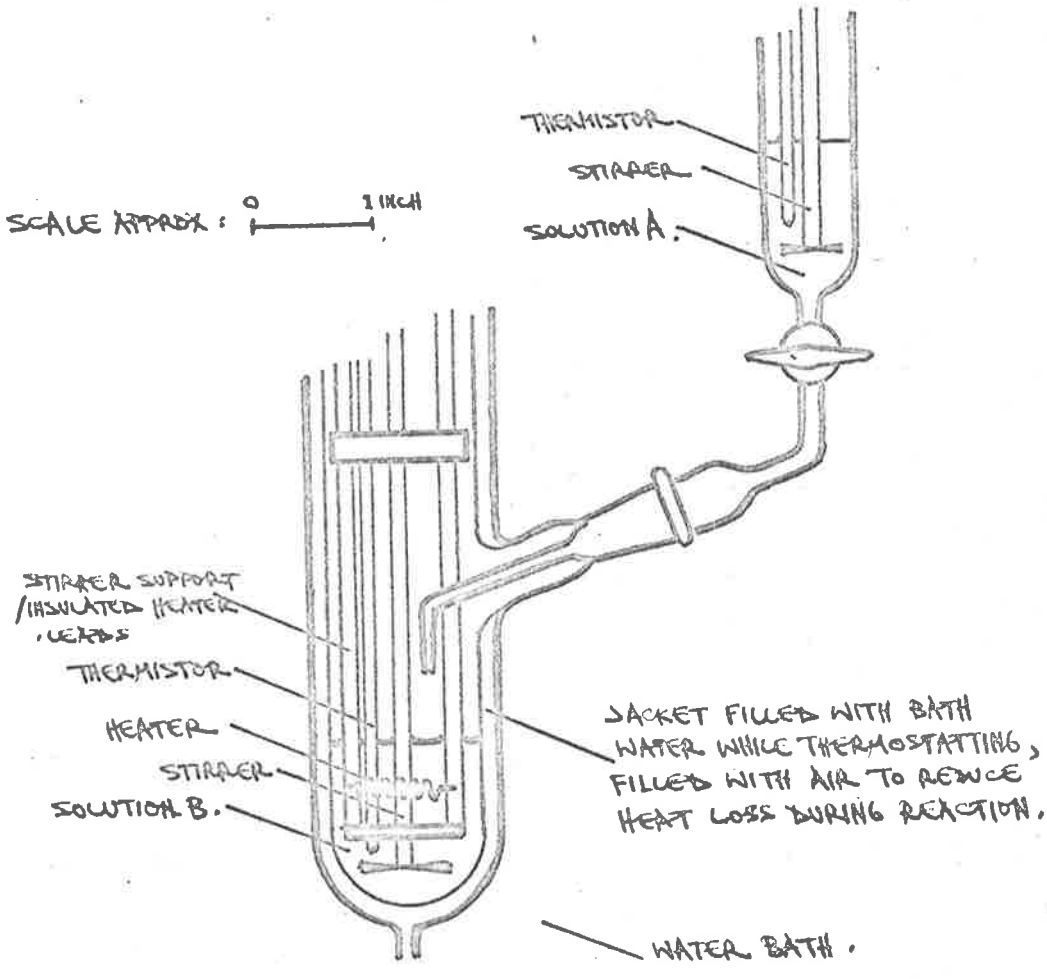

FIG. 2.6 SMALL VOLUME CALORIMETER.

comparable amount.

The results obtained from a series of determinations gave ΔH_h = 3.65 ± 0.1 kcals/mole compared with the value obtained by Gray (56G), of 3.60 ± 0.05 kcals/mole at 25°C.

It became possible, however, to continue measurements on a Beckman 190B microcalorimeter, and subsequent results were obtained on this instrument. The heat burst produced by reaction of a small accurately known volume (usually 50 - 200µl) of reactant A with 15ml of reactant B is compared with the heat produced by simultaneously diluting a similar volume of A into 15ml of solvent in a control cell; heating effects of dilution and mechanical stirring are cancelled. Both cells are mounted in copper/constantan thermopiles and the whole system encased in a large heat sink.

The instrument was calibrated by comparing the integrated heat flow through the thermopile with that for a standard reaction of well documented enthalpy change. Using the neutralisation of 196.4µl of 0.00967M HCl by 15ml of about 0.01M sodium hydroxide, the sensitivity of the instrument was found to be 0.358 ± 0.004 millicals/integrator division.

A series of measurements were made of the reaction of 101.3µl of 0.0766M sodium azide with 15ml of 0.1M perchloric acid, and the results are given in TABLE 2.11. The mean value of ΔH_h is 3.61 ± 0.06 kcals/mole at 18°C.

This value, combined with Gray's value of 3.60 ± 0.05 kcals/

TABLE 2.11

HEAT OF FORMATION OF HN_3aq FROM AQUATED IONS

Sample No.	Heat sink temperature	Integrator reading	ΔH kcals/mole
9	17.6	79.9	3.63
11	18.9	79.5	3.61
12	18.9	78.5	3.57

mole at 25°C, and the observation that ΔH_h calculated from our values of pKa at 25°C and 7.8°C is 3.78 kcals/mole, leads us to suggest that the enthalpy change for the dissociation of hydrazoic acid probably changes very little over the temperature range (10 - 40°C) in which our kinetic measurements were made. At worst estimate ΔH_h may have fallen to 3.4 kcals/mole at 40°C, in which case calculations, if the value of the dissociation constant based on the value of ΔH_h at 25°C, would be in error by only around 2%. This appears to be a different type of behaviour to that exhibited by many weak acids, where the ionisation constant may reach a maximum, often at temperatures close to room temperature (59R).

A microcalorimetric determination of the heat of neutralisation of azide ion in D_2O as solvent was carried out and the results are given in TABLE 2.12. The mean value is 4.07 ± 0.27 kcals/mole. Although our value of $\Delta H_h - \Delta H_d$ is subject to

considerable possible error, 0.46 kcals/mole compares quite reasonably with 0.38 kcals/mole for the second dissociation of phosphoric acid, calculated from the data of Gray, Bates and Robinson (64).

TABLE 2.12

HEAT OF FORMATION OF DN_3aq FROM SOLVATED IONS

101.3µl 0.0505M NaN_3 in D_2O + 15ml 0.1M DClO4

Sample No.	Heat sink temperature	Integrator reading	ΔH kcals/mole
13	18.9	63.1	4.37
14	18.6	55.2	3.82
15	18.6	63.8	4.41
16	18.7	53.7	3.72
17	18.6	58.0	3.95

CHAPTER III

RATE EQUATIONS AND KINETIC DERIVATIONS

The rate of formation of monoazideiron(III) ion was followed by measuring the concentration of the complex as a function of time, under conditions of total iron(III) ca. 0.01M, total azide ca. 0.005 and hydrogen ion ca. 0.007 to 0.42, at temperatures between 10° and 40°C. However, because the reactants and products are involved in a number of equilibria which may affect their concentration, and therefore may be expected to modify the kinetics of complex formation, the effect of these equilibria will now be considered in deriving a kinetic model against which the experimental results may be tested.

In acidic aqueous solutions of ferric iron containing low concentrations of azide, the possible equilibria to be considered have been shown in Chapter II to be

$$Fe^{+3} + HN_3 \rightleftharpoons FeN_3^{+2} + H^+ \qquad 3.1$$

$$Fe^{+3} \underset{k_{-H}}{\overset{k_H}{\rightleftharpoons}} FeOH^{+2} + H^+ \qquad 3.2$$

$$Fe^{+3} \underset{k_{-D}}{\overset{k_D}{\rightleftharpoons}} (FeOH)_2^{+4} + 2H^+ \qquad 3.3$$

$$HN_3 \underset{k_{-A}}{\overset{k_A}{\rightleftharpoons}} H^+ + N_3^- \qquad 3.4$$

The values and sources of the equilibrium constants, Keq, K_H, K_D and K_A, describing these equilibria, used in the treatment of the kinetic data are given in TABLE 3.1.

TABLE 3.1

EQUILIBRIUM CONSTANT DATA AT IONIC STRENGTH = 0.5M, TEMPERATURE = 25°C

	K	ΔH°	Reference
Keq	0.89	2.52	61B
K_H	1.87×10^{-3}	10.30	57M
K_D	1.49×10^{-3}	12.8	57M
K_A	3.45×10^{-5}		61B
K_A		3.60	56A

Consider the hydrolysis of Fe^{+3}_{aq} described by EQUATION 3.2. It has been shown that for a reaction of the form

$$C \underset{k_r}{\overset{k_f}{\rightleftharpoons}} A + B, \qquad 3.5$$

the relaxation time of the system to a small change in the condition of chemical equilibrium is described by

$$1/T = k_f + k_r (\bar{A} + \bar{B}) \qquad 3.6$$

where T is the relaxation time, and $\bar{A}$ and $\bar{B}$ are the equilibrium concentrations of components A and B.

Lua and Shulman (65L) have estimated from proton magnetic resonance shifts measured on ferric solutions, that $k_H = 2.8 \times 10^6$ sec^{-1}, so that $k_{-H} = 1.5 \times 10^9$ l/m/s at 25°C. The concentration of reactants in our runs performed at lowest acid are given in TABLE 3.2.

TABLE 3.2

CONCENTRATION OF REACTANTS AT t = o FOR RUN F162

(moles litre^{-1})

(Fe^{+3}) = 7.2×10^{-3}	(HN_3) = 4.8×10^{-3}	(H^+) = 7.3×10^{-3}
$(FeOH^{+2})$ = 1.9×10^{-3}	(N_3^-) = 2.3×10^{-5}	
$(Fe_2OH_2^{+4})$ = 4.4×10^{-3}		

If the concentration of any of the components involved in this equilibrium were disturbed by reaction to form FeN_3^{+2}, the equilibrium would respond with a relaxation time of 6×10^{-8} seconds. The $Fe^{+3}/FeOH^{+2}$ equilibrium described by EQUATION 3.2 will therefore apply throughout the kinetics of formation of the complex, for which the shortest half time for the conditions studied was around 5×10^{-3} seconds.

Similarly, the hydrolysis of hydrazoic acid can be considered mobile; by analogy to similar directly measured

protolytic reactions (64E), k_{-A} might be expected to be 5×10^{10} l/m/s, giving k_A a value of 2.5×10^{6} sec^{-1}. The relaxation time of this hydrolysis under our conditions would be about 3×10^{-9} seconds.

Wendt (62W) has measured the rate of the dimerisation

$$2\,FeOH^{+2} \underset{k'_{-D}}{\overset{k'_D}{\rightleftharpoons}} (FeOH)_2^{+4} \qquad 3.7$$

and obtained $k'_D = 450$ l/m/s, $k'_{-D} = 1$ sec^{-1}. The calculated relaxation time is 0.4 to 1 second for the range of conditions studied in our work. A similar range of relaxation times is suggested by the measurements of Sutin (65S). The dimerisation will be considered immobile for the period of measurement of FeN_3^{+2} formation. Assuming the dimer to be inert to direct reaction with ligand, the result of this equilibrium will be to reduce the effective concentration of Fe^{+3} available for reaction.

So possible reaction paths for the formation of FeN_3^{+2} are:

$$Fe^{+3} + N_3^- \underset{k_{-1}}{\overset{k_1}{\rightleftharpoons}} FeN_3^{+2} \qquad 3.8$$

$$FeOH + N_3^- \underset{k_{-2}}{\overset{k_2}{\rightleftharpoons}} FeN_3^{+2} + OH^- \qquad 3.9$$

$$Fe^{+3} + HN_3 \underset{k_{-3}}{\overset{k_3}{\rightleftharpoons}} FeN_3^{+2} + H^+ \qquad 3.10$$

$$FeOH^{+2} + HN_3 \underset{k_{-4}}{\overset{k_4}{\rightleftharpoons}} FeN_3^{+2} + H_2O \qquad 3.11$$

The rate of formation of the complex ion will be described by:

$$\frac{d(FeN_3)}{dt} = k_1(Fe)(N_3^-) + k_2(FeOH)(N_3^-) + k_3(Fe)(HN_3) + k_4(FeOH)(HN_3)$$
$$- k_{-1}(FeN_3) - k_{-2}(FeN_3)(OH^-) - k_{-3}(FeN_3)(H^+) - k_{-4}(FeN_3) \qquad 3.12$$

where ionic charges have been omitted for clarity.

However, as equilibrium conditions for hydrolyses 3.2 and 3.4 will apply throughout

$$(FeOH) = K_H(Fe)/(H) \qquad 3.13$$

$$(HN_3) = (N_3)(H)/K_A \qquad 3.14$$

also $(OH) = K_w/(H)$, where K_w is the ionisation of water.

So that 3.12 can be written as

$$\frac{d(FeN_3)}{dt} = (Fe)(N_3)\left[k_1 + \frac{k_2K_H}{(H)} + \frac{k_3(H)}{K_A} + \frac{k_4K_H}{K_A}\right]$$
$$- (FeN_3)\left[k_{-1} + \frac{k_{-2}K_w}{(H)} + k_{-3}(H) + k_{-4}\right] \qquad 3.15$$

$$= k_{OBS}(Fe)(N_3) - k'_{OBS}(FeN_3) \qquad 3.16$$

for a given free acid concentration, assuming (H) to remain essentially constant over the period of measurement, and where (Fe), (N_3^-) and (FeN_3^{+2}) refer to the 'free' concentrations of reactants and product at time t.

Subject to these assumptions, the system should be described by a reaction 'model',

$$Fe^{+3} + N_3^- \underset{k_r}{\overset{k_f}{\rightleftharpoons}} FeN_3^{+2} \qquad 3.17$$

Now at any time throughout the kinetics

Fe_T = total concentration of ferric available for reaction

= total concentration of ferric iron present - that ferric associated as dimer

$$= (Fe^{+3}_{aq}) + (FeOH^{+2}) + (FeN_3^{+2}) \qquad 3.18$$

$$= (Fe^{+3}_{aq})(1 + K_H/(H)) + (FeN_3^{+2}) \qquad 3.19$$

$$(Fe^{+3}_{aq}) = Fe_F = (Fe_T - x)/(1 + K_H/H) \qquad 3.20$$

where x is the concentration of the product, FeN_3^{+2}.

Similarly,

$$(N_3^-) = N_{3F} = (As_T - x)/(1 + H/K_A) \qquad 3.21$$

where As_T is total concentration of azide present.

So that on the basis of the model defined by EQUATION 3.17;

$$\frac{dx}{dt} = \frac{k_r(Fe_T - x)(As_T - x)}{(1 + K_H/H)(1 + H/K_A)} - k_r x \qquad 3.22$$

$$= k_r \frac{K(Fe_T - x)(As_T - x)H.K_A}{(H + K_H)(H + K_A)} - x \qquad 3.23$$

Under our conditions $H \gg 2000\ K_A$, so that

$$\frac{dx}{dt} = k_r \frac{(Fe_T - x)(As_T - x)\ K.K_A}{(H + K_H)} - x \qquad 3.24$$

Now in fast calculations including all possible equilibria, show that (H) at low values does change slightly during reaction; the best stoichiometric model for the system is

$$Fe^{+3} + HN_3 = FeN_3^{+2} + H^+ \qquad 3.25$$

So that $(H) = (H)_{initial} + x$

At the lowest acid studied, 7.2×10^{-3}M, this approximation is in error by 3%, although (H) changes by 20%; at the next lowest acid, 1.18×10^{-2}, which changes by 12% during reaction, the assumption is correct to within ½%. This can be included in

EQUATION 3.24 to give

$$\frac{dx}{dt} = k_r \frac{(Fe_T - x)(As_T - x)K_oK_A}{(H_0 + K_H + x)} - x \qquad 3.26$$

and rewritten, replacing the constants for clarity, as

$$\frac{dx}{dt} = k_r \frac{(a - x)(b - x)d}{(e + x)} - x \qquad 3.27$$

$$= k_r \frac{(abd) - (ad + bd + e)x + (d - 1)x^2}{(e + x)} \qquad 3.28$$

Therefore

$$\frac{e + x}{abd - (ad + bd + e)x + (d - 1)x^2} dx = k_r dt \qquad 3.29$$

So that, again replacing the constants for clarity,

$$p\int_o^x \frac{dx}{A + Bx + Cx^2} + \int_o^x \frac{x}{A + Bx + Cx^2} = \int_o^t k_r dt \qquad 3.30$$

where

$$A = abd = Fe_T.As_T.K_oK_A \qquad 3.31$$

$$B = -(ad + bd + e)$$

$$= -(Fe_TK_oK_A + As_TK_oK_A + H_0 + K_H) \qquad 3.32$$

$$C = \delta - 1 = K_0 K_A - 1 \qquad 3.33$$

$$p = e = H_0 + K_H \qquad 3.34$$

The integrals derived above are of a standard form and can be integrated exactly to give

$$\frac{p - (B/2C)}{\sqrt{B^2 - 4AC}} \ln \frac{2Cx + B - \sqrt{B^2 - 4AC}}{2Cx + B + \sqrt{B^2 - 4AC}} + \frac{1}{2C} \ln (A + Bx + Cx^2) \Big]_e^x = k_r t \Big]_o^t \qquad 3.35$$

Evaluation of this integral for corresponding values of (FeN_3^{+2}) at various times t, should be linear, with slope k_r, corresponding with the observed reverse rate constant defined in EQUATION 3.16.

Program RATE13, incorporating subroutines CONCS, DTATRY and LSTSQU, was written to evaluate the integral in EQUATION 3.24 for the conditions of concentration of reactants, temperature, instrument settings and thermodynamic data chosen for a given run, and to determine the 'observed' forward rate constant; it is given in full in APPENDIX 1.2.

CHAPTER IV

EXPERIMENTAL PROCEDURE AND TREATMENT OF RESULTS

Kinetic experiments were performed on a stopped flow apparatus with spectrophotometric detection, the specifications of which are given in APPENDIX 2. The principles and development of the stopped flow and other flow and relaxation techniques in the study of fast reactions have been surveyed in the literature (63R, 64C) and have been widely applied in the study of chemical kinetics in solution (64H, 65S).

In the stopped flow method, known ratios of the two reactant solutions are injected at high velocity into a small, efficient mixing chamber from which the mixed solution flows down an observation tube; the flow of reactants is suddenly stopped and the kinetics of reaction followed in that element of solution which stops at an observation point placed as close as practicable to the point of mixing. The prerequisite of the observation equipment is its ability to respond without distortion to the changes in concentration being followed.

A schematic diagram of the apparatus used in this study is given in FIGURE 4.1.

The kinetics of formation of the monoazidoiron(III) ion, initiated when equal volumes of acidified ferric solution (ca. 0.02M, ionic strength 0.5M) and sodium azide solution

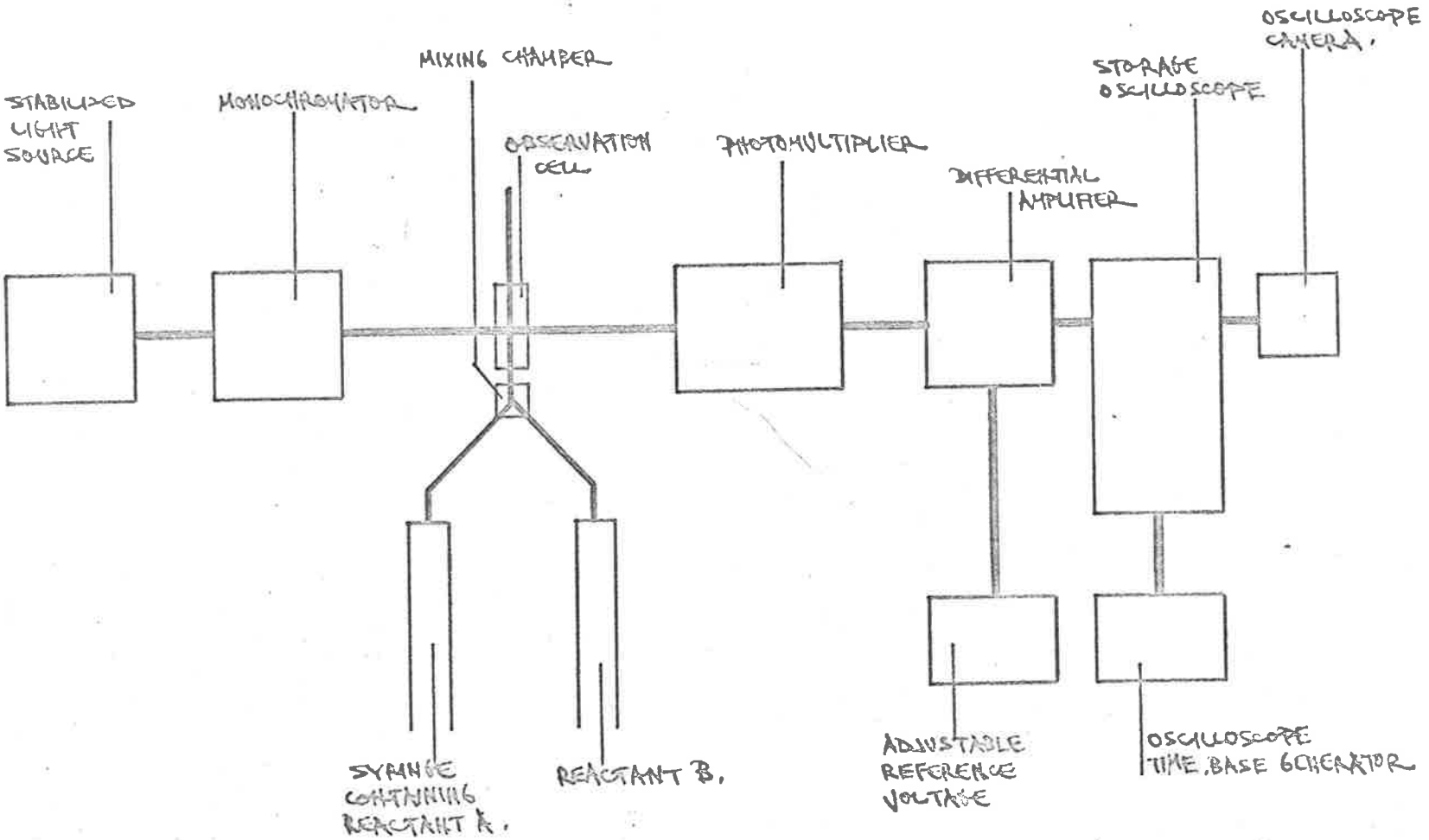

FIG. 4.1 SCHEMATIC DIAGRAM OF APPARATUS.

(ca. 0.01M, ionic strength 0.5M) were mixed, were measured by following the change in transmission through the solution of light at 460mμ. The reaction was studied at H^+ concentrations from 0.007M to 0.42M and at temperatures between 10° and 40°C.

The experimental procedure for kinetic measurement can be summarised:

(i) Preparation.

Reactant solutions of the desired concentrations were prepared by dilution of standardised stock. With the glassware used, and giving consideration to the uncertainty in concentration of the stock solution, possible errors in reactant concentrations are for ferric, ± 0.7%, hydrogen ion ± 3% to ± 0.5%, and azide ± 0.5%. Because of the volatility of hydrazoic acid, no solutions of acidified azide were prepared.

(ii) Degassing.

Reactant solutions were degassed by melting 50ml of frozen solution under vacuum in 100ml closed vessels. The procedure was necessary to prevent cavitation, which would otherwise occur when solutions flowed at high velocity through the apparatus. From vapor pressure and gas solubility data (59C), the concentration of dissolved gases is expected to fall by more than 98%, while the

solution concentration should be affected by less than 0.001% after one freeze/melting cycle under these conditions.

(iii) Thermostatting.

The apparatus was thermostatted by circulating water, controlled to ± 0.05°C, through the hollow thermal panels. Thermistor measurements of the reactant solutions indicated that temperature equilibrium was reached after 20 minutes; solutions were placed in the apparatus 20 - 30 minutes before any kinetic measurements were made.

(iv) Injection/Reaction.

Equal volumes of each reactant (0.45ml), enough to completely flush any reacted solution from the mixer and observation cell, were injected in 60 - 100 milliseconds. Just before the flow was stopped, the oscilloscope trace was triggered; the apparatus was set so that fast observation of reacting solutions was made 4 - 6 milliseconds after mixing, and reaction followed continuously for 4 - 6 half lives. Typical traces are shown in FIGURES 4.2 and 4.3.

(v) 'Infinite time' Reading.

After a few seconds a reading corresponding with the transmission of the solution after all reactions in the system had attained equilibrium was taken; the photomultiplier signal was balanced to electrical zero and the backing off voltage noted for later calculations. All

FIGURES 4.2 and 4.3. TYPICAL REACTION TRACES

FIGURE 4.2. RUN F20.1

(Fe^{+3})	0.01005 mole/litre
(Azide)	0.00450 mole/litre
(H^{+})	0.0615 mole/litre
Temperature	30.0°C
Trace speed	10 millsec/cm
CRO sensitivity	1.0 volt/cm
Total optical density change	0.20

FIGURE 4.3. RUNS F58.1, F58.2 and F58.3

(Fe^{+3})	0.01009 mole/litre
(Azide)	0.00464 mole/litre
(H^{+})	0.0108 mole/litre
Temperature	10.1°C
Trace speed	50 millsec/cm
CRO sensitivity	1.0 volt/cm
Total optical density change	0.84

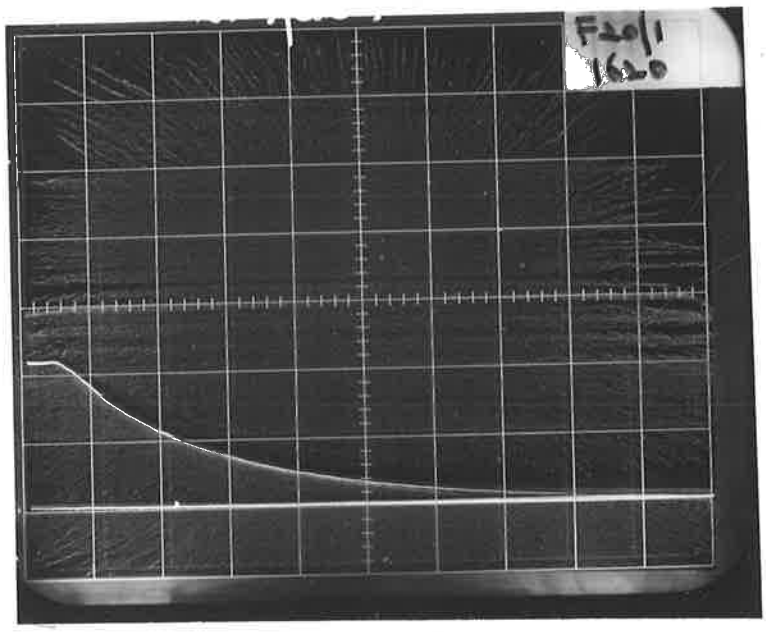
F20/1
1620

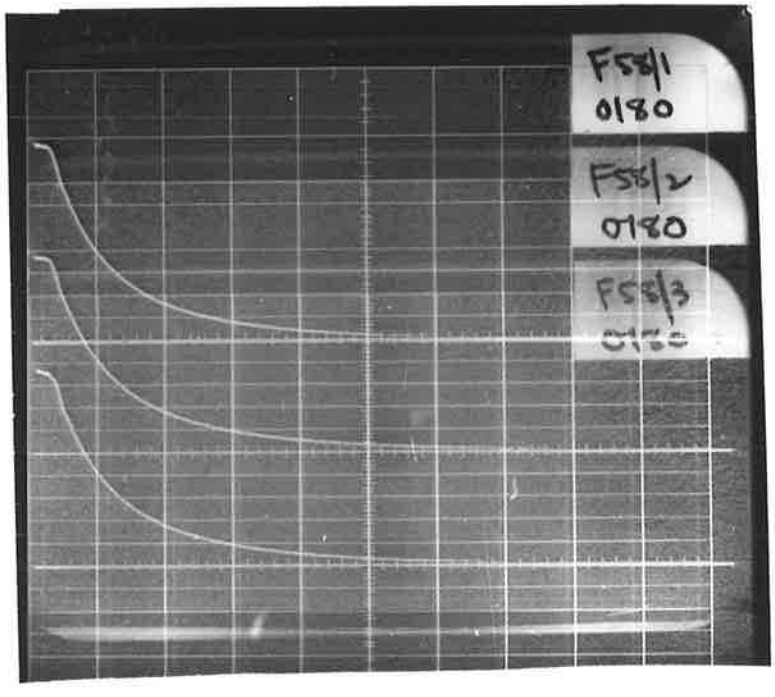
F58/1
0180
F58/2
0180
F58/3

measurements of transmission were taken with respect to this 'infinite time' sample.

The stored trace and base line were photographed for later measurement.

(vi) Trace Measurement.

Using a photographic enlarger, the trace was magnified to around four times screen size and the magnification noted; the image was projected onto graph paper and re-drawn. A typical displacement could be measured with an accuracy of 1%.

It will be later shown (APPENDIX 2) that the effective 'dead time' between mixing and observation is probably 2 - 3 milliseconds; it was assumed in the treatment of the data that at first observation the concentration of product was zero. For faster traces, this is obviously not true; a measurable reaction has taken place before observation, and mixing may not be 100% completed for 1 - 2 milliseconds after stopping. It was attempted to correct this by extrapolation of the smooth transmission vs time curve to zero time; curvature in the rate integral vs time at times less than a few milliseconds was eliminated through this procedure, and the extrapolation procedure is therefore assumed to be a reasonable one.

For each trace, usually twenty values of trace displacement at equal time intervals after stopping the flow were

measured, covering a period representing 70 - 90% of reaction, and these, together with the setting of the backing of potential at equilibrium, were recorded on punched cards.

In general, six runs were performed for any one given set of concentration conditions and temperature, and treated as described in steps (iv) to (vi) above. These conditions which applied to the whole set, total initial ferric and azide concentrations, the total initial hydrogen ion concentration, not allowing for hydrolysis of ferric or formation of hydrazoic acid, the temperature, oscilloscope settings of input amplifier and time base, and the enlargement factor in drawing the traces were recorded on punched cards.

The data was processed using a program RATE18 and associated subroutines, a complete listing of which is given in APPENDIX 1.2, and the operation of which is described below.

TREATMENT OF RESULTS - PROGRAM RATE13.

Leaving aside the input/output and housekeeping operations, the essential function of program RATE13 in processing a set of data will now be described.

Using the thermodynamic data chosen and the conditions of the run, the hydrolysis, dimerisation, acidity and complex formation equilibrium constants corresponding with the reactions below were calculated:

$$Fe^{+3} = FeOH^{+2} + H^{+} \qquad 4.1$$

$$2Fe^{+3} = (FeOH)_2^{+4} + 2H^{+} \qquad 4.2$$

$$HN_3 = N_3^{-} + H^{+} \qquad 4.3$$

$$Fe^{+3} + HN_3 = FeN_3^{+2} + H^{+} \qquad 4.4$$

This data is used in the calculation of the hydrolysis corrections of reactant concentrations in subroutine CONCS, where three stages during reaction are treated independently:

Firstly, the ferric solution is considered before reactants are mixed; reactions 4.1 and 4.2 equilibrate and the hydrogen and ferric concentrations are adjusted accordingly.

Secondly, at the instant of mixing, all reactants are diluted by a factor of two and reactions 4.1 and 4.3 come to equilibrium. As described in Chapter III, the dimerisation 4.2 can be considered immobile and, assuming no direct reaction with

ligand, its effect is to remove a certain concentration of ferric ion from the reaction scheme; any hydrogen ion increase due to dimerisation before mixing is included in the conditions at mixing.

Finally, the concentrations of all species when reactions 4.1, 4.2, 4.3 and 4.4 have equilibrated, the condition corresponding with the 'infinite time' reading, is calculated. The concentrations of ferric ion free for reaction, azide, hydrogen ion and the equilibrium concentration of complex product are returned to the main program.

Assuming the absorption of the solution at time = o to be that of the solvent, the concentration of product at time = t was calculated from the optical density at time = t, the optical density at equilibrium and the calculated equilibrium concentration of product.

The integral defined in EQUATION 3.35 was evaluated for these concentrations.

The purpose of subroutine DTATRY is to eliminate any punching errors in the data which may otherwise be very heavily weighted in a least squares fit to the function. The least squares slope of values of the integral vs time, passed by DTATRY, that is the observed aquation rate constant, was calculated, and the observed forward rate constant determined from this.

The calculations of product concentrations, integral and

observed rate constants were repeated for each run in the set, then the mean forward rate constant and probable error in the mean were calculated. This value was used in the analysis of the pH and temperature dependence.

An example of the output from RATE13 is shown in FIGURES 4.4 and 4.5; from the linearity of the rate plot to quite high degrees of conversion to product, the treatment appears to accurately describe the kinetics.

```
OUTPUT FOR RUN   54

 CALCULATION DETAIL FOR PUSH NUMBER 1

 FET1= 2.060E-02 FEF1= 1.995E-02 FEOH1= 4.629E-04 FEDI1= 9.174E-05 ACIDF1= 8.053E-02 NTRIAL=  2
 FET3= 1.021E-02 FEOH3= 5.050E-04 AZT3= 4.640E-03 HN3= 4.636E-03 ACIDF3= 3.590E-02 NTRIAL=  3
 FET4= 1.030E-02 FEF4= 8.854E-03 FEOH4= 4.501E-04 FEDI4= 8.675E-05 ACIDF4=3.6750E-02 HN4= 3.814E-03 FEN4= 8.227E-04 NTRIAL=  5
 EKHY= 1.868E-03. EKDI= 1.494E-03. EKAC= 3.446E-05. EQCON= 8.948E-01. YEQ= 5.908E+00/)
 POINT NO.  1     TIME=  0.            Y(J)=  1.841E+01     CONCN=  0.            FUNC=  0.
 POINT NO.  2     TIME=  4.160E-03     Y(J)=  1.621E+01     CONCN=  9.214E-05     FUNC=  8.714E-02
 POINT NO.  3     TIME=  8.320E-03     Y(J)=  1.451E+01     CONCN=  1.724E-04     FUNC=  1.726E-01
 POINT NO.  4     TIME=  1.248E-02     Y(J)=  1.321E+01     CONCN=  2.403E-04     FUNC=  2.537E-01
 POINT NO.  5     TIME=  1.664E-02     Y(J)=  1.216E+01     CONCN=  3.003E-04     FUNC=  3.336E-01
 POINT NO.  6     TIME=  2.080E-02     Y(J)=  1.125E+01     CONCN=  3.566E-04     FUNC=  4.175E-01
 POINT NO.  7     TIME=  2.496E-02     Y(J)=  1.050E+01     CONCN=  4.066E-04     FUNC=  5.008E-01
 POINT NO.  8     TIME=  2.912E-02     Y(J)=  9.908E+00     CONCN=  4.484E-04     FUNC=  5.788E-01
 POINT NO.  9     TIME=  3.328E-02     Y(J)=  9.408E+00     CONCN=  4.859E-04     FUNC=  6.563E-01
 POINT NO. 10     TIME=  3.744E-02     Y(J)=  8.908E+00     CONCN=  5.254E-04     FUNC=  7.479E-01
 POINT NO. 11     TIME=  4.160E-02     Y(J)=  8.558E+00     CONCN=  5.545E-04     FUNC=  8.231E-01
 POINT NO. 12     TIME=  4.576E-02     Y(J)=  8.198E+00     CONCN=  5.856E-04     FUNC=  9.132E-01
 POINT NO. 13     TIME=  4.992E-02     Y(J)=  7.948E+00     CONCN=  6.080E-04     FUNC=  9.857E-01
 POINT NO. 14     TIME=  5.408E-02     Y(J)=  7.698E+00     CONCN=  6.311E-04     FUNC=  1.069E+00
 POINT NO. 15     TIME=  5.824E-02     Y(J)=  7.508E+00     CONCN=  6.492E-04     FUNC=  1.141E+00
 POINT NO. 16     TIME=  6.240E-02     Y(J)=  7.298E+00     CONCN=  6.690E-04     FUNC=  1.232E+00
 POINT NO. 17     TIME=  6.656E-02     Y(J)=  7.108E+00     CONCN=  6.889E-04     FUNC=  1.328E+00
 POINT NO. 18     TIME=  7.072E-02     Y(J)=  7.008E+00     CONCN=  6.991E-04     FUNC=  1.385E+00
 POINT NO. 19     TIME=  7.488E-02     Y(J)=  6.908E+00     CONCN=  7.095E-04     FUNC=  1.448E+00
 LSTSQU GIVES   SLOPE  1.96392E+01  S.E.SLOPE   6.65E-02  INTERCEPT  6.9131E-03  S.E.INTERCEPT   2.75E-03  S.E.ORDINATE   6.09E-03
 EKHY= 1.868E-03. EKDI= 1.494E-03. EKAC= 3.446E-05. EQCON= 8.948E-01. YEQ= 5.908E+00/)
 EKHY= 1.868E-03. EKDI= 1.494E-03. EKAC= 3.446E-05. EQCON= 8.948E-01. YEQ= 5.988E+00/)
 EKHY= 1.868E-03. EKDI= 1.494E-03. EKAC= 3.446E-05. EQCON= 8.948E-01. YEQ= 5.988E+00/)
 EKHY= 1.868E-03. EKDI= 1.494E-03. EKAC= 3.446E-05. EQCON= 8.948E-01. YEQ= 5.988E+00/)
 EKHY= 1.868E-03. EKDI= 1.494E-03. EKAC= 3.446E-05. EQCON= 8.948E-01. YEQ= 6.068E+00/)
 EKHY= 1.868E-03. EKDI= 1.494E-03. EKAC= 3.446E-05. EQCON= 8.948E-01. YEQ= 6.068E+00/)
 EKHY= 1.868E-03. EKDI= 1.494E-03. EKAC= 3.446E-05. EQCON= 8.948E-01. YEQ= 5.988E+00/)
 EKHY= 1.868E-03. EKDI= 1.494E-03. EKAC= 3.446E-05. EQCON= 8.948E-01. YEQ= 6.068E+00/)


 KOBS( 1)= 5.099E+05 KOBS( 2)= 4.927E+05 KOBS( 3)= 4.890E+05 KOBS( 4)= 4.933E+05 KOBS( 5)= 4.992E+05 KOBS( 6)= 5.105E+05
 KOBS( 7)= 5.308E+05 KOBS( 8)= 5.134E+05 KOBS( 9)= 5.139E+05


 FOR RUN   54 CONCAO=  1.030E-02.CONCB=  4.640E-03.CONCDO=  3.530E-02.TEMP=  25.00
              MEAN RATE CONSTANT=  5.057E+05.P.F. RATE=   .6
```

FIGURE 4.4 . OUTPUT FROM PROGRAM RATE13 FOR RUN 54

9 TRACES , 19 POINTS PER TRACE.

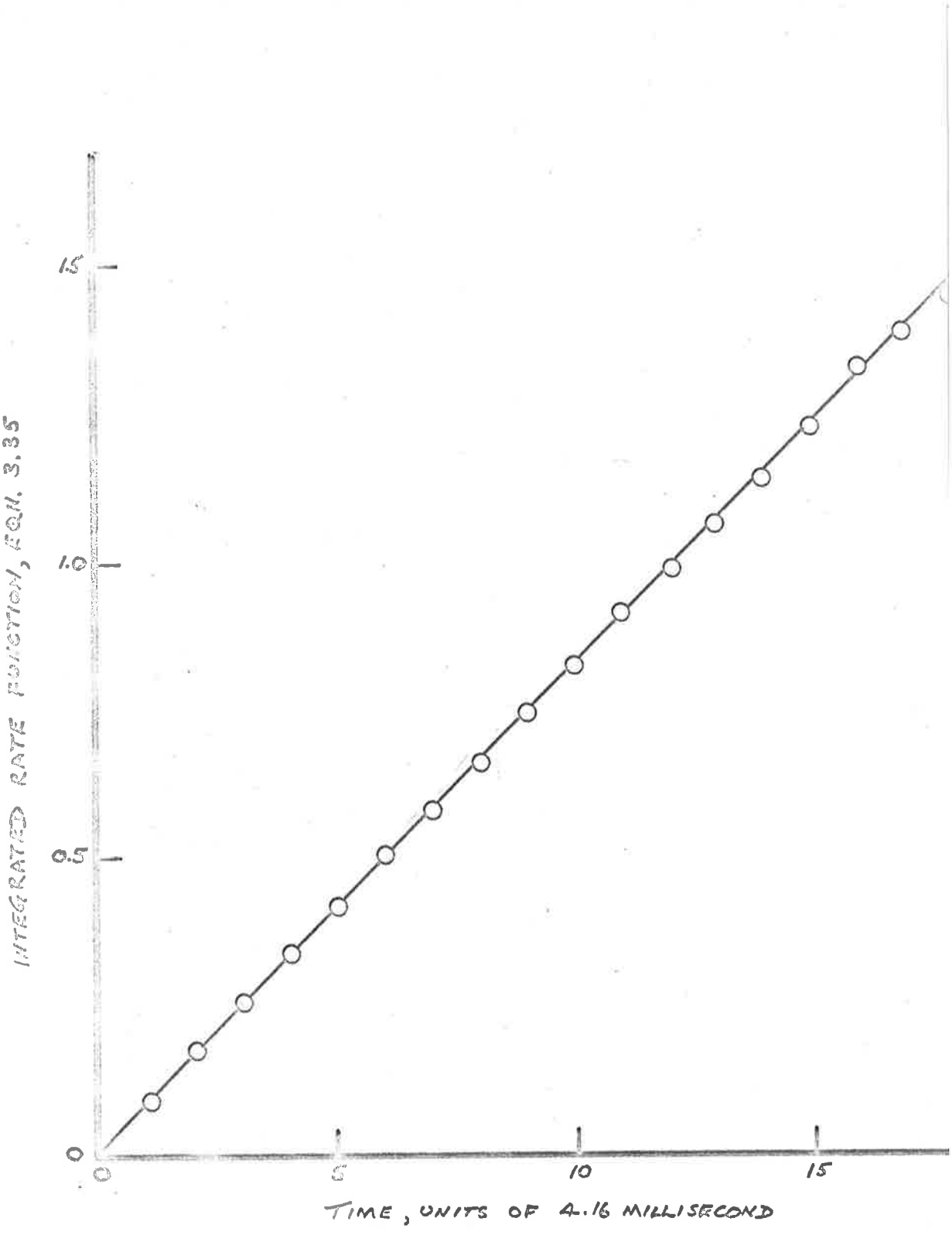

FIGURE 4.5 . RATE PLOT FOR RUN 54 ; OUTPUT FROM PROGRAM RATE 13.

CHAPTER V

RESULTS AND DISCUSSION

(a) Kinetics of ferric azide formation in water.

The value of the observed rate constant for runs in water at ionic strength 0.5M are given in TABLE 5.1. For a given temperature, the dependence on acid concentration (e.g. FIGURE 5.1) seems to verify that contributions do arise from the paths proposed in the derivation of k_{OBS} (EQUATIONS 3.12 to 3.17) from an acid independent term, a term proportional to (H^+) and a term inversely proportional to (H^+). Let us define the paths as before as

$$Fe^{+3} + N_3^- \underset{k_{-1}}{\overset{k_1}{\rightleftharpoons}} FeN_3^{+2} \qquad 5.1$$

$$FeOH^{+2} + N_3^- \underset{k_{-2}}{\overset{k_2}{\rightleftharpoons}} FeN_3^{+2} + OH^- \qquad 5.2$$

$$Fe^{+3} + HN_3 \underset{k_{-3}}{\overset{k_3}{\rightleftharpoons}} FeN_3^{+2} + H^+ \qquad 5.3$$

$$FeOH^{+2} + HN_3 \underset{k_{-4}}{\overset{k_4}{\rightleftharpoons}} FeN_3^{+2} + H_2O \qquad 5.4$$

The results from the acid and temperature dependences of k_{OBS} were analysed using program HTDP13 and its associated subroutines, given in full in APPENDIX 1.3; the procedure for the analysis of these dependences will now be described:

TABLE 5.1

SUMMARY OF OUTPUT FROM PROGRAM RATE 13

Mean values of observed rate constant in H_2O

(Concentrations in moles/litre)

Run	Fe^{+3}_{Tot}	As_{Tot}	H^+_{Free}	Temp.	Mean k_{OBS}	P.E. k_{OBS}
1	0.01010	0.00900	0.1079	25.00	4.939×10^5	0.5
2				31.30	9.464×10^5	0.6
3				39.10	1.999×10^6	1.2
4				21.20	3.347×10^5	0.8
5				28.10	7.050×10^5	0.4
6				35.30	1.436×10^6	3.1
7				10.10	9.289×10^4	1.9
8				15.70	1.891×10^5	3.0
9		0.00450	0.1124	25.00	5.137×10^5	0.3
10				30.00	8.348×10^5	0.6
11				35.30	1.435×10^6	0.8
12				39.10	2.094×10^6	1.4
13				10.10	9.448×10^4	0.9
14				15.70	1.612×10^5	1.7
15				21.20	3.315×10^5	1.2
16			0.0611	10.10	9.194×10^4	0.3
17				15.70	1.718×10^5	0.3
18				21.20	3.217×10^5	2.5
19				25.00	4.860×10^5	0.5
20				30.00	7.928×10^5	0.4
21				35.30	1.348×10^6	1.5
22				39.10	1.917×10^6	1.0

(contd.)

TABLE 5.1 (contd.)

Run	Fe^{+3}_{Tot}	As_{Tot}	H^{+}_{Free}	Temp.	Mean k_{OBS}	% P.E. k_{OBS}
37	0.01030	0.00464	0.1630	10.10	1.003×10^5	0.6
38				15.70	1.817×10^5	0.4
39				21.20	3.306×10^5	0.4
40				25.00	4.944×10^5	0.9
41				30.00	8.065×10^5	1.0
42				35.30	1.418×10^6	0.5
43				39.10	1.897×10^6	2.2
44			0.0864	10.10	9.501×10^4	0.2
45				15.70	1.754×10^5	0.3
46				21.20	3.256×10^5	0.3
47				25.00	5.025×10^5	0.9
48				30.00	8.232×10^5	0.4
49				35.30	1.350×10^6	0.6
50				39.10	1.922×10^6	0.7
51			0.0353	10.10	9.792×10^4	0.3
52				15.70	1.816×10^5	0.6
53				21.20	3.366×10^5	0.4
54				25.00	5.057×10^5	0.6
55				30.00	8.277×10^5	0.4
56				35.30	1.362×10^6	0.8
57				39.10	1.977×10^6	1.4
58	0.01030	0.00464	0.0099	10.10	1.416×10^5	0.9
59				15.70	2.596×10^5	0.6
60				21.20	4.651×10^5	0.5
61				25.00	6.839×10^5	0.9
62				30.00	1.066×10^6	1.7

(contd.)

TABLE 5.1 (contd.)

Run	Fe^{+3}_{Tot}	As_{Tot}	H^{+}_{Free}	Temp.	Mean k_{OBS}	% P.E. k_{OBS}
63	0.01020	0.00463	0.0203	10.10	1.006×10^{5}	0.6
64				15.60	1.864×10^{5}	0.3
65				21.20	3.370×10^{5}	1.6
66				25.00	4.982×10^{5}	0.5
67				30.00	7.924×10^{5}	0.6
68				35.30	1.153×10^{6}	0.9
69				39.10	1.738×10^{6}	2.6
70			0.0171	10.10	1.053×10^{5}	0.7
71				15.70	1.919×10^{5}	0.6
72				21.20	3.401×10^{5}	0.5
73				25.00	5.103×10^{5}	0.6
74				30.00	8.211×10^{5}	2.1
75				35.30	1.331×10^{6}	0.9
76				39.10	1.933×10^{6}	1.3
77			0.0129	10.10	1.186×10^{5}	1.6
78				15.70	2.118×10^{5}	0.3
79				21.20	3.670×10^{5}	1.0
80				25.00	5.649×10^{5}	1.7
81				30.00	8.524×10^{5}	0.8
82				35.30	1.528×10^{6}	1.7
83			0.4212	10.10	1.139×10^{5}	2.4
84				15.70	2.074×10^{5}	1.5
85				21.20	3.693×10^{5}	2.1
86				25.00	5.465×10^{5}	0.8
87				30.00	9.452×10^{5}	2.8
88				35.30	1.677×10^{6}	0.7
89				39.10	2.561×10^{6}	2.1

(contd.)

TABLE 5.1 (contd.)

Run	Fe^{+3}_{Tot}	As_{Tot}	H^{+}_{Free}	Temp.	Mean k_{OBS}	% S.E. k_{OBS}
90			0.1322	10.10	9.845×10^{4}	0.8
91				15.70	1.861×10^{5}	0.9
92				21.20	3.405×10^{5}	0.9
93				25.00	5.195×10^{5}	0.7
94				30.00	8.513×10^{5}	1.0
95				35.30	1.408×10^{6}	0.8
96				39.10	1.932×10^{6}	3.0
136	0.00976	0.00464	0.3870	10.10	1.076×10^{5}	0.5
137				15.70	1.935×10^{5}	0.5
138				21.20	3.575×10^{5}	0.8
139				25.00	4.927×10^{5}	1.2
140				30.00	7.633×10^{5}	1.6
141				35.30	9.387×10^{5}	0.9
142				39.10	1.849×10^{6}	4.9
143	0.00976	0.00464	0.0207	10.10	9.448×10^{4}	0.4
144				15.70	1.740×10^{5}	0.5
145				21.20	3.275×10^{5}	0.2
146				25.00	4.787×10^{5}	0.3
147				30.00	8.198×10^{5}	0.3
148				35.30	1.428×10^{6}	0.3
149	0.00995	0.00498	0.2431	10.20	9.969×10^{4}	0.2
150				15.80	1.874×10^{5}	0.5
151				21.20	3.449×10^{5}	1.1
152				25.00	5.058×10^{5}	0.6
153				30.00	8.413×10^{5}	0.9
154				35.30	1.439×10^{6}	1.4

(contd.)

TABLE 5.1 (contd.)

Run	Fe^{+3}_{Tot}	As_{Tot}	H^{+}_{free}	Temp.	Mean k_{OBS}	P.E. k_{OBS}
155			0.3391	10.30	1.045×10^5	0.7
156				15.80	2.047×10^5	1.1
157				21.20	3.599×10^5	0.3
158				25.00	5.296×10^5	0.5
159				30.00	8.727×10^5	1.7
160				35.30	1.351×10^6	1.7
161		0.00485	0.0092	25.00	5.622×10^5	1.1
162			0.0045	25.00	6.760×10^5	1.1
163		0.00098	0.0084	25.00	5.781×10^5	0.4
164			0.0151	25.00	5.376×10^5	0.8

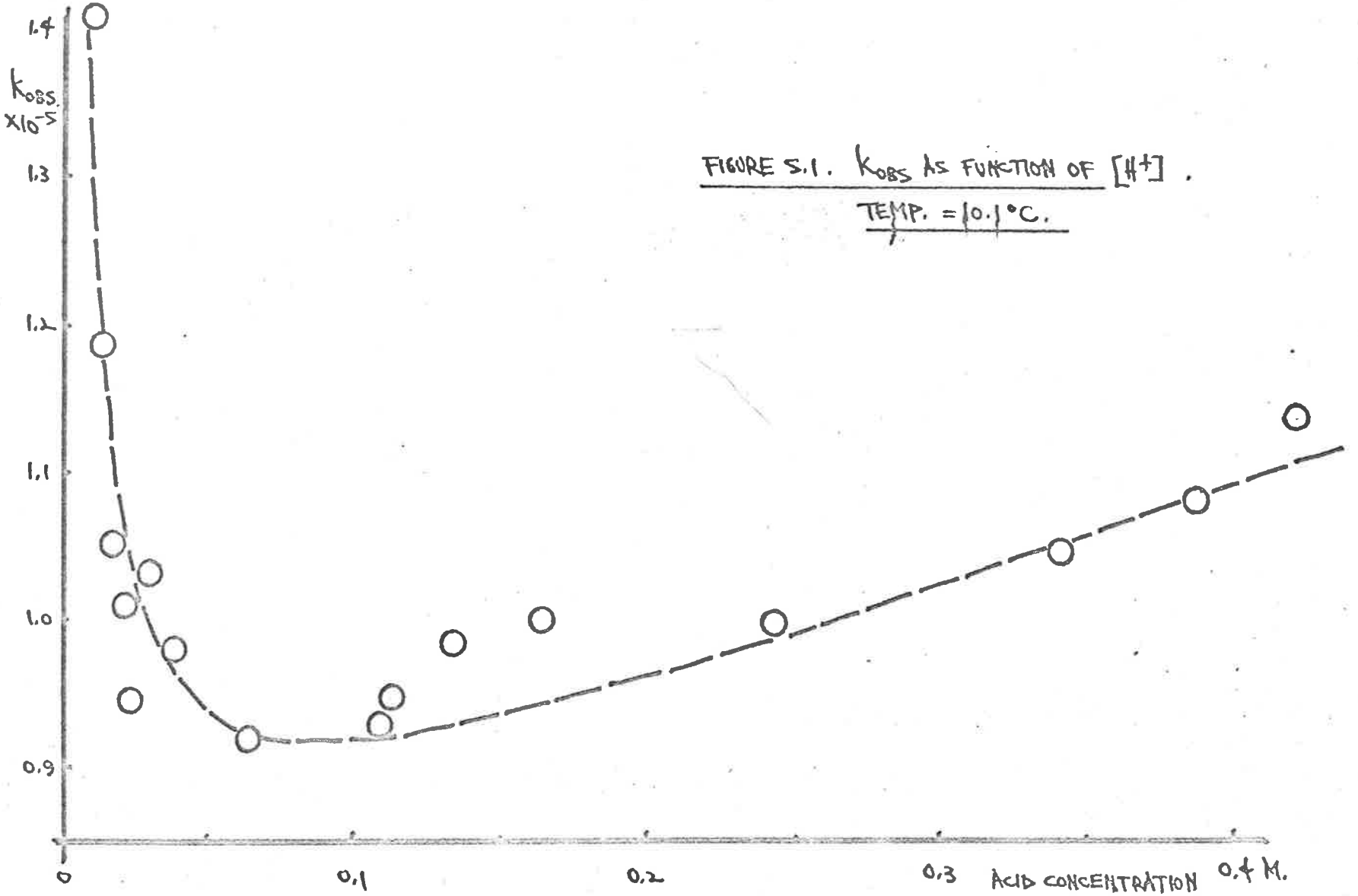

FIGURE 5.1. k_{OBS} AS FUNCTION OF $[H^+]$.

TEMP. = 10.1 °C.

(i) Temperature correction.

It was not always possible to perform runs over the whole temperature range at a given acid concentration and, to make full use of the data, it was considered desirable to be able to extrapolate the data to these temperatures. Inspection of the temperature dependence of k_{OBS} suggested that the observed activation energy was constant over the temperature range of interest. Using the activation parameters for the various acid dependent paths, determined by analysis of the data without using such an extrapolation, k_{OBS} at various temperatures was calculated; it was found that plots of $\log(k_{OBS})$ against reciprocal absolute temperature were indeed linear, with a standard error of 0.05% over the complete acid range. Values of the activation parameters for the individual paths were varied without affecting the linearity of the computed function. The extrapolation was therefore considered a valid one.

Because temperatures of the reactant solutions were not directly measured immediately prior to a kinetic run, but were assumed from the bath temperature after a sufficiently long thermostatting period determined from the experiments described earlier (Chapter IV), the method was used to extrapolate the data and to correct data at temperatures at which runs were performed, in an attempt to eliminate small thermostatting errors. Using this method, 17 points of the 109 sets of experiments performed were discarded from further calculation because they were considered to unduly weight the extrapolation; an example is shown in FIGURE 5.2, where run F68 was eliminated; including

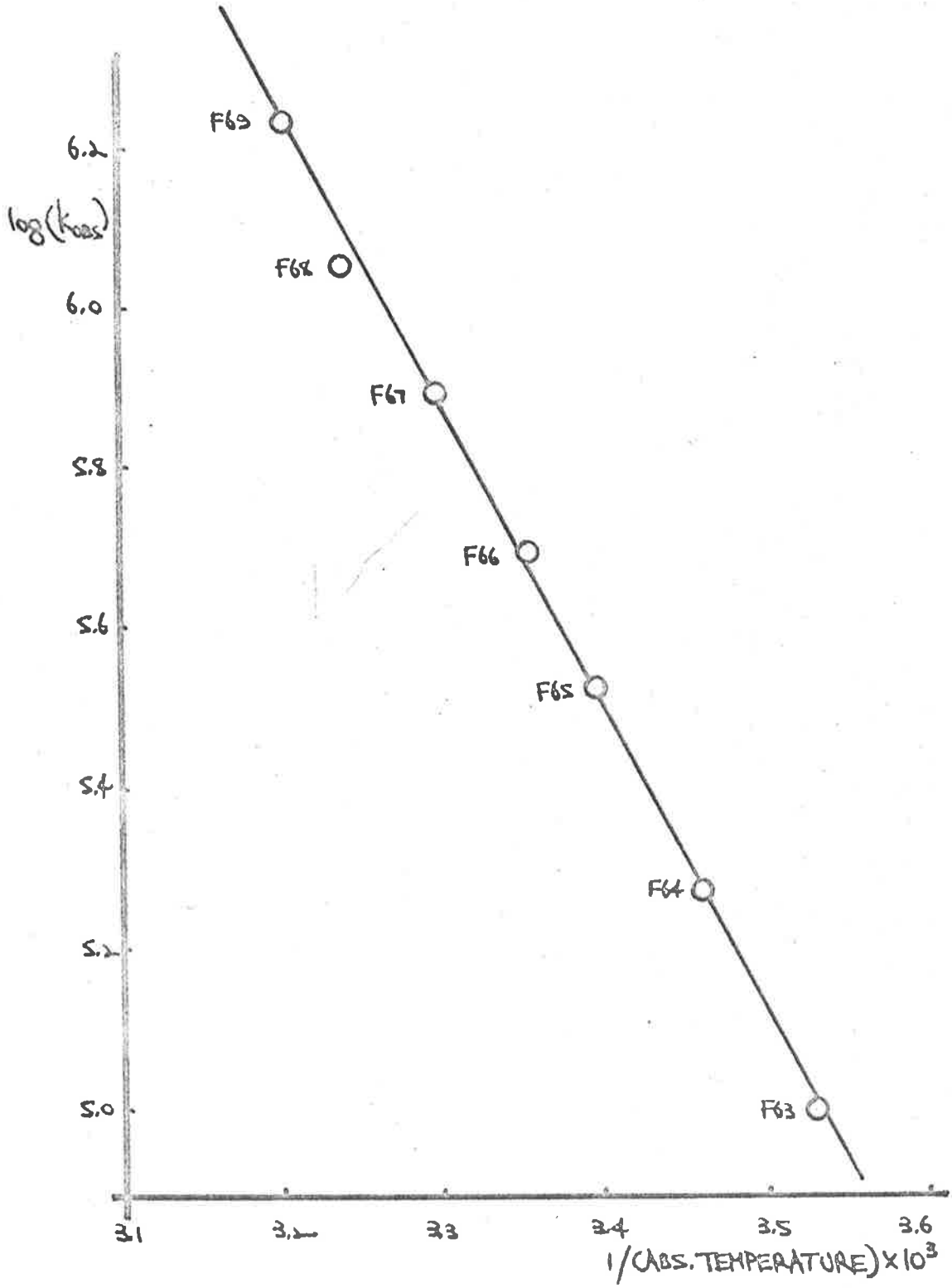

FIGURE 5.2. TEMPERATURE DEPENDENCE OF K_{OBS}.

F68 increased the standard error in the ordinate of the dependence by 50%. Of the 17 points discarded in this way, 41% were at 39°, 24% at 35° and 18% at 30°, indicating that thermostatting at higher temperatures was not very efficient or reliable.

Using this data for the runs in water at ionic strength 0.5M, k_{OBS} was recalculated for each acid concentration at temperatures between 10° and 40° at 5° intervals. The data used by HTDP13 included the total ferric concentration, the total azide concentration and the acid concentration free from hydrolytic effects. Using subroutine CONCS the total free hydrogen ion concentration was calculated for each run at the same temperature intervals.

Taking the points for a given temperature, the values of k_1 (or k_4, both of which are acid independent and therefore indistinguishable), k_3 and k_2 were determined.

In general, for acid above 0.05M, the effect of k_2 appears from the data (e.g. FIGURE 5.1) to be having little effect; the least squares slope and intercept for points in this region were used as a first approximation to calculate k_3 and $k_{1/4}$. From the calculated contributions of these paths at lower acid concentrations, the effect due to path 2 was computed and the least squares slope of this contribution against reciprocal acid concentration used to calculate k_2. This first approximation to k_2 was used to correct k_{OBS} over the whole acid range so that a corrected value of k_3 and $k_{1/4}$ could be calculated; using this, a new value of k_2 was obtained. Five such iterations were performed and k_3, the path most sensitive to these approximations,

changed typically by 14%, 4%, 2%, and 1% after each iteration. Performing this analysis at each temperature, the activation parameters for each path were calculated. The results for calculation run R13/H13/3 are given in TABLE 5.2. The results for paths 1 and 4 are

TABLE 5.2

FERRIC/AZIDE FORMATION KINETIC IN WATER

CALCULATION RUN R13/H13/3

Path	k_{25} (litre/mole/sec.)	Activation energy (kcals/mole)	Activation entropy (e.u.)
1	$4.3 \times 10^5 \pm 2.5\%$	18.35 ± 0.001	28.78 ± 0.003
2	$1.0 \times 10^6 \pm 15\%$	2.49 ± 0.31	-22.8 ± 1.0
3	$9.6 \pm 20\%$	17.9 ± 0.1	6.0 ± 0.5
4	$8.0 \times 10^3 \pm 2.5\%$	11.65 ± 0.001	-1.62 ± 0.003

calculated assuming the acid independent path is completely path 1 or 4. Errors quoted are the standard errors in the least squares slopes or intercepts used to calculate the quantity referred to. Allowing for errors in reactant concentrations, injection ratios, trace measurement, etc., the maximum expected error in k_{OBS} is around 3½%; compared with a typical standard error in the mean of a number of determinations of 1½%, and the standard error in the value of k_4, which generally makes up 80 - 90% of k_{OBS}, of 2½%, it seems reasonable to assume that k_{OBS}

is subject to an uncertainty of 3%.

The first point of interest is the appearance of reaction path 2 corresponding to the reaction of $FeOH^{+2}/N_3^-$, first suggested as a possibility by Sutin (63S). While the present work was in progress, however, Cavasino (67A) and Espenson (67C) both published results on the kinetics of ferric/azide interactions.

The results of Cavasino et al. are confined to (H^+) from 0.01M to 0.05M, and in this range, the observed rate constant was found to be independent of acid concentration; based on the assumption that the function is at minimum in this range, with the effects of k_3 and k_2 compensating to within his experimental error (8%), Cavasino used the earlier value of 4/litre/mole/sec for k_3 (63S), measured at ionic strength 1.0M, and calculated that k_2 under his conditions (ionic strength 0.1M) was in the range 3×10^3 to 4×10^5 litre/mole/sec. Using our value for k_3, Cavasino's data suggest an upper limit of 9.6×10^5 litre/mole/sec for k_2, in agreement with our value of $(1.0 \pm 0.15) \times 10^6$ litre/mole/sec.

Carlyle and Espenson's results extended over a wide acid concentration range, the lowest being at 0.005M, with no curvature at low acid that would suggest a contribution from our path 2. As has been pointed out in Chapter II, investigations prompted by Carlyle and Espenson's equilibrium measurements of the second azido complex did not suggest any significant concentrations of the diazido complex under our conditions, but it can be shown that the ratio of second to first complex will be given by:

$$\frac{(Fe(N_3)_2)}{(FeN_3)} = \frac{K_{eq2}}{K_{eq}} \cdot \frac{(HN_3)}{(H^+)} \qquad 5.5$$

$$K_{eq} = (FeN_3^{+2})(H^+)/(Fe^{+3})(HN_3) \qquad 5.6$$

$$K_{eq2} = (Fe(N_3)_2^+)(H^+)^2/(Fe^{+3})(HN_3)^2 \qquad 5.7$$

So that any effect on the observed rate due to simultaneous second complex formation might well be expected to interfere in a way which resembled an inverse acid contribution.

New runs F1 to F160 were carried out with total ferric and total azide concentrations constant at 0.01M and 0.005M respectively; runs were therefore performed at 25°C in which the total azide concentration was reduced to 0.001M, and the results of runs F161 to F164 are given in TABLE 5.3. Although the proportion of second complex should have fallen for the low azide runs to 20% of that in the runs at higher azide, the calculated values of the contribution from path 2 fit quite well the points from calculation R13/H13/3 (where they were not included); FIGURE 5.3 shows this contribution as a function of $1/(H^+)$, and it appears that any effect of second complex is probably not important.

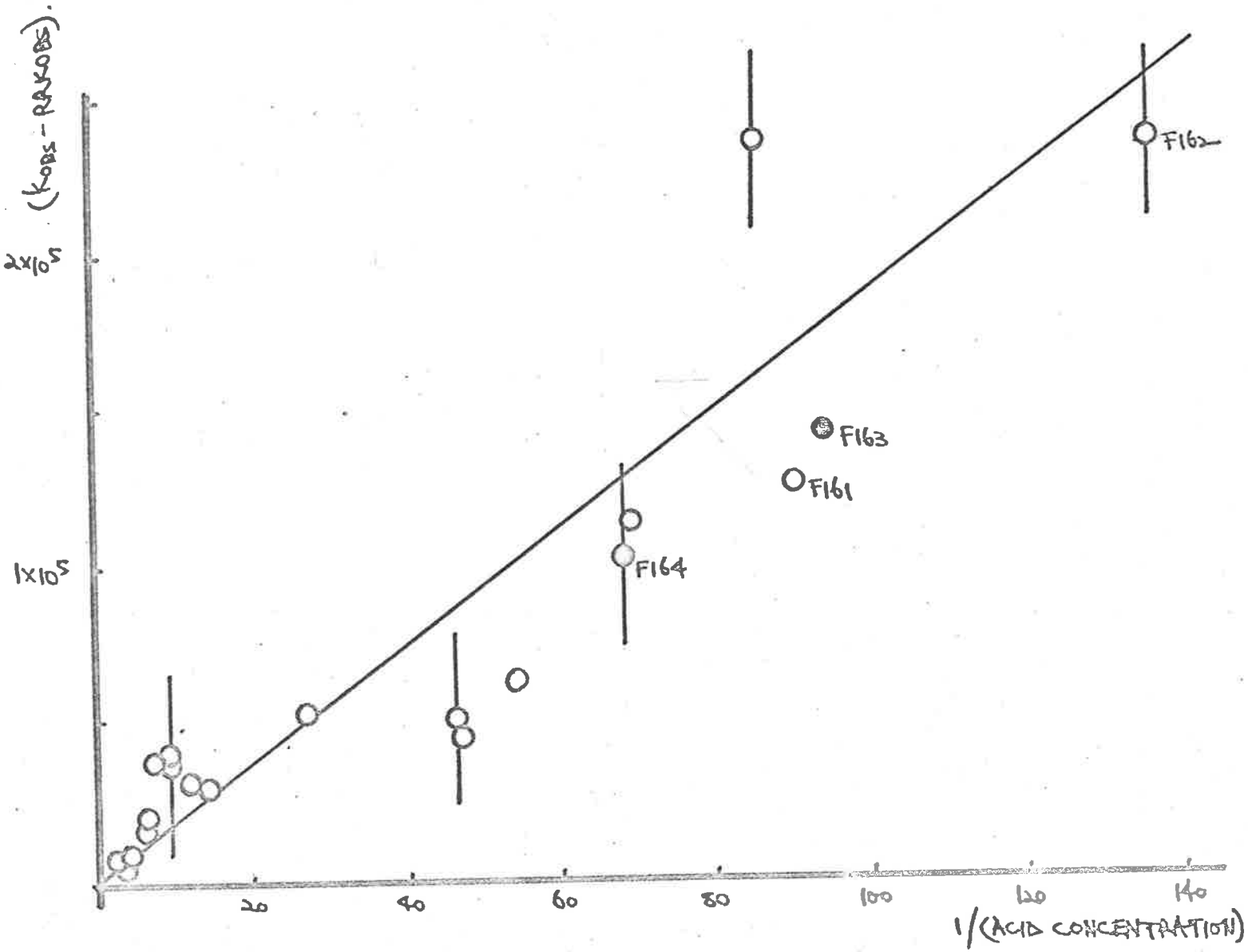

FIGURE 5.3. CONTRIBUTION TO k_{OBS} BY PATH 2 VS 1/(H).

TABLE 5.3

FERRIC/AZIDE FORMATION KINETICS

AZIDE DEPENDENCE AT LOW (H^+) and 25°C

Run	k_{OBS} (l./m./s.)	(HN_3) (mole/litre)	(H^+) (mole/litre)	$1/(H^+)$	$(k_{OBS}$ - ARKOBS)
F161	5.62×10^5	0.00485	0.0111	90	1.26×10^5
F162	6.76×10^5	0.00485	0.0074	136	2.42×10^5
F163	5.78×10^5	0.00098	0.0106	94	1.43×10^5
F164	5.38×10^5	0.00098	0.0147	68	1.02×10^5

(ARKOBS is the calculated contribution of paths 3 and 1/4 to the observed rate constant).

The possibility that the method used to determine k_{OBS} in RATE13, in particular the extrapolation to correct for any reaction between mixing and first observation was responsible for the apparent inverse acid path (k_2), was investigated. In program RATE10, from the calculated equilibrium concentration of ferric azide, knowing the path length of the observation cell, the extinction coefficient of FeN_3^{2+} at 460 mμ, and the light transmission at equilibrium (proportional to the 'infinite time' balancing potential), the signal corresponding to the incident light intensity (I_o) could be calculated. Knowing the transmission at a particular time during reaction, the optical density and therefore the concentration of the product was then calculated. The calculation of the integrated rate expression and subsequent operations were identical to those in RATE13.

Because the concentration of product at first observation was not zero in these cases, the apparent 'dead time' between mixing and first observation could be calculated from the extrapolated X - intercept of the integrated rate expression vs time plot. An example of the predicted zero time displacement is shown in FIGURE 5.4; although the calculated 'dead time' is longer than would be expected, the extrapolation is not unreasonable. The results returned from RATE10 and RATE13 over the complete acid range agree closely, and typical examples at 25° are given in TABLE 5.4.

TABLE 5.4

COMPARISON OF TREATMENT OF DATA USING COMPUTER PROGRAM RATE10 AND RATE13

Run	(H^+) (mok/litre)	k_{OBS} from RATE13/1	k_{OBS} from RATE10/2
F68	0.421	5.46×10^5 l/m/s.	5.46×10^5 l/m/s.
F9	0.113	5.14×10^5	5.13×10^5
F61	0.012	6.84×10^5	6.87×10^5

To ensure that the results at low acid were not an artefact produced by the thermodynamic data used, program RATE10 was run with the thermodynamic data from the same sources as were used by Carlyle and Espenson. For the hydrolysis of Fe(III), the data of Milburn (57M) was again used; Espenson had made assumptions identical to ours concerning the immobility of the dimerisation of $FeOH^{+2}$ over the

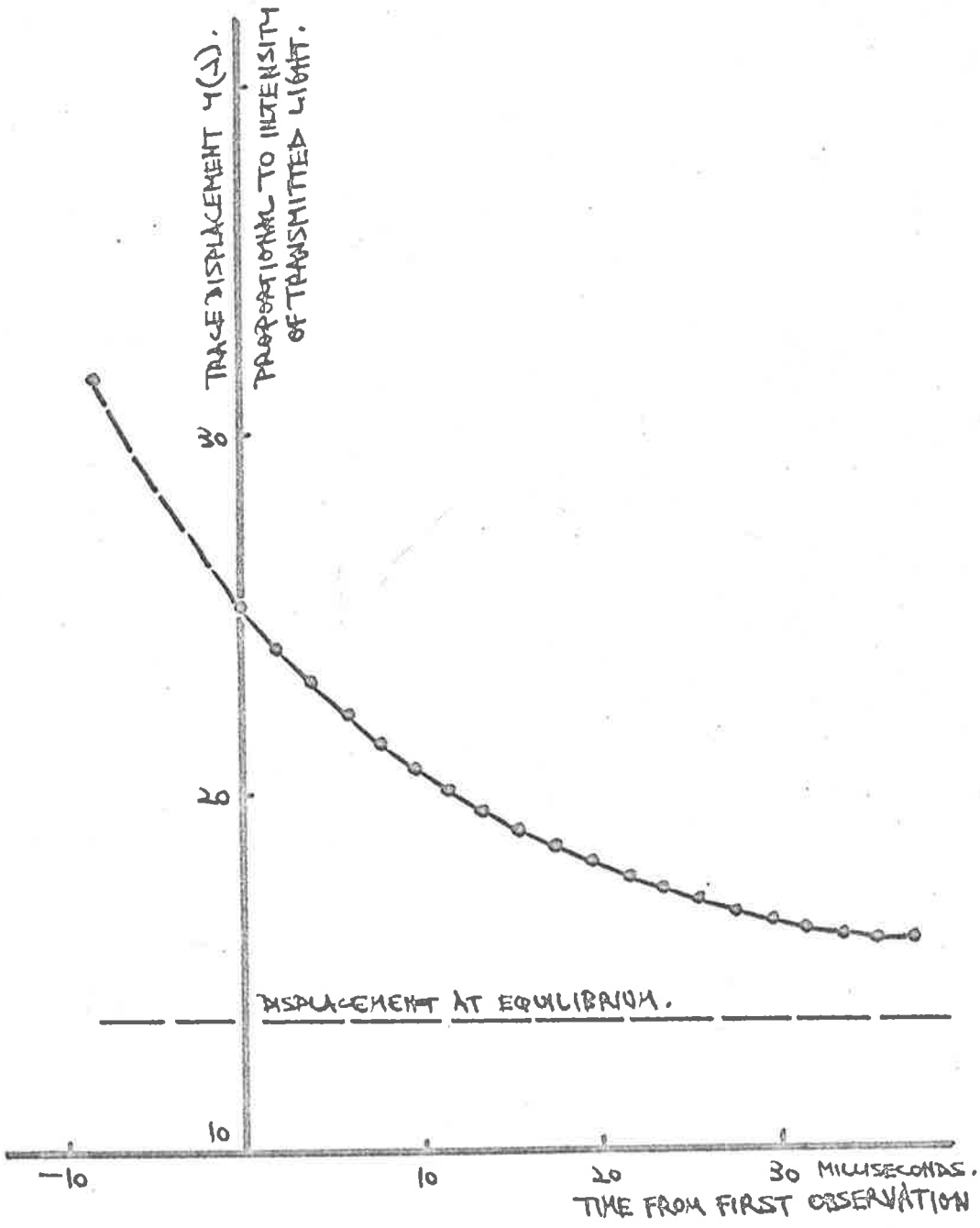

FIGURE 5.4. OUTPUT FROM RATE10. RUN F20/1

period of ferric azide formation. Data of Quintin (40Q) for the dissociation constant and ionic strength dependence of the ionization of hydrazoic acid was used. Rapenson's value of 0.512 for the FeN_3^{+2} equilibrium formation constant was corrected from an ionic strength of 1.0M to 0.5M, to give 0.600, using the dependence of Bunn, Dainton and Duckworth (61B). The thermodynamic data used at 25° are given and compared to those otherwise used in this work in TABLE 5.5.

TABLE 5.5

EQUILIBRIUM CONSTANTS CALCULATED AT 25° AND IONIC STRENGTH 0.5M

	K_{eq}	K_H	K_D	K_A
Normally used (e.g. in calculation R10/2)	0.894	1.87×10^{-3}	1.49×10^{-3}	3.45×10^{-5}
Used in calculation R10/6	0.600	1.87×10^{-3}	1.49×10^{-3}	3.25×10^{-5}

Because the values of K_{eq}/K_A (i.e. the formation constant of FeN_3^{+2} from Fe^{+3} and free N_3^-) differ by a factor of 1.4, and this quantity enters directly into the calculation of the value of the forward rate constant from the slope of the integrated rate expression, a comparison of the aquated rate constants was considered a more valid test of the effect of the thermodynamic data on the analysis of the rate data; a sample of these results is given in TABLE 5.6, and

results for the aquation rate over the whole acid range are shown directly compared with Carlyle and Espenson's data in FIGURE 5.5. The results for aquation are very similar, and could probably be explained by the ionic strength difference between the two sets of data except for acid concentrations below 0.05M; the point measured by Espenson is a logical extension of the trend at higher acids, whereas our results show a smooth deviation from that trend;

TABLE 5.6

EFFECT OF THERMODYNAMIC DATA ON ANALYSIS OF RATE DATA

		R10/2		R10/6	
Run	(H^+) (mole/litre)	k_{OBS} $l.mole^{-1}sec^{-1}$	$k_{AQUATION}$ (sec^{-1})	k_{OBS} $(l.mole^{-1}sec^{-1})$	$k_{AQUATION}$ (sec^{-1})
F86	0.421	5.46×10^5	21.1	2.43×10^5	21.3
F9	0.113	5.13×10^5	19.8	2.33×10^5	20.4
F61	0.012	6.87×10^5	26.5	3.30×10^5	28.9

results of Cavasino and coworkers on the reactions of Fe^{+3}_{aq} with sulphate and chloracetic acid (68C, 69A) have demonstrated that, in these systems, reaction pathways with (H^+) dependances $(H^+)^{-1}$, $(H^+)^0$, $(H^+)^1$ have been observed and measured. We are therefore of the opinion that the contribution attributed to $FeOH^{+2}/N_3^-$ reaction as a possible reaction path is a real phenomenon, and that the parameters given in TABLE 5.2 provide an accurate representation of the

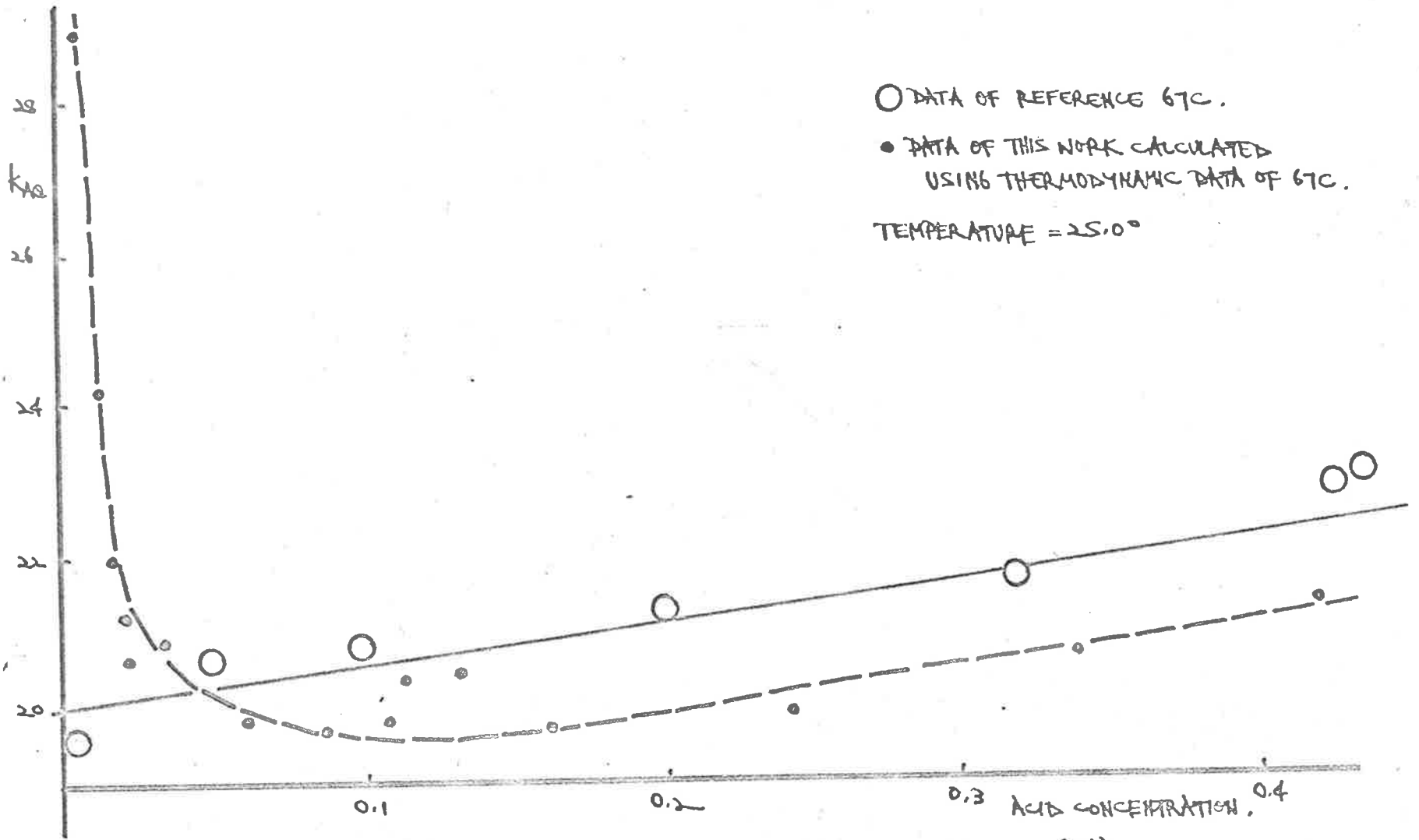

FIGURE 5.5. OBSERVED AQUATION RATE CONSTANT VS (H+).

formation kinetics of the FeN_3^{+2} ion in aqueous solution at ionic strength 0.5M.

(b) Kinetics of ferric azide formation in deuterium oxide.

Measurements were made of the rate of formation of the FeN_3^{+2} complex ion D_2O over a range of temperatures and acid concentrations using the same experimental techniques and methods of analysis of the data as for runs in water. Reagents were prepared as described in Chapter II (Materials (vi)).

Thermodynamic data used in the analysis of the results is given in TABLE 5.7.

TABLE 5.7

EQUILIBRIUM CONSTANT DATA AT IONIC STRENGTH 0.5M AND 25°C

	K	ΔH° (kilocal/mole)	Reference
K_{eq}	0.74	2.45	61B
K_H	1.09×10^{-3}	9.3	64F
K_b	1.49×10^{-3}	12.8	57M
K_A	1.19×10^{-5}		61B
K_A		4.1	This work

Data used to correct for dimerisation of $FeOD^{+2}$ is not available and the value was assumed equal to that for $FeOH^{+2}$ in

TABLE 5.8

SUMMARY OF OUTPUT FROM PROGRAM RATE 13

Mean values of observed rate constant in D_2O

(Concentrations in moles/litre)

Run	Fe^{+3}_{Tot}	As_{Tot}	D^+_{Free}	Temp.	Mean k_{OBS}	% P.E. k_{OBS}
23	0.01030	0.00464	0.1122	10.10	9.026×10^4	0.6
24				21.20	2.856×10^5	0.4
25				15.70	1.671×10^5	0.3
26				25.00	4.416×10^5	0.6
27				30.00	7.333×10^5	0.3
28				35.20	1.261×10^6	0.8
29				39.10	1.830×10^6	1.6
30			0.0590	10.10	8.568×10^4	0.3
31				15.70	1.689×10^5	3.4
32				21.20	2.827×10^5	0.3
33				25.00	4.349×10^5	0.4
34				30.00	7.233×10^5	0.4
35				35.30	1.259×10^6	0.4
36				39.10	1.796×10^6	0.6
108	0.00976		0.1477	10.10	8.864×10^4	0.2
109				15.70	1.661×10^5	0.1
110				21.20	2.937×10^5	0.5
111				25.00	4.524×10^5	0.4
112				30.00	7.587×10^5	0.4
113				35.30	1.223×10^6	0.3
114				39.10	1.885×10^6	3.1
115			0.0527	10.10	8.591×10^4	0.5
116				15.70	1.639×10^5	1.0
117				19.30	2.379×10^5	0.2
118				25.00	4.475×10^5	0.2

(contd.)

TABLE 5.8 (contd.)

Run	Fe^{+3}_{Tot}	As_{Tot}	D^{+}_{Free}	Temp.	Mean k_{OBS}	% P.E. k_{OBS}
119				29.90	7.341×10^{5}	0.2
120				35.20	1.221×10^{6}	0.2
121				39.10	1.806×10^{6}	2.2
122			0.0157	10.10	8.932×10^{4}	0.1
123				15.70	1.669×10^{5}	0.2
124				21.20	3.033×10^{5}	0.4
125				25.00	4.663×10^{5}	0.3
126				30.00	7.763×10^{5}	0.5
127				35.20	1.262×10^{6}	4.5
128				38.90	1.990×10^{6}	6.2
129		0.00460	0.0819	10.10	8.856×10^{4}	0.6
130				15.70	1.680×10^{5}	0.4
131				21.20	2.987×10^{5}	0.2
132				25.00	4.572×10^{5}	0.2
133				30.00	7.470×10^{5}	0.3
134				35.20	1.269×10^{6}	0.3
135				39.10	1.887×10^{6}	0.6

water. For this reason, only one measurement was made at low (D^+) to investigate whether a path corresponding to the $FeOD^{+2}/N_3^-$ reaction could be observed; it is considered that this does occur, and that the rate constant at 25° is about half of that measured for the reaction in water. It was felt, however, that, as the value ascribed to k_2 is based only on this one point, the analysis of which is approximate, it should be used only as a second order correction term for the measurements at higher acid concentrations.

A summary of the output from RATE13 for runs in D_2O is given in TABLE 5.8 and the observed rate constants at 25° shown in FIGURE 5.6, together with the function for the observed rate calculated on the basis of constants for the various acid dependent paths returned from program HTDP13. These rate constants and activation parameters are given in TABLE 5.9.

TABLE 5.9

FERRIC/AZIDE FORMATION KINETICS IN D_2O

CALCULATION RUN R13/H13/6

Path	$k_{25°}$ (litre/mole/sec)	Activation energy (kcals/mole)	Activation entropy (e.u.)
1	$5.4 \times 10^5 \pm$	17.1 ± 0.01	26.5 ± 0.01
2	$5 \times 10^5 \pm$	(16)	(22)
3	2.0 ±	22.3 ± 0.03	17.7 ± 0.1
4	$5.9 \times 10^5 \pm$	12.5 ± 0.01	0.5 ± 0.1

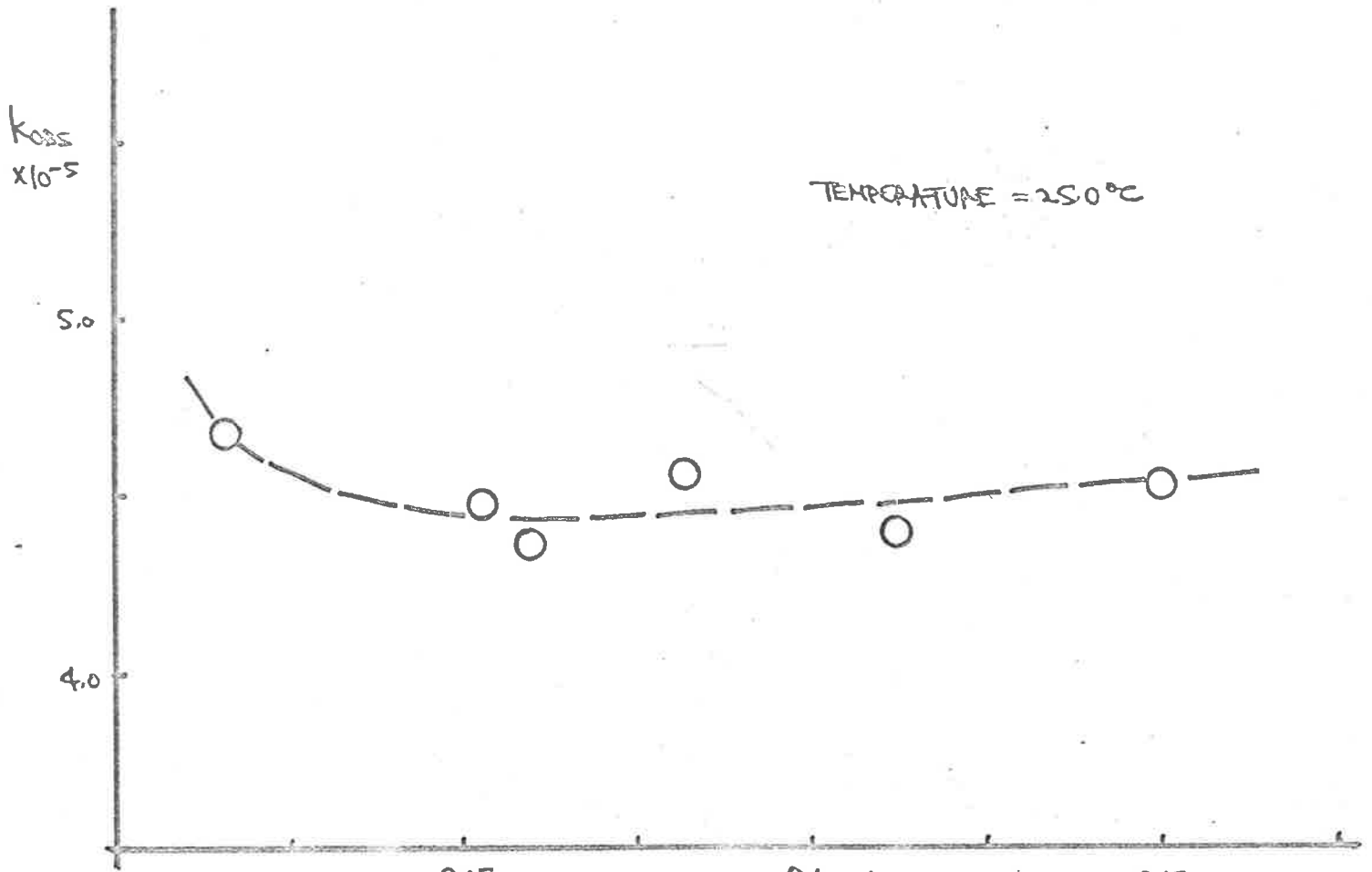

FIGURE 5.6. OBSERVED RATE CONSTANTS IN D_2O.

(e) Assignment of the acid independent rate constant.

As has been pointed out in the introduction to this work, the first question to be decided before any discussion of the mechanisms of complex ion formation between Fe^{+3} and basic ligands can take place, is the assignment of the relative contributions of paths 1 and 4 to the observed acid independent rate constant:

$$Fe^{+3}_{aq} + B^- \underset{}{\overset{k_1}{\rightleftharpoons}} FeB^{+2}_{aq} + H_2O \qquad 5.8$$

$$FeOH^{+2}_{aq} + HB \overset{k_4}{\rightleftharpoons} FeB^{+2}_{aq} + H_2O \qquad 5.9$$

Paths 3 and 2 on the other hand have unique acid dependences and can therefore be assigned unambiguously:

$$Fe^{+3}_{aq} + HB \overset{k_3}{\rightleftharpoons} FeB^{+2}_{aq} + H^+ + H_2O \qquad 5.10$$

$$FeOH^{+2}_{aq} + B^- \overset{k_2}{\rightleftharpoons} Fe(OH)B^{+}_{aq} + H_2O \qquad 5.11$$

presumably followed as suggested by Conniek (58B) and others later (68C) by a fast proton attachment:

$$Fe(OH)B^{+}_{aq} + H^+ \longrightarrow FeB^{+2}_{aq} \qquad 5.12$$

Assignment has usually been made on the assumption that the

system is accurately described by the Eigen-Wilkins mechanism, i.e. that the rate of complex formation is essentially independent of the nature of the incoming group, allowing for an electrostatic pre-association, and those systems in which path 1 (EQUATION 5.8) was predominant should have similar rates which are close to the first order water exchange rate for Fe^{+3}_{aq}, and those systems in which path 4 (EQUATION 5.9) predominated should have rates similar to the solvent exchange rate for $FeOH^{+2}$. Any system which did not fit either of those two criteria should, on the basis of the relative concentrations of Fe^{+3}, $FeOH^{+2}$, B and HB have an observed rate which was a reasonable combination of k_1 and k_4. As has been noted in Chapter I, although the apparent dependence of the rate on the basicity of ligand B is considerably reduced, this approach has not been completely successful in systematically describing ferric systems.

Data for those ligands which are not strongly basic, and can therefore be assigned to path 1 or path 3 with some degree of confidence are given in TABLE 5.10.

TABLE 5.10

KINETIC AND THERMODYNAMIC DATA FOR COMPLEX ION FORMATION BY Fe^{+3}_{aq} AT 25°

Ligand	k_{25} l/m/s	$\log(k_{25})$	K_{25}	$\log(K_{25})$	Reference
HN_3	9.6 ± .2	0.98	0.88	-0.06	This work
HN_3	2.8 ± .8	0.45	0.51	-0.29	67C
HN_3	4.0 ± 1	0.60	0.88	-0.06	63S
CH_3CO_2H	4.8 ± .8	0.68	0.044	-1.36	[a]69A
$ClCH_2CO_2H$	2.2 ± .4	0.34	0.31	-0.51	[a]69A
$C_2H_5CO_2H$	5.7 ± .8	0.76	0.062	-1.21	[a]69A
HF	11.4 ± .1	1.06	184	2.26	60P
Br^-	3.4	0.53	0.37	-0.43	69C
Br^-	20 ± 6	1.30	1.6	.2	[b]61M
Cl^-	9.4 ± 1	0.97	4.1	0.61	59Co
HSO_4^-	40	1.60	8.6	0.95	68C
SCN^-	132 ± 50	2.12	269	2.43	64Ca
SCN^-	127 ± 10	2.10	140	2.16	58B
SCN^-	150 ± 50	2.18	140	2.15	62W
$HC_2O_4^-$	1440 ± 100	3.16	2.2×10^4	4.34	65B
$HC_2O_4^-$	860 ± 40	2.93	1.1×10^4	4.04	66M
$Fe(CN)_6^{-3}$	1750 ± 250	3.24	117	2.07	67S
$Fe(CN)_6^{-3}$	800 ± 80	2.90	36	1.56	68W

a. 20°C. b. 22 ± 2°C.

Uncertainties in rate are those quoted by the original authors or were estimated from the original results where possible; equilibrium data is that quoted for the original experimental conditions.

The data for HSO_4^- and $HC_2O_4^-$ use the equilibrium data for the simple replacement by the ligand of a water molecule in the hydration shell of the metal ion to form $Fe(H_2O)_5SO_4^+$ and $Fe(H_2O)_5C_2O_4^+$, without the possible hydrolysis to $Fe(H_2O)_5HSO_4^{+2}$ and $Fe(H_2O)_5HC_2O_4^{+2}$, or in the case of the oxalate, the formation of the first chelate $Fe(H_2O)_4C_2O_4^+$.

If the ligands of charge -1 are first considered, so that the question of differences in simple ionic preassociation can be temporarily put aside, it can be seen (FIGURE 5.7) that the rates of complex formation are, in fact, significantly dependent on the nature of the entering group, and log(rate constant) and log(equilibrium constant) can reasonably be correlated in a Bronsted Type relationship with a slope of 0.44 ± 0.1. If, for those systems where more than one determination of the rate has been made, only the most recent data is considered, on the grounds that the quoted errors imply that it is generally more accurate, and presumably the workers have given due consideration to the earlier results, a correlation with a slope of $0.48 \pm .1$ (FIGURE 5.8) is obtained.

Such linear free energy relationships have been shown to hold for large numbers of organic reactions following similar reaction mechanisms, and the slope has been taken as a measure of the degree of participation, by the group being varied in the series, in the formation of the transition state (63). More convincing arguments can be based on correlations of the enthalpy and entropy of activation with the corresponding parameters for the equilibrium,

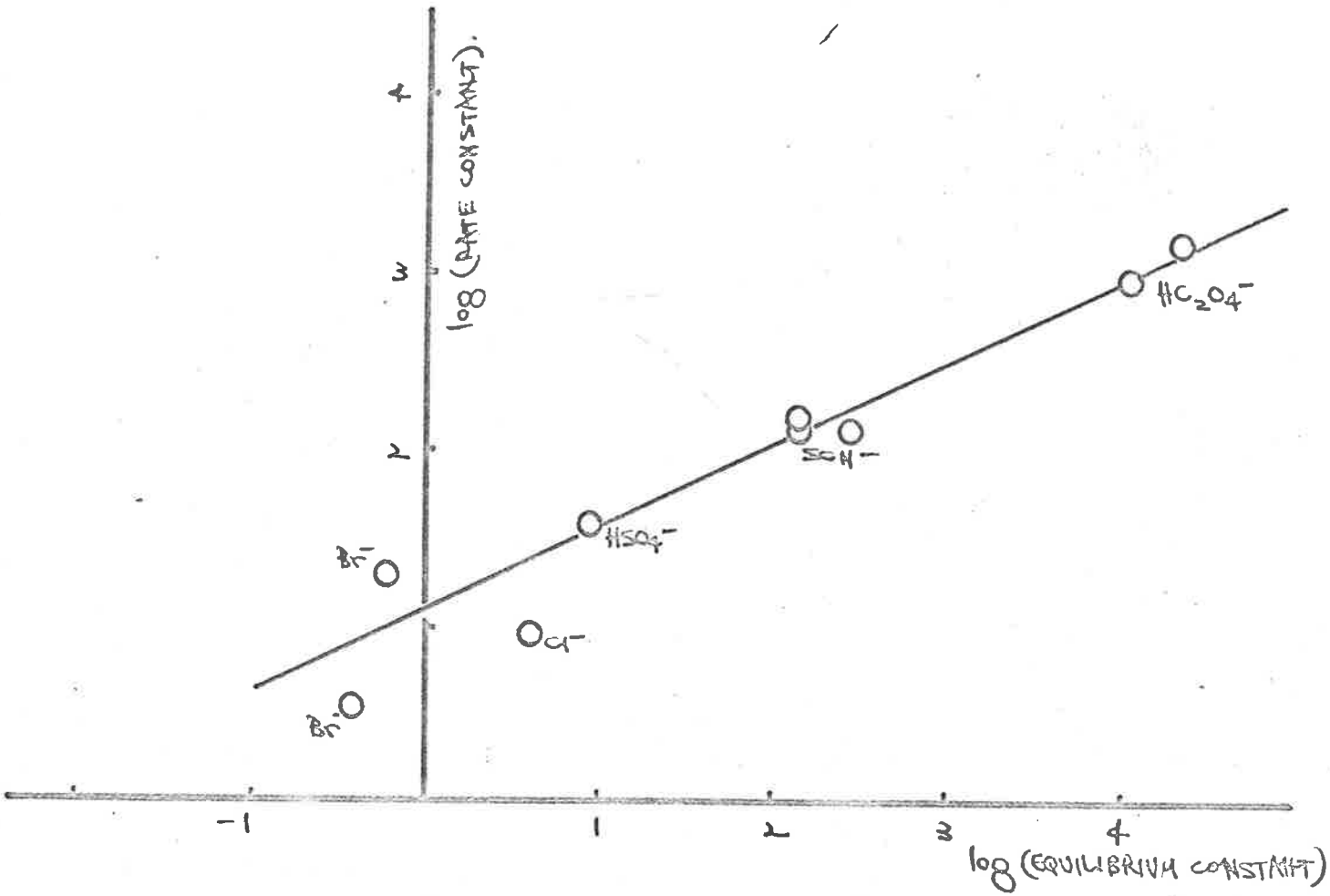

FIGURE 5.7. REACTIONS OF $Fe^{+3} + L^-$ AT 25°

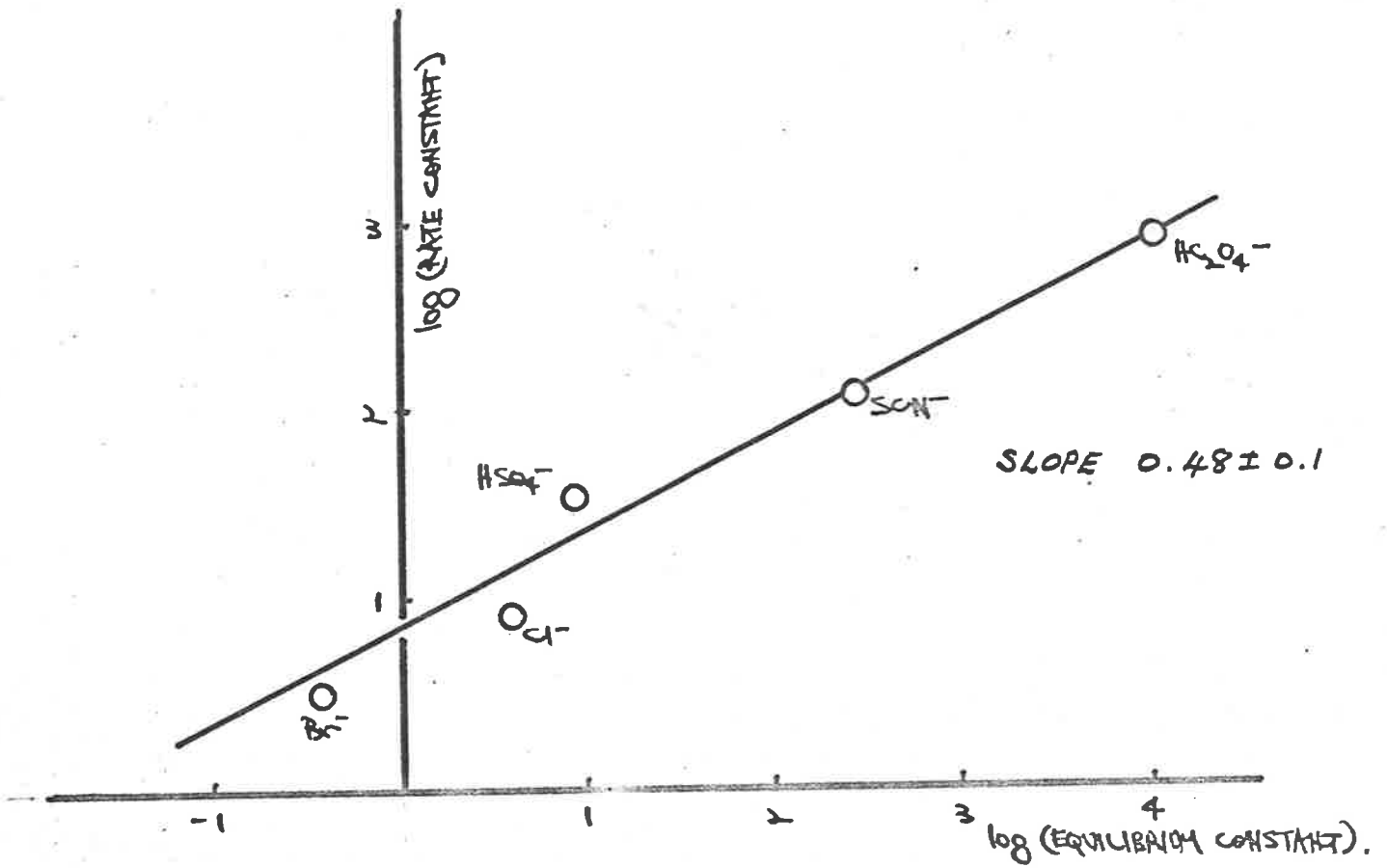

FIGURE 5.8. REACTIONS OF $Fe^{+3} + L^-$. MOST RECENT DATA.

but often sufficient data is not available, as is the case substitution reactions at Fe^{+3}_{aq}, or the activation data is subject to considerable experimental inaccuracy.

Correlation of log(k) and log(K) for the aquation of $Co(NH_3)X^{+2}$, which has a slope of 1.0, has been cited by Langford (65La) as evidence that the environment of the leaving group X closely resembles its environment in the products as the free solvated ion; that is, that the mechanism is strongly dissociative. For the aquation of $Cr(H_2O)_5X^{+2}$, Swaddle and Guastalla (68S) have shown that the function has a slope of 0.56, and conclude that the separation of group X is only partially complete in the transition state; in this system correlation of the entropy of activation and partial molar entropy of the aquated ion, with a slope of 0.53 (67Sw) also supports this view. It is interesting that log k vs log K for the aquation of $Fe(H_2O)_5X^{+2}$ (for the data of TABLE 5.10) has a slope of 0.52, extremely close to the value for the $Cr(H_2O)_5X^{+2}$ series.

It would seem, therefore, that to recognise that the rates of Fe^{+3}_{aq} substitution may be correlated in a way which does not assume that they must have the same value may be a more stable basis on which to examine them. Certainly, to consider that log (k) may be a function of log (K) with a standard error of 0.1 would seem better than to assume it constant independent of log (K) with a standard error of 1.4. Even if the data for $HC_2O_4^-$ as ligand is considered unsuitable because it is a moderately strong base with pK_b = 12.8 to 12.9 under the kinetic conditions, the assumption that log (k) is independent of

log (K) has a standard error of 0.6.

For ligands of charge other than -1, there is not sufficient data for a clear cut decision to be made (FIGURE 5.9). The data for neutral ligands is heavily weighted by the position of HF, but the results certainly appear to show a much less marked dependence on the ligand; the assumption that the rates are independent of ligand has a standard error of 0.2, while the least squares slope of the data without this assumption is 0.12 ± 0.1.

The triply charged ferricyanide has been shown to be involved in a considerable ionic preassociation with Fe^{3+}, K = 35 (67S); assuming that the only difference in the behaviour of $Fe(CN)_6^{-3}$ and the -1 ligands is a difference in the preassociation, and correcting the data of Silber and Swinehart (67S) accordingly, brings the data (open circle in FIGURE 5.9) reasonably into line.

Data for complex formation by reaction with $FeOH^{+2}$ which can be assigned unambiguously to pathway 2 (EQUATION 5.11) is presented in TABLE 5.11 and FIGURE 5.10. Scatter of data is considerable, but by releasing the restriction that the rates should be constant at a value around the water exchange rate (i.e. 3.0 to 6.0 x 10^4 l/m/s (62E, 67J)), and instead assuming that they may be a function of log (K), the least squares slope is 0.40 ± 0.1. All of the data can be reasonably accommodated, including that determined in this work for N_3^-, which, on the assumption that the rates are approximately constant, was well outside the range which could be accounted for by a simple ionic pre-

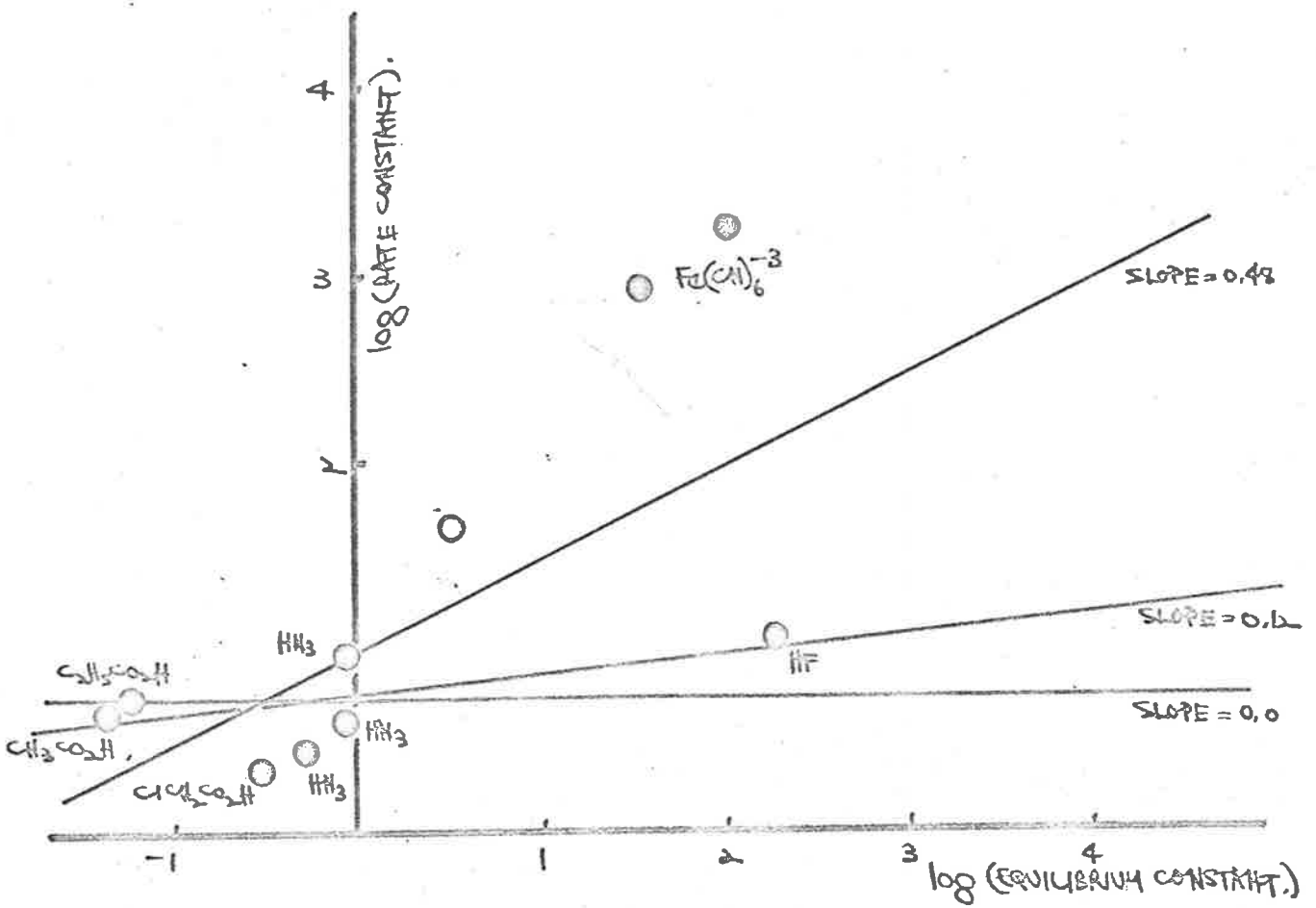

FIGURE 5.9 REACTIONS OF Fe^{+3}.

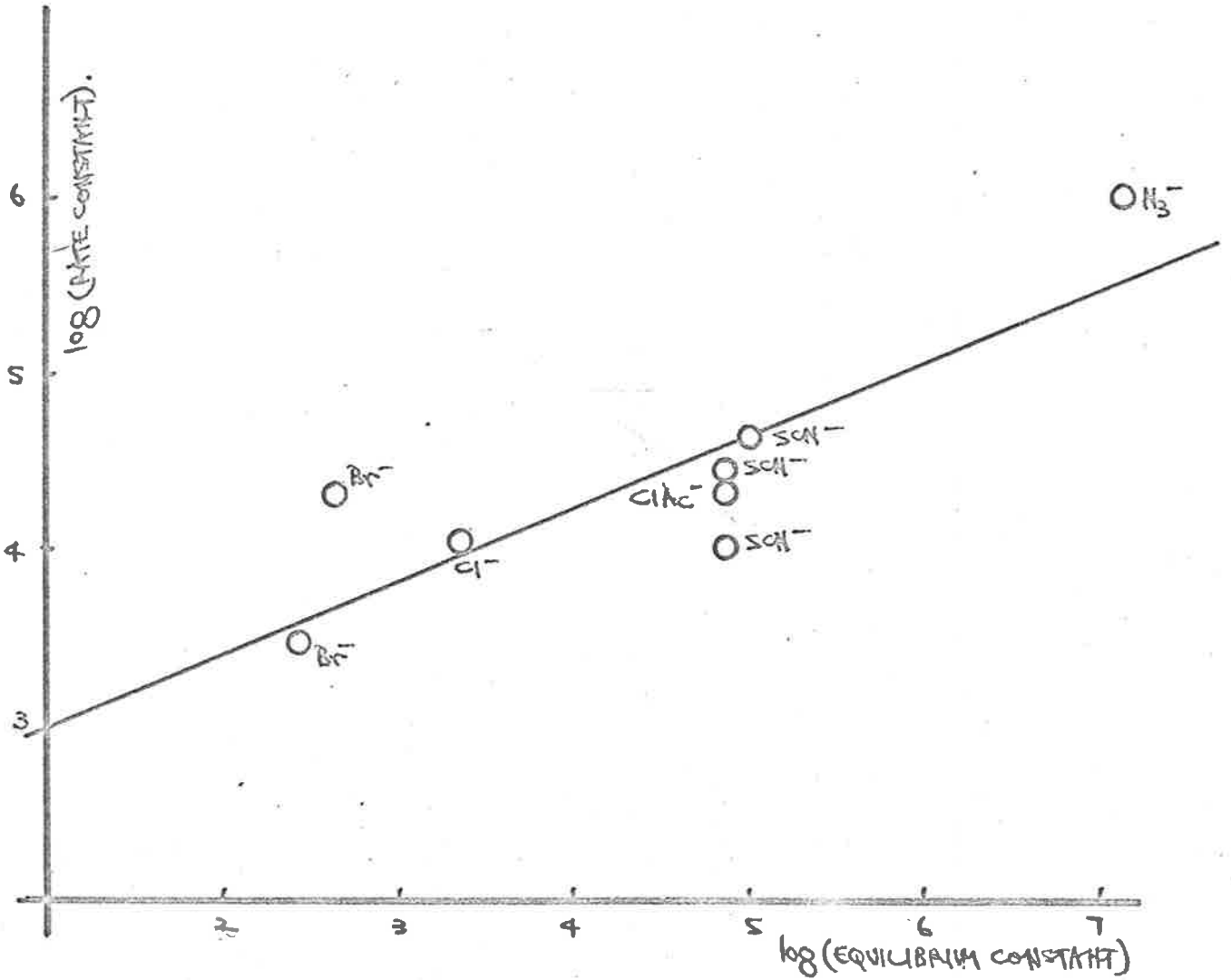

FIGURE 5.10 REACTIONS OF $FeOH^{+2} + L^-$.

association. Once again, if only the most recent data on duplicated systems is considered (FIGURE 5.11), the slope is 0.50 ± 0.07.

TABLE 5.11

KINETIC AND THERMODYNAMIC DATA FOR COMPLEX ION FORMATION BY $FeOH^{+2}$ AT 25°

Ligand	k_{25} l/m/s	$\log(k_{25})$	K_{25}	$\log(K_{25})$	Reference
Br^-	$2.1 \pm .5 \times 10^4$	4.32	4.2×10^2	2.62	61M
Br^-	3×10^3	3.48	2.5×10^2	2.40	69C
Cl^-	$1.1 \pm .1 \times 10^4$	4.04	2.2×10^3	3.34	59Co
SCN^-	$4.2 \pm .5 \times 10^4$	4.62	9.8×10^4	4.99	64Ca
SCN^-	$1 \pm .1 \times 10^4$	4.00	7.3×10^4	4.86	58B
SCN^-	$2.4 \pm .2 \times 10^4$	4.32	7.4×10^4	4.87	62W
$ClAc^-$	$2.8 \pm$ x 10^4	4.45	6.9×10^4	4.84	69A
N_3^-	$1.0 \pm .1 \times 10^6$	6.00	1.25×10^4	7.10	This work
SO_4^{-2}	$2.4 \pm .1 \times 10^5$	5.38	2.0×10^5	5.30	62W
SO_4^{-2}	$2.3 \pm .6 \times 10^5$	6.36	7.5×10^4	4.87	68C
$Fe(CN)_6^{-3}$	$3.6 \pm .4 \times 10^4$	4.55	2.4×10^4	4.38	68W

The thermodynamic data used in TABLE 5.11 is necessarily that for the overall reaction:

$$(H_2O)_5FeOH^{+2} + L^- \underset{}{\overset{k_2}{\rightleftharpoons}} (H_2O)_4Fe(OH)L \rightleftharpoons (H_2O)_5FeL \qquad 5.13$$

Information is not available for the hydrolysis of $Fe(H_2O)_5L^{+2}$,

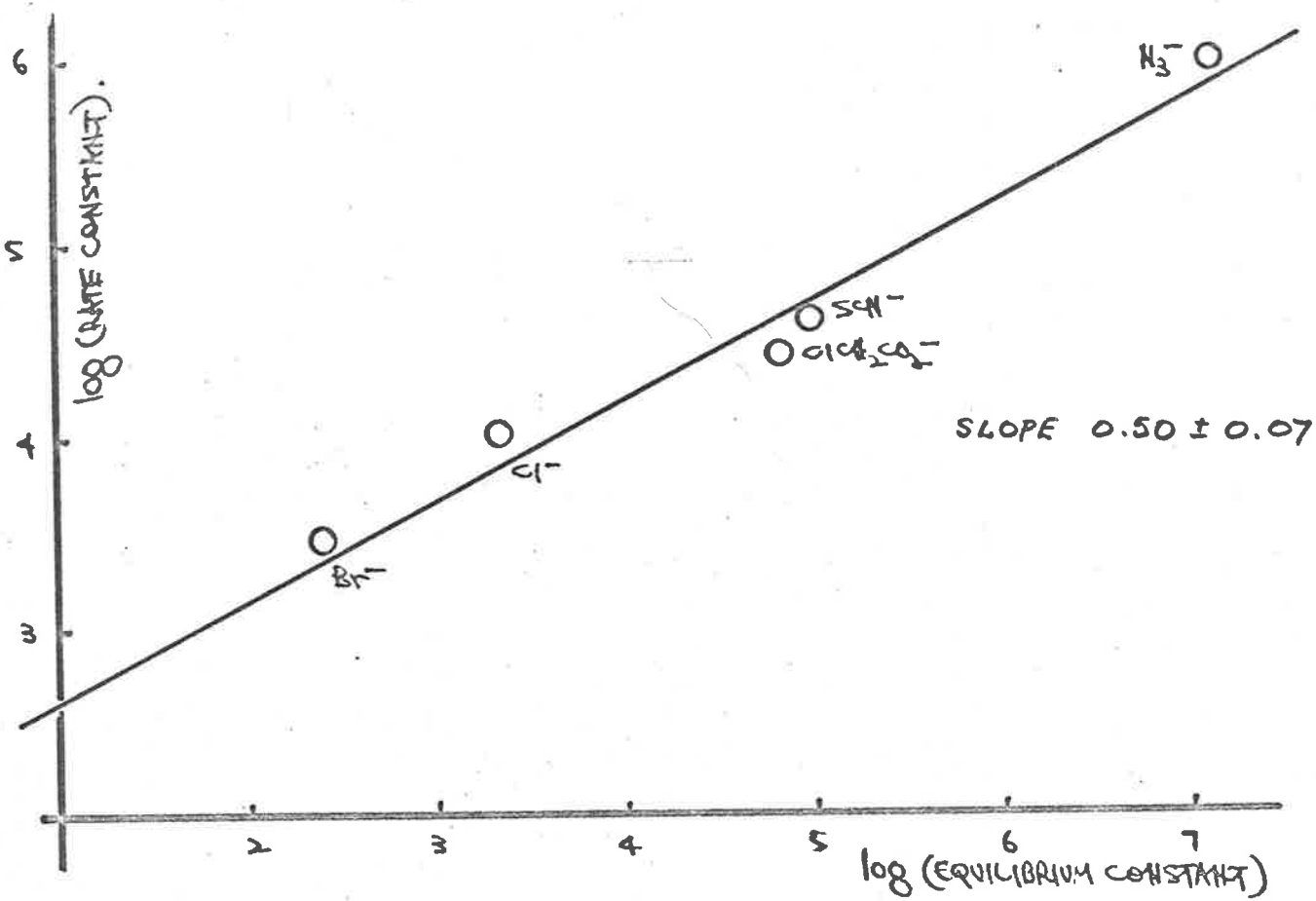

FIGURE 5.11. REACTIONS OF $FeOH^{+2}$. MOST RECENT DATA.

except an approximate value for the thiocyanate complex (6×10^{-5}(5%Li)), so that, for any rigorous comparison with the reactions of Fe^{+3}_{aq}, the degree of hydrolysis of the complex must be assumed to be approximately constant for all ligands. The similarity in free energy correlation slopes for the Fe^{+3}_{aq} and $FeOH^{+2}_{aq}$ reactions with similar ligands, however, lends some support to this assumption.

On the basis of this empirical correlation of the observed data, making no assumptions carrying any mechanistic implications, those ferric/ligand systems with more basic ligands which cannot be unambiguously assigned to a reaction pathway, will now be considered.

The data are presented in TABLE 5.12 for all such systems, on the assumption that the observed acid-independent rate constant does, in fact, correspond entirely to path 1. Included are the thiocyanate and acid oxalate ions, on the grounds that the oxalic acid is not entirely dissociated in solution, and information is available for the existence of HSCN in solution (65M).

TABLE 5.12

KINETIC AND THERMODYNAMIC DATA ASSUMING REACTION PATH 1:

$Fe + L \rightleftharpoons FeL$

Ligand	k_{25}	$\log(k_{25})$	K_{25}	$\log(K_{25})$	Reference
SCN^-	132	2.12	269	2.43	64Ca
SCN^-	127	2.10	140	2.16	58B
SCN^-	150	2.18	140	2.16	62We
$HC_2O_4^-$	1.4×10^3	3.15	2.2×10^4	4.34	65B
$HC_2O_4^-$	8.6×10^2	2.93	1.1×10^4	4.04	66M
F^-	5.4×10^3	3.73	1.5×10^5	5.18	60P
acetate	3.4×10^5	5.53	1.6×10^3	3.20	69A
propionate	4.2×10^5	5.62	2.8×10^3	3.45	69A
chloracetate	4.9×10^3	3.69	126	2.10	69A
formate	1.3×10^4	4.11	1.3×10^3	3.11	66M
N_3^-	1.6×10^5	5.20	8.4×10^3	3.92	63S
N_3^-	5.2×10^5	5.72	3.2×10^4	4.51	67A
N_3^-	1.4×10^5	5.15	7.3×10^3	3.86	67C
N_3^-	4.3×10^5	5.63	2.4×10^4	4.38	This work
SO_4^{-2}	10^3	3.00	600	2.78	62We
SO_4^{-2}	6.4×10^3	3.81	205	2.31	62D
SO_4^{-2}	4.6×10^3	3.66	205	2.31	68C
$C_2O_4^{-2}$	1.2×10^5	5.08	6.9×10^3	3.84	66M

The equilibrium constant for the oxalate is that calculated from Moorhead and Sutin's data (66M), for the monodentate attachment to the metal ion for valid comparison to be made with the other ligands. The data are shown in FIGURE 5.12, together with that of FIGURE 5.8,

and the suggested dependence extrapolated from the data of FIGURE 5.8. It can be seen that, while the data for fluoride falls reasonably within the range of this extrapolation, data for the chloracetate propionate, formate, acetate, azide, sulphate and oxalate do not.

The same data, recalculated on the assumption that the acid independent path can be entirely associated with path 4, is given in TABLE 5.13 and presented in FIGURE 5.13 with the expected dependence for -1 ligands in their reaction with $FeOH^{+2}$ taken from FIGURE 5.10, and the assumption that reactions of neutral ligands would be expected to show little or no variation in rate by analogy with the Fe/HL systems in FIGURE 5.9.

The data for the azide, acetate, propionate, formate and chloracetate fit a model with reactants FeOH/HL better than for a model Fe/L; the data for the fluoride appears to fit both trends equally well, and the acidoxalate and thiocyanate fit the FeOH/HL model slightly worse than the Fe/L model.

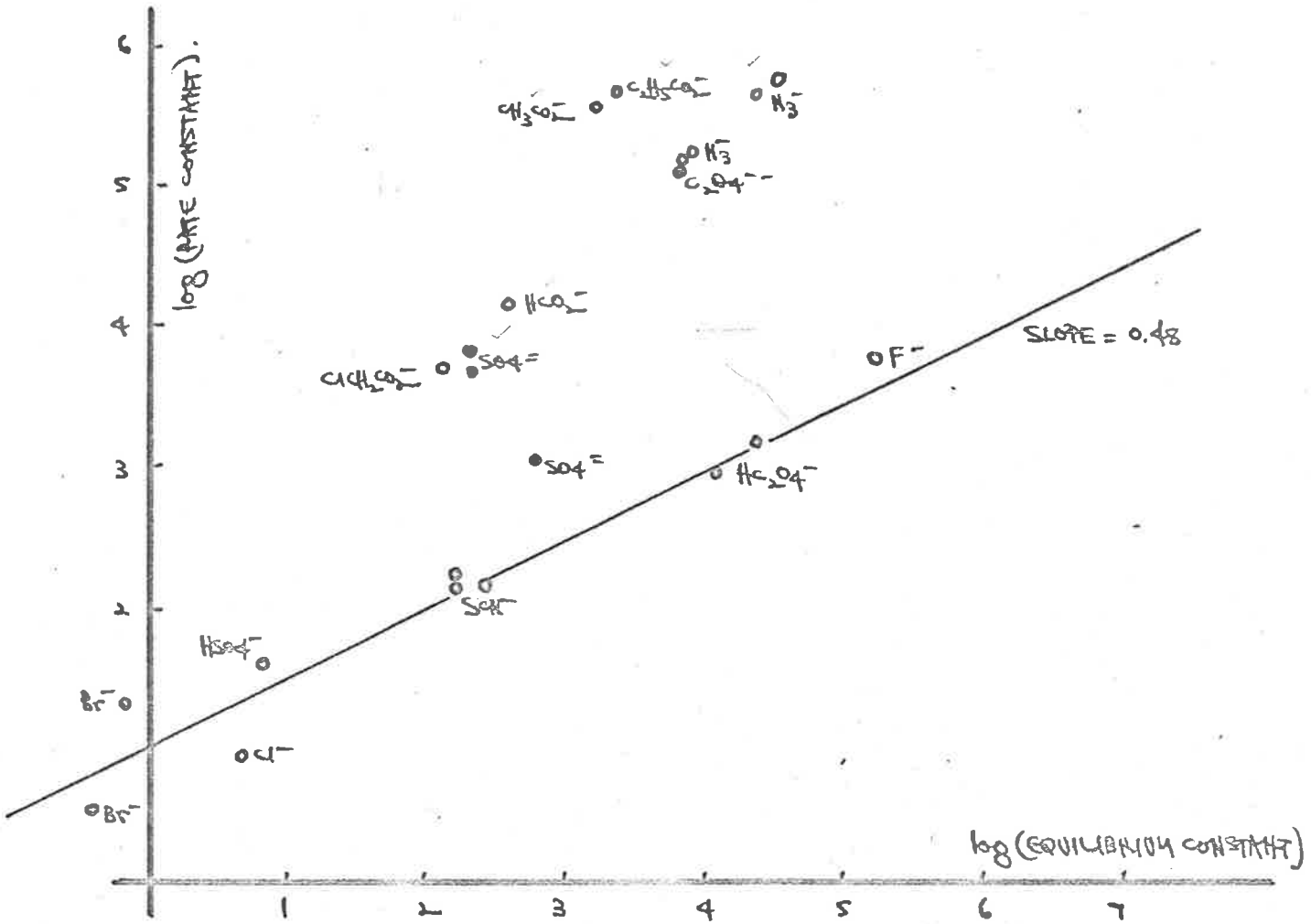

FIGURE 5.12 — ALL AVAILABLE DATA ASSUMING PATH 1 AS ACID INDEPENDENT PATHWAY.

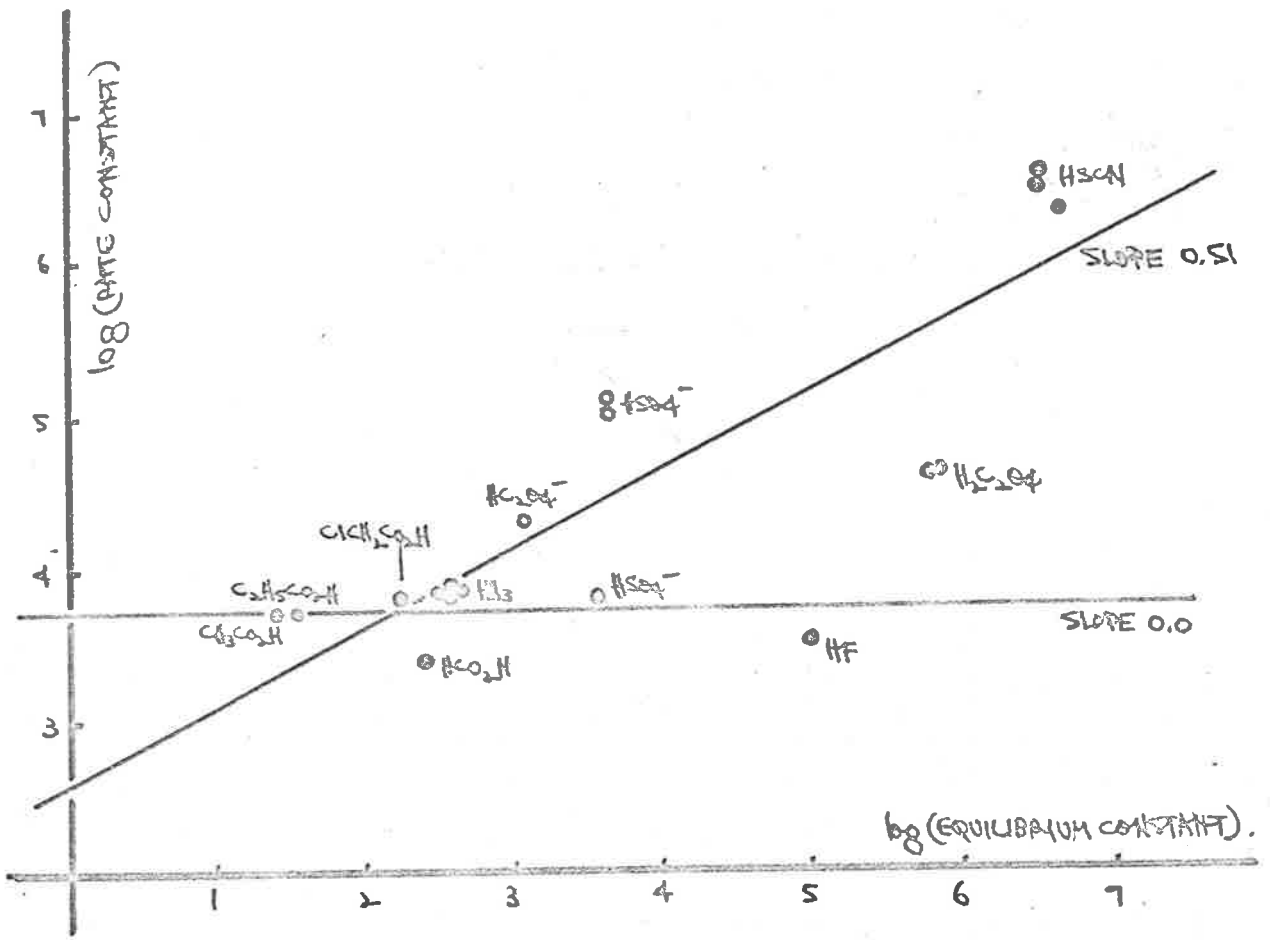

FIGURE 5.13. ALL AVAILABLE DATA ASSUMING PATH 4 AS ACID INDEPENDENT PATHWAY

TABLE 5.13

KINETIC AND THERMODYNAMIC DATA ASSUMING REACTION PATH 4:

$FeOH + HL \rightleftharpoons FeL$

Ligand	k_{25}	$\log(k_{25})$	K_{25}	$\log(K_{25})$	Reference
HSCN	2.2×10^6	6.34	4.4×10^6	6.64	64Ca
HSCN	3.0×10^6	6.48	3.3×10^6	6.52	58B
HSCN	3.6×10^6	6.56	3.3×10^6	6.52	62We
$H_2C_2O_4$	4.6×10^4	4.66	7.2×10^5	5.86	65B
$H_2C_2O_4$	4.4×10^4	4.64	5.6×10^5	5.75	66M
HF	3.5×10^3	3.54	9.7×10^4	4.99	60P
acetate H	5.3×10^3	3.72	25	1.40	69A
propionate H	5.1×10^3	3.71	34	1.53	69A
chloroacetate H	6.8×10^3	3.83	1.7×10^2	2.34	69A
formate H	2.5×10^3	3.40	2.5×10^2	2.40	66M
HN_3	6.8×10^3	3.83	3.6×10^2	2.56	63S
HN_3	7.4×10^3	3.87	4.5×10^2	2.65	67A
HN_3	6.1×10^3	3.79	3.1×10^2	2.49	67C
HN_3	8.0×10^3	3.90	4.7×10^2	2.67	This work
HSO_4^-	6.2×10^3	3.79	3.7×10^3	3.57	62We
HSO_4^-	1.4×10^5	5.15	4.6×10^3	3.66	62D
HSO_4^-	1.0×10^5	5.00	4.6×10^3	3.66	68C
$HC_2O_4^-$	2.0×10^4	4.30	1.2×10^3	3.06	66M

Of the doubly charged ligands, the deviant oxalate data is considerably improved by assuming that the kinetic pathway is $FeOH^{+2}/HC_2O_4^-$ but the sulphate data seems to fit both interpretations

equally badly. In TABLE 5.14, k_1 and k_4 have been estimated from the lines of best fit for the appropriate ligand charge types in reaction with Fe^{+3}_{aq} and $FeOH^{+2}_{aq}$ from FIGURES 5.12 and 5.13 and their relative contributions to the observed rate constant

$$k_{obs} = k_1 + (K_H/K_A)k_4 \qquad 5.14$$

have been calculated:

TABLE 5.14

Ligand	k_1	K_H/K_A	k_{obs}	% due to k_1	Reference
SCN^-	139	6.1×10^{-5}	139	100	64Ca
SCN^-	107	4.2×10^{-5}	107	100	58B
SCN^-	107	4.2×10^{-5}	107	100	62We
$HC_2O_4^-$	870	3.1×10^{-2}	1030	84	65B
$HC_2O_4^-$	1230	1.9×10^{-2}	1330	92	66M
F^-	3240	1.5	1.11×10^4	29	60P
chloroacetate	100	0.72	3.88×10^3	2.6	69A
formate	174	5.2	2.75×10^4	0.6	66M
N_3^-	758	24	1.27×10^5	0.6	63S
N_3^-	1180	71	3.74×10^5	0.4	67A
N_3^-	708	24	1.27×10^5	0.6	67C
N_3^-	1290	51	2.69×10^5	0.5	This work
acetate	339	64	3.36×10^5	0.1	69A
propionate	447	82	4.31×10^5	0.1	69A

$k_4 = 5.25 \times 10^3$ l/m/s for all ligands.

The calculations confirm what has been observed in general from FIGURES 5.12 and 5.13; all ligands are assignable fairly conclusively to either path 1 or path 4, except the fluorides, for which the observed acid independent rate involves significant proportions of each.

To summarise, the basis of the assignments is that there are two possible contributions to the acid independent rate, referred to as paths 1 and 4, and that for neutral ligands the rates are approximately independent of ligand; for ligands of charge -1, however, the rate constants for these paths may be correlated with their equilibrium constants in a way which suggests that the nature of the incoming group may play an appreciable role in the rate of complex ion formation. It would seem, therefore, that to interpret the reactions of the ferric ion in terms of a classical Eigen-Wilkins mechanism (65E), as is perhaps best documented for the reactions of Ni^{+2}_{aq}, may well be an oversimplification. Examination of the data compiled by Rorabacher (66R) for reactions of Ni^{+2}_{aq} gives for twelve neutral ligands, log k = 3.4 $\pm$ 0.1, and for five ligands of charge -1, log k = 3.8 $\pm$ 0.2; for the second order exchange of water from Ni^{+2}_{aq}, log k = 3.4. The data extends over a range of equilibrium constants of 10^{11} (64S).

(d) Ferric/azide interactions.

The data presented in the previous section for ferric/

ligand interactions suggest that for ferric/azide the acid independent path can be assigned almost completely to path 4, so that the contributing reactions observed in this study will be considered to be:

$$FeOH^{+2} + HN_3 \underset{}{\overset{k_4}{\rightleftharpoons}} FeN_3^{+2} \qquad 5.15$$

$$Fe^{+3} + HN_3 \overset{k_3}{\rightleftharpoons} FeN_3^{+2} + H^+ \qquad 5.16$$

$$FeOH^{+2} + N_3^- \overset{k_2}{\rightleftharpoons} Fe(OH)N_3^+ \xrightarrow{H^+} FeN_3^{+2} \qquad 5.17$$

The discussion of the substitution reactions of labile metal ions at present centres on a comparison with the rate of exchange of solvent in the first coordination shell of the ion and the suggestion that it is this rate which determines the rate of complex formation.

A number of determinations of the rate of water exchange in the coordination shell of Fe^{+3}_{aq} have been made using O^{17} nuclear magnetic relaxation techniques and the results of these studies are given in TABLE 5.15. The values represent a steady refinement of technique and analysis; the values of Grenser (62G) are those which have been generally used in a discussion of mechanism of Fe^{+3}_{aq} substitution. The more recent values of Judkins (67J) were obtained from a much more comprehensive study of acid and temperature dependences; it was noted that at room temperature or below, other effects, originating in the outer coordination sphere sites of the ferric ion, became comparable with exchange from the first coordination sphere.

TABLE 5.15

RATES OF EXCHANGE OF WATER IN Fe^{+3}_{aq} SOLUTION

	k sec^{-1}	H	Reference
$Fe(H_2O)_6^{+3}$	2.4×10^4		61C
	2.6×10^3	8.9	62E
	625	12.8	67J
	150	18.4	67J
$Fe(H_2O)_5OH^{+2}$	2.0×10^5		62E
	6.6×10^5		67J

The faster rate obtained by Genser from measurements at 27°, was attributed by Judkins to the outer sphere exchange not being allowed for, and the two values quoted by Judkins are the result of a different model being used in the correction of data for the outer sphere relaxation. A similar effect was observed by Conniek and Poulson (59Cn) for Cr^{+3}_{aq}, although relaxation could be accounted for entirely by exchange from the first coordination sphere for the doubly charged ions studied.

If the data determined in this work are analysed in the terms of an Eigen-Wilkins mechanism, using the solvent exchange data of references 62E and 67J, the results are as shown in TABLE 5.16.

TABLE 5.16

Reaction path	k l/m/sec	k_{ex} sec^{-1}	K_o*	Reference
Fe/HN_3	9.6	150	0.06	This work/67J
$FeOH/HN_3$	8.0×10^3	6.6×10^5	0.01	
$FeOH/N_3^-$	1.0×10^6	6.6×10^5	1.5	
Fe/HN_3	9.6	2.6×10^3	0.004	This work/62E
$FeOH/HN_3$	8.0×10^3	2.0×10^5	0.025	
$FeOH/N_3^-$	1.0×10^6	2.0×10^5	5.0	

*Preassociation constant of Eigen-Wilkins mechanism.

Values for the preassociation constant K_o for the reactions of HN_3, and therefore for other neutral ligands, are much lower than would be expected from calculated values of ion/dipole interactions which give 0.2 to 0.4 litres/mole using the model of Fuoss (58F); they are also lower than that determined by a similar treatment of the experimental data for reactions of Ni^{+2} with neutral ligands (66R) (0.2 litres/mole), which might be expected to have values comparable with those of the $FeOH/HN_3$ system. The values of K_o for $FeOH/N_3^-$ are of the order of that calculated using the Fuoss model (2 litres/mole) assuming a separation of 5Å in the ion pair. Using the data of Judkins, however, seems to give best support to the mechanism, especially when the comparison is extended to the activation parameters. The activation energy for Fe/HN_3 (17.9 kcals/mole) is very similar to

that for the water exchange (18.4 kcals/mole) and the value for $FeOH/N_3$ (2.5 kcals/mole), which is abnormally low when compared with other FeOH/ligand reactions (e.g. FeOH/HF = 10 kcals/mole, FeOH/Cl = 13 kcals/mole), appears to be matched by a low value for the water exchange at FeOH (4 kcals/mole). The activation energy for $FeOH/HN_3$ (11.6 kcals/mole) is, however, significantly higher than the water exchange value and difficult to rationalise in terms of the very weak ion/dipole preassociation. The values for the suggested pre-association for Fe/HN_3 and $FeOH/HN_3$ are, in fact, much lower than would be obtained from a random distribution of uncharged reaction partners in solution (0.15 litres/mole (66R)).

It appears, therefore, that our observations cannot be completely explained in terms of this simple model.

As was mentioned above, it has been reported (67J) that at room temperature or below, Fe^{+3}_{aq} appears to have an observable outer hydration shell, held strongly enough that these interactions may provide an alternative mechanism for O^{17} relaxation. At higher temperatures presumably as thermal agitation in the bulk solvent becomes more violent, it is disrupted and becomes a less important mechanism for relaxation. A comparison of the data of references 62E and 67J is shown in FIGURE 5.14. It would appear that, in the range of 95-100°, the role of the second sphere is negligible and the data neglecting its presence and variously allowing for its effect are equivalent to well within their experimental errors ($\pm$ 0.2 log units).

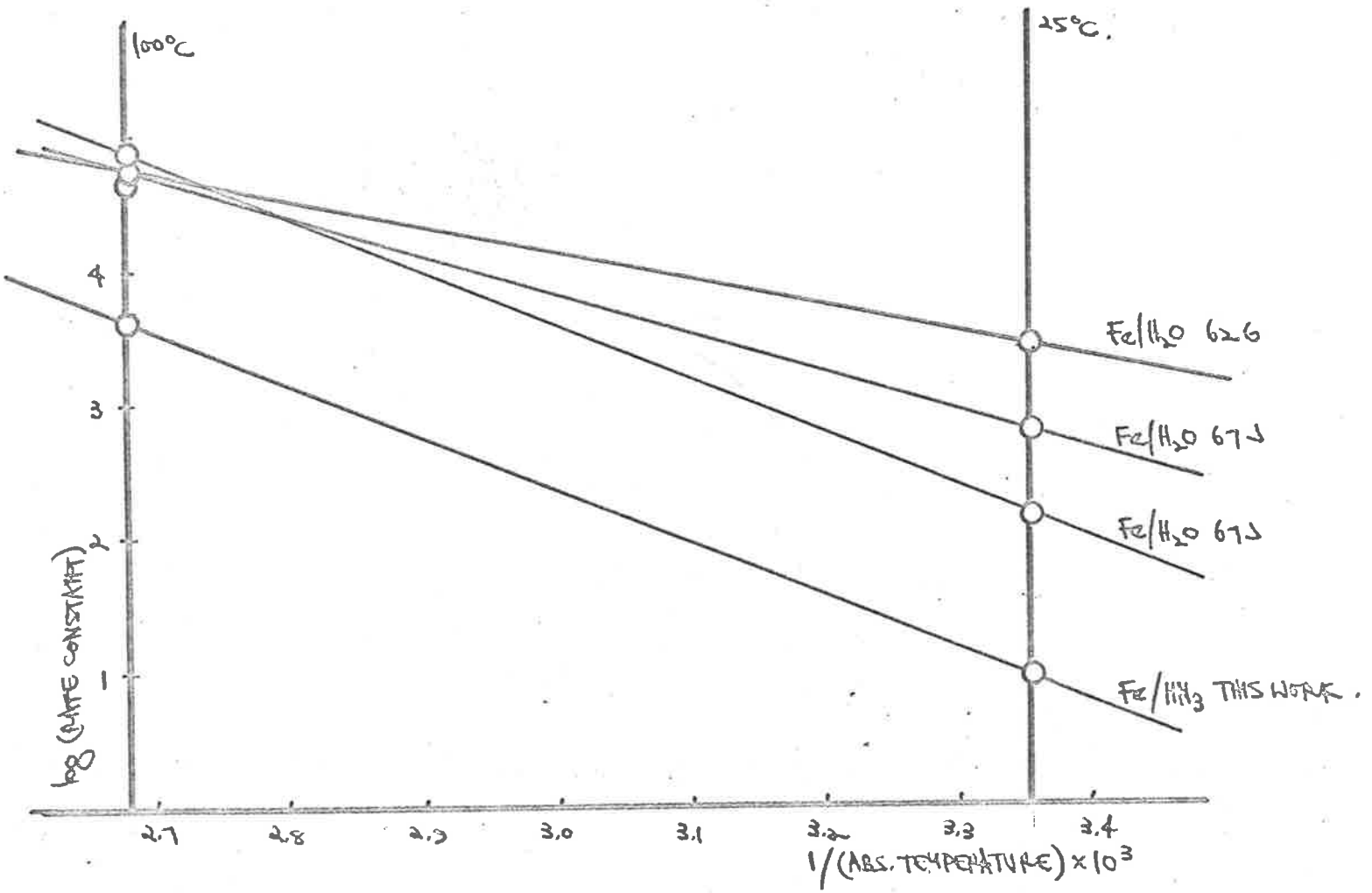

FIGURE 5.14. EXTRAPOLATION OF RATE DATA TO 100°C

Because of their very similar activation energies the comparison of the inner sphere exchange rate and the Fe/HN_3 reaction rate is hardly affected by the higher temperatures, and the K_o calculated from the mean water exchange rate (5.9×10^4 sec^{-1}) is 0.07 litre/mole.

A similar treatment may be carried out on the data for $FeOH^{+2}$ reactions, and this is given in TABLE 5.17.

TABLE 5.17

		k(25°)	k(100°)	$k/k^{100°}_{exchange}$
Fe/H_2O	(62B)	2.6×10^3	$5.4 \times 10^4 sec^{-1}$	
	(67J)	625	$4.8 \times 10^4 sec^{-1}$	
	(67J)	150	$7.6 \times 10^4 sec^{-1}$	
$FeOH/H_2O$	(67J)	6.6×10^5	2.6×10^6	
Fe/HN_3		9.6	$4.1 \pm .2 \times 10^3$ l/m/s	0.07
$FeOH/HN_3$		8.0×10^3	$4.0 \pm .1 \times 10^5$ l/m/s	0.15
$FeOH/N_3$		1.0×10^6	$2.3 \pm .6 \times 10^6$ l/m/s	0.9

It can be seen that the preassociation constant, assuming a straightforward Eigen-Wilkins mechanism for $FeOH/N_3$, is again reasonable, but that the $FeOH/HN_3$ value is now of a similar order to that for Fe/HN_3. Of the other data available for reaction with $FeOH^{+2}$, that for the chloride and thiocyanate, because of much less accurate activation energy values, cannot be extrapolated with the

certainty of the data for azide, but within these errors they agree with our results for azide. The values in TABLE 5.18 indicate that, although the data for our reaction 2 appear seriously in conflict with that for other univalent ligands at 25°, agreement is much improved at 100°. The values of the preassociation constant K_o, determined as before from the ratio of the observed rate and water exchange rate, for the chloride and the thiocyanate, are also much more reasonable at 100°.

TABLE 5.18

Ligand	k_{N_3}/k_{ligand}	K_o(25°)	k_{N_3}/k_{ligand}	K_o(100°)	Reference
Cl^-	91	0.02	3	0.3	59Co
SCN^-	24	0.06	2	0.5	64Ca
SCN^-	100	0.02	8	0.1	58B
SO_4^{-2}	4.4	0.3	0.2	4.3	68C

The data for the sulphate changes from being slower than the azide at 25° to being faster at 100° (FIGURE 5.15), as might be expected for more highly charged ligand. The plot of $\log(K_o)$ at 100°, for HN_3, N_3^- and SO_4^{-2} reactions with $FeOH^{+2}$, as a function of charge product shown in FIGURE 5.16 gives a good linear correlation, suggesting that an electrostatic model for the preassociation applies at this temperature whereas at 25° no such correlation can be obtained. If

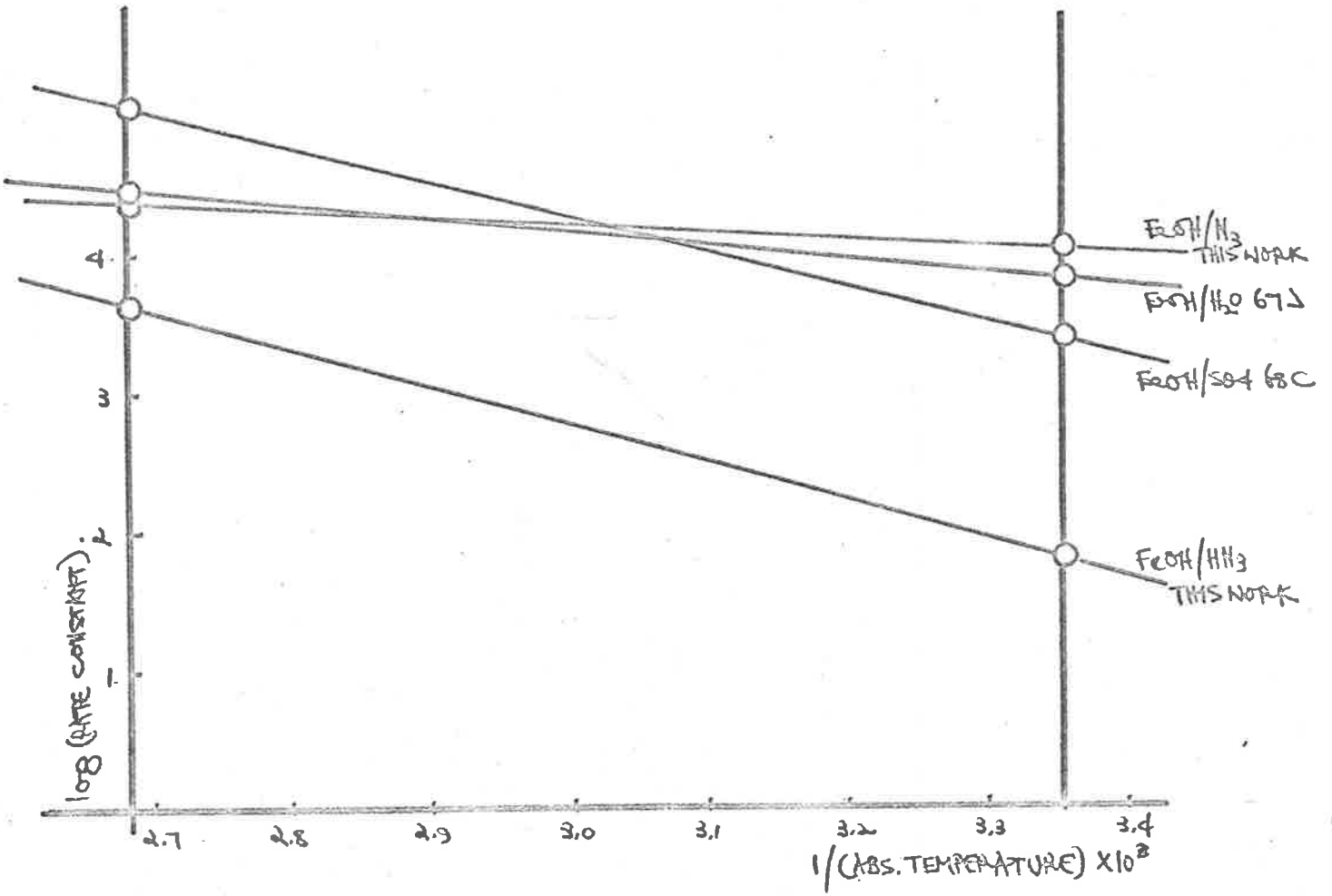

FIGURE 5.15 EXTRAPOLATION OF FeOH RATE DATA TO 100°C.

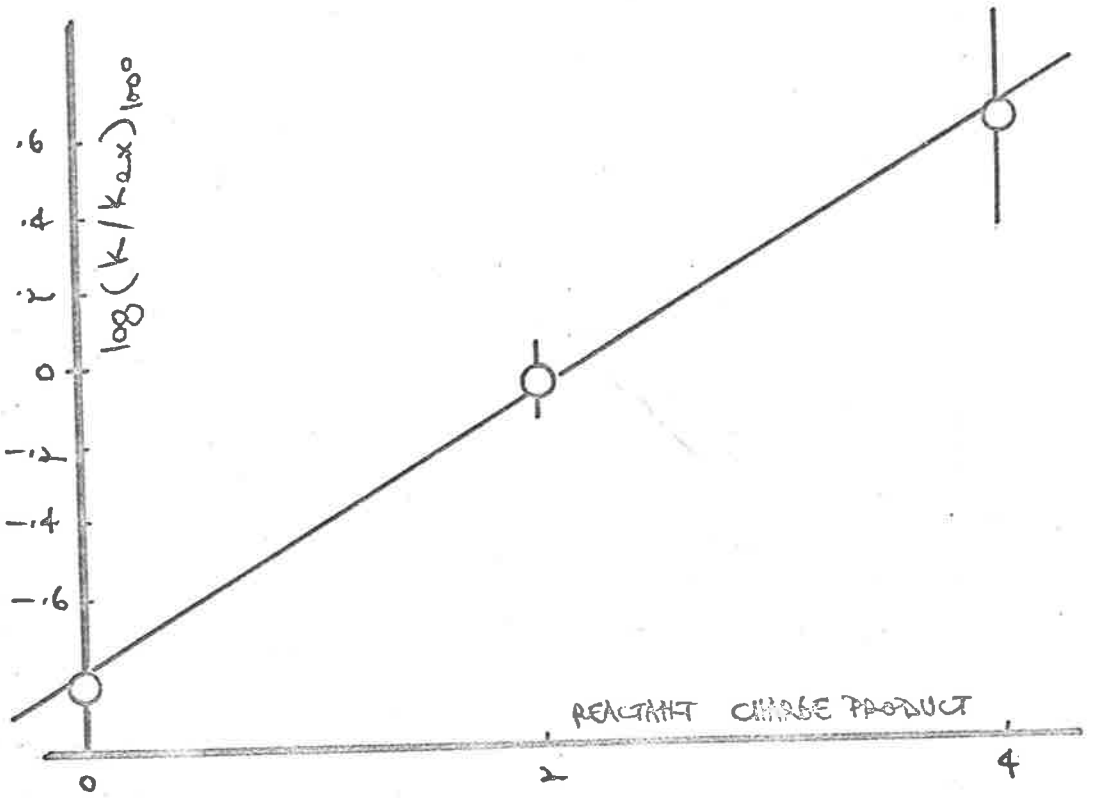

FIGURE 5.16.

it is assumed that the size of the ligands is constant, that the bulk dielectric constant (55 at 100°C in water) applies, and that the model of Fuoss can be used to describe the association, the slope of FIGURE 5.16 (0.36), corresponding to a value of (ionic separation) x (dielectric constant) of 5.4 x 10^{-6}cm, gives a separation in the suggested complex of 9.8Å; the separation calculated from the radius of Fe^{+2} (0.7), diameter of H_2O (3.6) and half the length of HN_3 (1.4) is 5.7Å.

These results would tend to suggest that at 100° when any effects due to secondary solvation at Fe^{+3}_{aq} would appear to be negligible, and certainly where the free energy for the removal of a solvent molecule from any point in the bulk solvent is zero, the effects which give such a wide range of rates for reaction of $FeOH^{+2}$ with HN_3 and N_3^- and between N_3^- and other monovalent cations are also much reduced and the system can reasonably be described by a simple Eigen-Wilkins mechanism.

Of the data for reaction of univalent cations with Fe^{+3}_{aq} only that of Conniek and coworkers for the chloride (59Co) and thiocyanate (58B) have activation parameters which can be used for extrapolation over this temperature range with an accuracy of better than an order of magnitude; the data is given in TABLE 5.19 and agreement between the ligands is improved by a factor of four at 100°C.

TABLE 5.19

Ligand	$k_{25°}$	$\Delta H^{\ddagger}$	$k_{100°}$
Cl^-	9.4	17 ± 2	3.0×10^3
SCN^-	127	13 ± 1	10.0×10^3

All of the data available for other ligand systems do not support a comparison at 100°, however. For some, activation data is not available or accurate enough for a meaningful extrapolation to be considered. There is a serious discrepancy between the extrapolation of the data for HF and our data for HN_3 (60P); while the agreement in rates at 25° is good, the activation energy is such that the rates differ by a factor of 20 at 100°. For FeOH/HF, although, as has been suggested above, there may be some simultaneous contributions to reaction via Fe^{+3}/F^*, the agreement at 25° is as good as the agreement at 100°, but the discrepancy is outside the experimental error.

The data for FeOH/HN_3 determined by Cavasino (67A) agrees within experimental error with our value at 100°; activation parameters for the data of Carlyle and Espenson (67C) cannot be determined from their equation kinetics, as no information on the temperature dependence of their separately determined equilibrium constant is available.

The rate of solvent exchange, if predominantly determined by the strength of the metal-oxygen interaction in the aquated ion,

would be expected to be much the same in deuterium oxide as in water. Ultrasonic measurements by Smithson and Litowitz (56S) of manganous sulphate in H_2O and D_2O showed no shift in the frequency of absorption attributed to the metal solvent exchange rate on changing solvents. From its higher viscosity, temperature of maximum density and heat capacity, D_2O would appear to be a more structured solvent; calculations by Nemethy and Scheraga (64N), using the 'flickering cluster' model of Frank and Wen, could reproduce the experimental data for those properties if hydrogen-bonding in D_2O was assumed to be stronger than that in H_2O by 0.24 kcals/mole. Because of this greater structure, it has been suggested that D_2O solvates cations less strongly than H_2O, but solvates anions more strongly (60Bi). The molar volume measurements of Wirtz (37W) suggest that, although the degree of structural order in D_2O is greater than H_2O at lower temperatures, the rate of breakdown with increasing temperature is greater for D_2O until at higher temperatures both forms appear to have similar degrees of order.

The results of ferric azide kinetics determined in this work are given in TABLE 5.20.

TABLE 5.20

KINETICS OF FERRIC/AZIDE INTERACTION IN H_2O AND D_2O

	k_{25}	$\Delta H^{\ddagger}$	$\Delta S^{\ddagger}$	k_{100}
$Fe/HN_3/H_2O$	9.6	17.9	6.0	4.1×10^3
D_2O	2.0	22.3	17.7	3.8×10^3
$FeOH/HN_3/H_2O$	8.0×10^3	11.6	-1.6	4.0×10^5
D_2O	5.9×10^3	12.5	0.5	4.1×10^5

It can be seen that the significant isotope effects observed for both reaction paths at 25° have virtually disappeared at 100°, when, it is assumed, both solvents have similar degrees of solvating power. It is not thought that the data for Fe/HN_3 is accurate enough for any more than this qualitative observation. The data for $FeOH/HN_3$, however, makes up about 95% of the observed rate constant and has been measured quite accurately; the solvent isotope effect at 25°, $k_H/k_D = 1.35 \pm 0.05$. The difference in activation energy could be entirely accounted for if, assuming the value of Nemethy and Scheraga above, only four hydrogen bonds are broken in the attainment of the transition state; assuming that the major contribution to the activation entropy difference is only in the 'thawing' of solvating water molecules, the observed difference would correspond to the 'desolvation' of eight solvent molecules.

LIBRARY OF THE UNIVERSITY OF ADELAIDE

Based mainly on the quantities measured in this work, a case has been presented which is substantiated by data available in other ferric systems, that differences in the rates of reaction for various ligands at 25°, and discrepancies between the observed data and the general mechanism which seems to apply in other labile metal ion substitution reactions, can at least be partly accounted for by comparing the data under conditions, where differences in secondary solvation characteristics of the reactants can be assumed negligible. The major limitation has been that sufficient other accurate activation data is not available, nor are the phenomena of ion solvation so well understood that a critical comparison of a large number of ligand systems can be made.

There seems little doubt that at least for charged ligands at 25°, the character of the entering group plays a significant part in the rate of complex formation for reaction both at Fe^{+3}_{aq} and $FeOH^{+2}_{aq}$. The high rate constant and negative entropy of activation for the reaction path $FeOH^{+2}/N_3^-$ (-23 e.u.) would indicate an ordered transition state not inconsistent with an associative mechanism.

APPENDIX 1

COMPUTER PROGRAMS

Computer programs were written in FORTRAN IV to operate on the University of Adelaide CDC 6400 computer using the Scope 2 compiler.

Complete main program and subroutine listings are given; where two main programs use similar subroutines, reference is made to the earlier listing.

The programs listed in this Appendix are:

(i) PROGRAM EQUIL including subroutines CONCS 2 and LSTSQU, for the analysis of concentration and optical density data for the determination of the extinction coefficients and association equilibrium constant for the FeN_3^{+2} complex ion. Subroutine CONCS 2 applies concentration corrections for the various hydrolysed species present under the experimental conditions and subroutine LSTSQU calculates the linear least squares fit to the data.

(ii) PROGRAM RATE 13 with subroutines CONCS, BRATH and LSTSQU is the final version of a series of programs used to analyse the concentration, optical transmission and instrument conditions used in kinetic runs, to determine the second order (reversible) kinetic rate constants for the formation of the FeN_3^{+2} complex ion.

(iii) PROGRAM STEP 13 with subroutines TEMDEP, CONC2 and LSFSQU is the final version of a series of programs analysing the second order formation rate constant data from RATE 13, as a function of hydrogen ion concentration and temperature. It calculates the activation parameters of the various acid dependent and acid independent paths leading to the formation of the FeN_3^{+2} complex ion.

APPENDIX 1.1

```
      PROGRAM EQUIL(INPUT,OUTPUT)
      DIMENSION HEADER(8),FET(40),AZT(40),ACIDO(40),D(40),X(40),Y(40)
C
C
   99 READ 2,(HEADER(J),J=1,8),N
    2 FORMAT(8A10/I3)
      IF(HEADER(1).EQ.10H          )STOP
      PRINT 3,(HEADER(J),J=1,8)
    3 FORMAT(1H1//1X8A10/24X*FET*9X*AZT*9X*ACIDO*19X*D.D.*)
C
      DO 6 J=1,N
      READ 4,IDENT,FET(J),AZT(J),ACIDO(J),D(J)
    4 FORMAT(A10,3F10.3,F6.3)
    6 PRINT 5,IDENT,FET(J),AZT(J),ACIDO(J),D(J)
    5 FORMAT(10XA10,3E12.3,12XE12.3)
C
C
      EQCON=0.0
      DO 13 I=1,3
      PRINT 14,I
   14 FORMAT(/* TRIAL NUMBER=*I2/24X*FEF*9X*HN3*9X*ACIDF*7X*FEN3*8X*D.D*
     .18X*D.D. CORR*3X*A/D*9X*H/B*)
C
      DO 10 J=1,N
      CALL CONCS2(FET(J),AZT(J),ACIDO(J),EQCON,FEF,HN3,FEN3,ACIDF)
      DCORR=D(J)-0.244*FEF-13.30*FEF*0.00187/ACIDF
C
      IF(FEF.GT.HN3) GO TO 7
      X(J)=ACIDF/HN3
      Y(J)=(FEF+FEN3)/DCORR
      GO TO 8
    7 X(J)=ACIDF/FEF
      Y(J)=(HN3+FEN3)/DCORR
    8 CONTINUE
C
   10 PRINT 9,FEF,HN3,ACIDF,FEN3,D(J),DCORR,Y(J),X(J)
    9 FORMAT(20X8E12.3)
C
      PRINT 11
   11 FORMAT(//* A/D VS ACID/B*)
      CALL LSTSQU(X,Y,N,SLOPE,SI,1)
      EXT=1.0/SI
      EQCON=SI/SLOPE
      PRINT 12,EXT,EQCON
   12 FORMAT(1X*EXTINCTION COEFF =*E10.3,10X*EQUILIBRIUM CONST =*E10.3/)
C
   13 CONTINUE
      GO TO 99
C
      END
```

APPENDIX 1.1

```
      SUBROUTINE CONCS2(FET,AZT,ACIDO,EQCON,FEE,HN3,FEN3,ACIDF)
C     DATA FOLLOWING IS FOR 25 DEGREES ONLY
      DATA EQKH,EQDI,EQKA/1.87E-03,1.49E-03,3.45E-05/
      FEE=FET  $  HN3=AZT  $  ACIDF=ACIDO-AZT
   30 ACTEN=ACIDF
C
      BB=1.0+EQKH/ACIDF+EQCON*HN3/ACIDF
      FEE=(SQRT(BB*BB+8.0*EQDI*FET/(ACIDF*ACIDF))-BB)*ACIDF*ACIDF
     1/(4.0*EQDI)
      FEOH=FEE*EQKH/ACIDF
      FEDI=FEE*FEE*EQDI/(ACIDF*ACIDF)
      FEN3=FEE*EQCON*HN3/ACIDF
      HN3=(AZT-FEN3)/(1.0+EQKA/ACIDF)
      ACIDF=ACIDO+FEOH+2.0*FEDI-HN3
C
      DIFF=ABS((ACTEN-ACIDF)*100.0/ACIDF)
      IF(DIFF.LT.0.01)32,30
   32 CONTINUE
C
      RETURN
      END

      SUBROUTINE LSTSQU(X,Y,N,SLOPE,INTCPT,PTEST)
      DIMENSION X(40),Y(40)
      REAL INTCPT
      INTEGER PTEST
      IF(N.LT.2)38,40
   38 PRINT 39
   39 FORMAT(40H  N.LT.2  EXECUTION TERMINATED IN LSTSQU)
      STOP
   40 CONTINUE
      SX=SXX=SY=SYY=SYX=0
      DO 41 J=1,N
      SX=SX+X(J)
      SXX=SXX+X(J)*X(J)
      SY=SY+Y(J)
      SYY=SYY+Y(J)*Y(J)
   41 SYX=SYX+Y(J)*X(J)
      SXX=SXX-SX*SX/N
      SYY=SYY-SY*SY/N
      SYX=SYX-SY*SX/N
      SLOPE=SYX/SXX
      INTCPT=(SY-SLOPE*SX)/N
      IF(N.EQ.2)43,44
   43 SERY=SERS=SERINT=0.0
      GO TO 45
   44 SERY=SQRT((SYY-SLOPE*SLOPE*SXX)/(N-2.0))
      SERS=SERY/SQRT(SXX)
      SERINT=SERY*SQRT(1.0/N+(SX/N)*(SX/N)/SXX)
   45 CONTINUE
      IF(PTEST.EQ.0)RETURN
      PRINT 42,SLOPE,SERS,INTCPT,SERINT,SERY
   42 FORMAT(1X21HLSTSQU GIVES    SLOPE E12.5,12H   S.F.SLOPE E10.2,12H   I
     1NTERCEPT E11.4,16H   S.F.INTERCEPT E10.2,15H   S.E.ORDINATE E10.2)
      RETURN
      END
```

```
      PROGRAM RATE13(INPUT,OUTPUT,PUNCH)
C     REDUCTION OF STOPPED FLOW DATA TO OBSERVED RATE CONSTANTS USING
C     INTEGRATED RATE EXPRESSION FOR REACTIONS OF THE FORM  A+B=C+D.
C     INFLUENCE OF FORWARD AND REVERSE REACTIONS TAKEN INTO ACCOUNT.
C     INITIAL CONCENTRATION OF PRODUCT C IS ASSUMED TO BE ZERO.
C
C
      DIMENSION T(40),Y(40),TIME(40),FUNC(40),CONCN(40),OD(40)
      DIMENSION RASS(40),DR(40)
C
C     FUNCTION DEFINITION AND DATA FOR EQUILIBRIUM CONSTANTS
C     DATA FOLLOWING IS FOR H2O RUNS AT MU=0.50
      DATA DELHEQ,DELSEQ/ 2520.0,8.23/
      DATA DELHHY,DELSHY/ 10360.0,22.06/
      DATA DELHDI,DELSDI/12800.0,30.0/
      DATA DELHAC,DELSAC/ 3600.0,-8.34/
      CALCK(DELH,DELS,TEMP)=EXP((DELS-DELH/(273.2+TEMP))/1.9865)
C
      PRINT 2000
 2000 FORMAT(1H1)
C
C
C     READ REACTANT CONCENTRATIONS AND CONDITIONS FOR RUN
   99 READ 80,IRNO,CONCAO,CONCB,CONCC,CONCDO,TEMP,SCALE,SENS,SPEED,N,
     1IPNO
   80 FORMAT(1X,I3,4E10.3,F6.2,3F6.3,2I3)
      IF(IRNO.EQ.0) STOP
C
C
C     CALCULATE EQUILIBRIUM CONSTANTS AND HYDROLYSIS CORRECTIONS
      EQCON=CALCK(DELHEQ,DELSEQ,TEMP)
      EKHY=CALCK(DELHHY,DELSHY,TEMP)
      EKDI=CALCK(DELHDI,DELSDI,TEMP)
      EKAC=CALCK(DELHAC,DELSAC,TEMP)
      CONCA=CONCAO
      PRINT 81,IRNO
   81 FORMAT(1H1////* OUTPUT FOR RUN *I4///* CALCULATION DETAIL FOR PUSH
     1 NUMBER 1 */)
      CALL CONCS(CONCA,CONCB,CONCDO,CONCD,CONCEQ,EKHY,EKDI,EKAC,EQCON)
C
C
C     CALCULATE CONSTANT PARAMETERS FOR INTEGRATED RATE EXPRESSION
      P=CONCD+EKHY
      A=CONCA*CONCB*EQCON
      B=-(CONCA*EQCON+CONCB*EQCON+P)
      C=EQCON-1.0
      SQRTF=SQRT(B*B-4.0*A*C)
      PP=(P-B/(2.0*C))/SQRTF
      E=B-SQRTF   $  H=B+SQRTF
```

```
      DO 100 IP=1,IPNO
C
C     READ BACKING OFF AND CHANGES IN TRANSMISSION PER PUSH
      READ 95,RES,(Y(J),J=1,N)
   95 FORMAT(F4.0,19F4.2)
C
C     CALCULATE EQUILIBRIUM TRANSMISSION
      YEQ=RES*19.23/((1.0+107.0+RES)*SENS*SCALE)
      PRINT 92,EKHY,EKDI,EKAC,EQCON,YEQ
   92 FORMAT(* EKHY=*E10.3*, EKDI=*E10.3*, EKAC=*E10.3*, EQCON=*E10.3*,
     1YEQ=*E10.3*/)
C
C
C     CALC. REACTION TIME AND ABSOLUTE TRANSMISSION VALUES FOR DATA POINTS
      DO 10 J=1,N
      T(J)=TIME(J)=SCALE*SPEED*(J-1)
   10 Y(J)=Y(J)+YEQ
C
C
C     CALCULATE CONCN. AND INTEGRATED RATE FUNCTION
C
      YA=ALOG10(Y(1)/YEQ)
      DO 11 J=1,N
      CONCN(J)=CONCCFO*ALOG10(Y(1)/Y(J))/YA
      FUNC(J)=PP*ALOG((H*(2.0*C*CONCN(J)+E))/(E*(2.0*C*CONCN(J)+H)))
     1+0.5/C*ALOG((A+B*CONCN(J)+C*CONCN(J)*CONCN(J))/A)
C
C     PRINT VALUES OF CONC AND INTEG RATE FUNCTION FOR PUSH 1
      IF(IP.EQ.1)94,11
   94 PRINT 96,J,TIME(J),Y(J),CONCN(J),FUNC(J)
   96 FORMAT(1X*POINT NO. *I2,5X*TIME= *E10.3,5X*Y(J)= *E10.3,5X*CONCN=
     1*E10.3,5X*FUNC= *E10.3)
   11 CONTINUE
C
C
C     CALCULATE LEAST SQUARES SLOPE OF INTEG. RATE FUNCTION VS TIME
      CALL DTATRY(TIME,FUNC,N)
      IPRINT =0
      IF(IP.EQ.1)IPRINT=1
      CALL LSTSQU(TIME,FUNC,N,RATED,INTCPT,IPRINT)
C
C     SET UP ARRAY RASS(J) WITH SUCCESSIVE VALUES OF KOBS
      RASS(IP)=RATED*EQCON/EKAC
  100 CONTINUE
C
      PRINT 200,(J,RASS(J),J=1,IPNO)
  200 FORMAT(///(6(6H KOBS(I2,2H)=E10.3)))
```

APPENDIX 1.2

```
C       CALCULATE MEAN RATE CONSTANT AND P.E. IN MEAN RATE FOR RUN
        SR=SDD=0.0
        DO 201 J=1,IPNO
  201   SR=SR+RASS(J)
        AVR=SR/IPNO
        DO 202 J=1,IPNO
        DR(J)=AVR-RASS(J)
  202   SDD=SDD+DR(J)*DR(J)
        PPEAVR=67.45*SQRT(SDD/((IPNO-1)*IPNO))/AVR
C
C        PUNCH AND PRINT SUMMARY OF OUTPUT
        PUNCH 203,IRNO,CONCAO,CONCB,CONCDO,TEMP,AVR,PPEAVR
  203   FORMAT(I4,3E10.3,F6.2,E10.3,F4.1)
        PRINT 204,IRNO,CONCAO,CONCB,CONCDO,TEMP,AVR,PPEAVR
  204   FORMAT(//* FOR RUN *I4* CONCAO= *E10.3*,CONCB= *E10.3*,CONCDO= *
       1E10.3*,TEMP= *F6.2/14X*MEAN RATE CONSTANT= *E10.3*,P.E. RATE= *
       1F4.1)
C
        GO TO 99
        END
```

APPENDIX 1.2

```
        SUBROUTINE DTATRY(X,Y,N)
C       TESTS AND REJECTS POINTS OUTSIDE EXPERIMENTAL ERROR
C       STRAIGHT LINE RELATIONSHIP ONLY
C
C
        DIMENSION X(40),Y(40),DEVN(40),MESAGE(16)
        REAL MDEVN
        K=1
        GO TO 1
   99   N=I-1
        K=K+1
    1   I=2
        SS=SDEVN=0
        DO 10 J=2,N
   10   SS=SS+Y(J)/X(J)
        SMEAN=SS/(N-1)
        DO 11 J=2,N
        DEVN(J)=ABS(Y(J)-SMEAN*X(J))
   11   SDEVN=SDEVN+DEVN(J)
        MDEVN=SDEVN/(N-1)
        IF(K.EQ.5)100,30
C
C       REJECTION OF DATA POINTS WITH DEVN GREATER THAN 4*MEAN DEVN
   30   DO 33 J=2,N
        IF (DEVN(J).GT.4*MDEVN) 31,32
   31   CONTINUE
        GO TO 33
   32   X(I)=X(J)
        Y(I)=Y(J)
        I=I+1
   33   CONTINUE
        IF ((I-1).LT.N)99,100
  100   CONTINUE
        RETURN
        END
```

APPENDIX 1.2

```
      SUBROUTINE CONCS(CONCA,CONCB,CONCDO,CONCD,CONCCEQ,EKH,EQDI,
     1EQKA,EQCON)
      FET1=2.0*CONCA  $  ACIDF1=ACIDO1=2.0*(CONCDO+CONCB)
      NTRIAL=0
   10 ACTEM=ACIDF1
      NTRIAL=NTRIAL+1
      AA=1.0+EQKH/ACIDF1
      FEF1=(SQRT(AA*AA+8.0*EQDI*FET1/(ACIDF1*ACIDF1))-AA)*ACIDF1*ACIDF1
     1/(4.0*EQDI)
      FEOH1=FEF1*EQKH/ACIDF1
      FEDI1=FEF1*FEF1*EQDI/(ACIDF1*ACIDF1)
      ACIDF1=ACIDO1+FEOH1+2.0*FEDI1
      DIFF=ABS((ACIDF1-ACTEM)*100.0/ACIDF1)
      IF(NTRIAL.EQ.20) GO TO 39
      IF(DIFF.LT.0.01)12,10
   12 PRINT 13,FET1,FEF1,FEOH1,FEDI1,ACIDF1,NTRIAL
   13 FORMAT(6H FET1=E10.3,6H FEF1=E10.3,7H FEOH1=E10.3,7H FEDI1=E10.3,
     18H ACIDF1=E10.3,8H NTRIAL=I3)
      FET3=(FEF1+FEOH1)/2.0  $  ACIDO3=(ACIDF1-FEOH1)/2.0
      AZT3=CONCB  $  ACIDF3=ACIDO3-AZT3
      NTRIAL=0
   20 ACTEM=ACIDF3
      NTRIAL=NTRIAL+1
      HN3=AZT3/(1.0+EQKA/ACIDF3)
      FEOH3=FET3/(1.0+EQKH/ACIDF3)*EQKH/ACIDF3
      ACIDF3=ACIDO3-HN3+FEOH3
      DIFF=ABS((ACTEM-ACIDF3)*100.0/ACIDF3)
      IF(NTRIAL.EQ.20) GO TO 39
      IF(DIFF.LT.0.01)22,20
   22 PRINT 23,FET3,FEOH3,AZT3,HN3,ACIDF3,NTRIAL
   23 FORMAT(6H FET3=E10.3,7H FEOH3=E10.3,6H AZT3=E10.3,5H HN3=E10.3,
     18H ACIDF3=E10.3,8H NTRIAL=I3)
      CONCA=FET3  $  CONCB=AZT3  $  CONCD=ACIDF3
      FET4=FET1/2.0  $  ACIDO4=ACIDO1/2.0  $  HN4=HN3  $  AZT4=AZT3
      ACIDF4=ACIDF3
      NTRIAL=0
   30 ACTEM=ACIDF4
      NTRIAL=NTRIAL+1
      BB=1.0+EQKH/ACIDF4+EQCON*HN4/ACIDF4
      FEF4=(SQRT(BB*BB+8.0*EQDI*FET4/(ACIDF4*ACIDF4))-BB)*ACIDF4*ACIDF4
     1/(4.0*EQDI)
      FEOH4=FEF4*EQKH/ACIDF4
      FEDI4=FEF4*FEF4*EQDI/(ACIDF4*ACIDF4)
      FEN4=FEF4*EQCON*HN4/ACIDF4
      HN4=(AZT4-FEN4)/(1.0+EQKA/ACIDF4)
      ACIDF4=ACIDO4+FEOH4+2.0*FEDI4-HN4
      DIFF=ABS((ACTEM-ACIDF4)*100.0/ACIDF4)
      IF(NTRIAL.EQ.40) GO TO 39
      IF(DIFF.LT.0.01)32,30
   32 PRINT 33,FET4,FEF4,FEOH4,FEDI4,ACIDF4,HN4,FEN4,NTRIAL
   33 FORMAT(6H FET4=E10.3,6H FEF4=E10.3,7H FEOH4=E10.3,7H FEDI4=E10.3,
     18H ACIDF4=E10.4,5H HN4=E10.3,6H FEN4=E10.3,8H NTRIAL=I3)
      CONCCEQ=FEN4
      RETURN
   39 PRINT 40
   40 FORMAT(44H  NTRIAL LIMIT EXCEEDED,EXECUTION TERMINATED)
      STOP
      END
```

APPENDIX 1.2

```
      SUBROUTINE LSTSQU(X,Y,N,SLOPE,INTCPT,PTEST)
******SEE APPENDIX 1.1
```

```
      PROGRAM HTDP13(INPUT,OUTPUT)
C
C
C     REDUCTION OF ACID DEPENDENCE OF OBSERVED RATE CONSTANT FOR
C     FERRIC/AZIDE INTERACTIONS .
C     ASSUME POSSIBLE CONTRIBUTING PATHS AS ...
C     (FE+3)+(N3-) =(FEN3+2)+(H2O)      K1
C     (FEOH+2)+(N3-) = (FEN3+2)+(OH-)   K2
C     (FE+3)+(HN3) =(FEN3+2)+(H+)       K3
C     (FEOH+2)+(HN3) =(FEN3+2)+(H2O)    K4
C
C     **DATA MUST BE IN ORDER OF DECREASING ACID
C
C
      DIMENSION IRNO(20),FETO(20),AZTO(20),ACIDO(20),ACID(20),TEMP(20),
     1RKOBS(20)
      DIMENSION RKREC(40,20),ACREC(40,20),RRKOBS(20),RRRKO(20),RECAC(20)
     1,RCAC2(20),RK1(20),RK2(20),RK3(20),RK4(20),ERK1(20),ERK2(20),
     1ERK3(20),ERK4(20),RLCTEM(20),EQKH(40),EQKA(40)
      DIMENSION EACT(10),EFACT(10),SACT(10),ESACT(10)
      DIMENSION RKOBSP(20),RECACP(20),RRRKOP(20),RCAC2P(20),HCON(20)
      DIMENSION EQDI(40),EQCON(40)
C
      DATA PLANCK,BOLTZK/6.625E-27,1.380E-16/
C     DATA FOLLOWING IS FOR H2O RUNS AT MU=0.50
      DATA DELHEQ,DELSEQ/ 2520.0,8.23/
      DATA DELHH,DELSH/ 10300.0,22.96/
      DATA DELHDI,DELSDI/12800.0,30.0/
      DATA DELHA,DELSA/ 3600.0,-8.34/
      CALCK(H,S,T)=EXP((S-H/(273.2+T))/1.9865)
C
      PRINT 500
  500 FORMAT(1H1)
      M=0
C
C
C     CALCULATE EQUILIBRIUM CONSTANTS AT REQUIRED TEMPERATURES
      DO 6 I=10,40,5
      EQCON(I)=CALCK(DELHEQ,DELSEQ,FLOAT(I))
      EQKH(I)=CALCK(DELHH,DELSH,FLOAT(I))
      EQDI(I)=CALCK(DELHDI,DELSDI,FLOAT(I))
      EQKA(I)=CALCK(DELHA,DELSA,FLOAT(I))
    6 CONTINUE
C
   99 READ 1,N
    1 FORMAT (I3)
      IF(N.EQ.0)100,2
C
C     READ DATA FOR GIVEN ACID CONCENTRATION
    2 READ 3,(IRNO(J),FETO(J),AZTO(J),ACIDO(J),TEMP(J),RKOBS(J),PE,
     1J=1,N)
    3 FORMAT(A4,3E10.3,F6.2,F10.3,F4.1)
C
C     ASSUME R*LN(KOBS) VS 1/TEMP IS LINEAR ,RECALCULATE KOBS AT REQUIRED TEMPS
      PRINT 4,ACIDO(1)
    4 FORMAT(1X22HR*LNKOBS VS 1/T FOR H=E7.4)
```

```
      PRINT 44,(IRNO(J),J=1,M)
   44 FORMAT(26H RUNS SENT TO TEMDER ARE  9(1XA4,1H,))
      CALL TEMDER(RKOBS,TEMP,M,DELH,DELS,SEH,SES,0)
      M=M+1
      DO 5 I=10,40,5
      RKREC(I,M)=(BOLTZK*(273.2+FLOAT(I))/PLANCK)*CALCK(DELH,DELS,FLOAT(
     1I))
C
C     CALCULATE HYDROLYSIS AND TEMP CORRECTIONS TO ACID CONCENTRATION
    5 CALL CONCS(FETO(1),AZTO(1),ACIDO(1),ACREC(I,M),DUMMY,EQKH(I),
     1EQDI(I),EQKA(I),EQCON(I))
      GO TO 99
C
  100 CONTINUE
      DO 115 JRUN=1,3
C
C     DEFINE ACID LIMITS WHERE PATH 2 IS TO BE CONSIDERED SIGNIFICANT
      GO TO(52,53,54) JRUN
   52 DIV12=DIV21=0.050  $  GO TO 59
   53 DIV12=0.050  $  DIV21=0.10  $  GO TO 59
   54 DIV12=DIV21=0.050  $  GO TO 59
   59 CONTINUE
C
      DO 57 J=1,20
   57 PK2(J)=RECACP(J)=RRKCP(J)=RCAC2P(J)=0.0
C
C
      DO 40 NO=1,5
      L=0
      IF(NO.EQ.5)48,49
   48 PRINT 12,JRUN,NO
   12 FORMAT(1H1//* JRUN= *I3*    TRIAL NUMBER= *I2//)
   49 IF(JRUN.EQ.3.AND.NO.GT.1)50,51
   50 DIV12=0.0
      DIV21=1.0
   51 CONTINUE
C
C
      DO 20 I=10,40,5
      K=KL=KP=0
C
C     SET UP ONE DIMENSIONAL ARRAYS OF ACID(J) AND OBSERVED RATE CONSTANT
C     CORRECT KOBS FOR PATH 2 IF DATA OF PREVIOUS TRIALS IS AVAILABLE
      DO 14 J=1,M
      ACID(J)=ACREC(I,J)
      RRKOBS(J)=RKREC(I,J)-RK2(I/5-1)*EQKH(I)/ACID(J)
C
C     SEPARATE DATA INTO REGIONS WHERE PATH 2 IS/IS NOT CONSIDERED SIGNIFICANT
      IF(ACID(J).GT.DIV12)60,61
   60 K=K+1
   61 IF(ACID(J).GT.DIV21)62,63
   62 KP=KP+1
   63 CONTINUE
   14 CONTINUE
C
C     CALC. LEAST SQUARES SLOPE OF KOBS, CORRECTED FOR PATH 2, VS ACID CONC.
      CALL LSTSQU(ACID,RRKOBS,K,RS,RT,RES,RET,0)
```

```
C     CORRECT KOBS FOR CONTRIBUTIONS OF PATH 1/4 AND PATH 3 TO DETERMINE
C     EFFECT OF PATH 2
      KP=KP+1
      DO 15 J=KP,M
      KL=KL+1
      RRRKO(KL)=RKREC(I,J)-RS*ACID(J)-RT
   15 RECAC(KL)=1.0/ACID(J)
      KL=KL+1
      RRRKO(KL)=0.0
      RECAC(KL)=0.0
C
C     CALC. LEASTSQUARES SLOPE OF CONTRIB. OF PATH 2 VS 1/(ACID CONC.)
      CALL LSTSQU(RECAC,RRRKO,KL,RRS,RRT,RRES,RRET,0)
C
C     CALCULATE RATE CONSTANTS AND ERRORS IN RATE CONSTANTS
      L=L+1
      TEMP(L)=I
      RECTEM(L)=1.0/(273.2+I)
      RK1(L)=RT
      RK2(L)=RRS/EQKH(I)
      RK3(L)=RS*EQKA(I)
      RK4(L)=RT*EQKA(I)/EQKH(I)
      ERK1(L)=ERK4(L)=RET*100.0/RT
      ERK2(L)=RRES*100.0/RRS
      ERK3(L)=RES*100.0/RS
C
C     PRINT DATA AND CONTRIBUTIONS OF VARIOUS PATHS FOR FIFTH TRIAL AND
C     AT 25.0 DEGREES.
      IF(NO.EQ.5.AND.I.EQ.25)16,20
   16 PRINT 17,I
   17 FORMAT(//10H FOR TEMP=I3,4X5HRKREC10X4HACID10X6HRRKOBS11X5HRRRKO11X
     13H1/H)
      DO 18 J=1,KL
      RRRKOP(KP-1+J)=RRRKO(J)
   18 RECACP(KP-1+J)=RECAC(J)
      PRINT 19,(RKREC(I,J),ACID(J),RRKOBS(J),RRRKOP(J),RECACP(J),J=1,M)
   19 FORMAT(8X5(5XE10.3))
   20 CONTINUE
   40 CONTINUE
C
C     PRINT RATE CONSTANTS AND ERRORS FOR EACH SET OF CONDITIONS DEFINED
C     BY DIV12 AND DIV21
      PRINT 27
   27 FORMAT(//1CX4HTEMP13X3HRK14X8HP/C S.E.8X3HRK24X8HP/C S.E.8X3HRK34X
     18HP/C S.E.8X3HRK44X8HP/C S.E.)
      PRINT 28,(TEMP(J),RK1(J),ERK1(J),RK2(J),ERK2(J),RK3(J),ERK3(J),RK4
     1(J),ERK4(J),J=1,L)
   28 FORMAT(6XE10.3,4(E17.3,F6.1))
C
C     CALCULATE ACTIVATION PARAMETERS FOR EACH PATH
      PRINT 26
   26 FORMAT(1H1)
      PRINT 31
   31 FORMAT(/1X21HTEMP DEPENDENCE OF K1)
      CALL TEMDEP(RK1,TEMP,L,EACT(1),SACT(1),EEACT(1),ESACT(1),1)
      PRINT 32
   32 FORMAT(/1X21HTEMP DEPENDENCE OF K2)
      CALL TEMDEP(RK2,TEMP,L,EACT(2),SACT(2),EEACT(2),ESACT(2),1)
```

```
      PRINT 33
   33 FORMAT(/1X21HTEMP DEPENDENCE OF K3)
      CALL TEMDEP(RK3,TEMP,L,EACT(3),SACT(3),EEACT(3),ESACT(3),1)
      PRINT 34
   34 FORMAT(/1X21HTEMP DEPENDENCE OF K4)
      CALL TEMDEP(RK4,TEMP,L,EACT(4),SACT(4),EEACT(4),ESACT(4),1)
C
C
C     FOR CONDITIONS WHERE ALL POINTS ARE CONSIDERED CALCULATE AND PRINT VALUES
C     OF KOBS AT VARIOUS ACID CONCS FROM  VALUES OF K1,K2,K3, AND K4.
      IF(JRUN.NE.3) GO TO 115
  110 PRINT 111
  111 FORMAT(1H1,26H CALCULATED VALUES OF KOBS//)
      DO 114 I=10,49,15
      PRINT 112,I
  112 FORMAT(//13H TEMPERATURE=I3//5X4HACID14X5HKCALC)
      HCON(1)=0.007071
      DO 114 J=1,14
      RKCALC=RK1(I/5-1)+RK2(I/5-1)*EQKH(I)/HCON(J)+RK3(I/5-1)*HCON(J)/
     1EQKA(I)
      PRINT 113,HCON(J),RKCALC
  113 FORMAT(8X,F16.3,F20.2)
  114 HCON(J+1)=HCON(J)*1.4142
C
C
  115 CONTINUE
      STOP
      END


      SUBROUTINE TEMDEP(RK,T,N,DELH,DELS,SEH,SES,PTEST)
      DIMENSION RK(40),T(40),RECTEM(40),A(40)
      INTEGER PTEST,TEST
      DATA PLANCK,BOLTZK,R/6.625E-27,1.3804E-16,1.9865/
      TEST=0
      DO 10 J=1,N
      RECTEM(J)=1.0/(273.2+T(J))
      A(J)=R*ALOG(RK(J)*PLANCK*RECTEM(J)/BOLTZK)
      PRINT 9,T(J),RK(J),A(J),RECTEM(J)
    9 FORMAT(10X*TEMP= *F10.3*   KOBS= *E10.3*   R.LN(KOBS)= *E10.3
     1*   1/(ABS. TEMP)= *E10.3)
   10 CONTINUE
      IF(PTEST.EQ.0)TEST=1
      CALL LSTSQU(RECTEM,A,N,DELH,DELS,SEH,SES,TEST)
      DELH=-DELH
      IF (PTEST.EQ.0)RETURN
      SACTE=SEH/1000.0
      ACTE=DELH/1000.0
      PRINT 20,ACTE,SACTE,DELS,SES
   20 FORMAT (044H SUBROUTINE TEMDEP GIVES ACTIVATION ENERGY  F8.2,F9.3,
     1 10H   KILOCAL,5X21HENTROPY OF ACTIVATION,F9.2,F9.3,7H   E.U.)
      RETURN
      END
```

APPENDIX 1.3

```
      SUBROUTINE LSTSQU(X,Y,N,SLOPE,INTCPT,SERS,SERINT,PTEST)
******SEE APPENDIX 1.1
```

APPENDIX 1.3

```
      SUBROUTINE CONCS(CONCA,CONCB,CONCDO,CONCD(CONCCEQ,EQKII,EQDI(
     1EQKA,EQCON)
******SEE APPENDIX 1.2
```

APPENDIX 2

APPARATUS

1. Stopped flow apparatus.

(i) Description.

Initial kinetic experiments were performed on a stopped flow apparatus built from plans provided by Professor J. M. Sturtevant, and which has been described adequately elsewhere (64S). The drive was modified by addition of a pneumatic actuator to the syringe piston trolley; this was found to increase the reproducibility of kinetic results by a factor of about 5 over measurements for injection by hand. The actuator was operated with compressed nitrogen at 40 - 60 p.s.i. applied via a quick release valve which could be fully opened in ca. 0.01 seconds. At each push 0.45ml of each reactant was injected in 60 - 100 milliseconds, depending on the drive pressure; injection times, and therefore flow rates and 'dead time' between mixing and first observation were found to be reproducible to 1-2% for a given driving pressure. This system appears to be as effective as the hydraulic and motor drives used by other workers (64Gi, 63D).

On the basis of the experience gained with this apparatus (hereafter referred to as Mk.II), another stopped flow apparatus (Mk.III) was designed and built, with the hope of overcoming some of the disadvantages of the Mk.II apparatus, and having some features which the other machine had not. The Mk.III apparatus is shown and

design drawings of the major parts are given in FIGURES A2.1 to A2.27.

The main design points of the apparatus, and differences between it and the Mk.II apparatus will be discussed.

The apparatus is designed on a fully horizontal format, in contrast to the vertical cell and overflow of the Mk.II. This is to minimise the marked diffusion of reactants of different density through the vertical cell from the mixing chamber directly below, a few seconds after the flow has stopped. This has been pointed out by Sturtevant (64S) and observed in this work.

The apparatus is essentially modular in construction, compared with the 'unified' form of the Mk.II, to allow for the probable redesign of individual sections for application to a particular chemical problem. Many designs, for instance, have been published for mixing chambers, operation at very high flow velocities (68B) or very low resistance to fluid flow; these could be incorporated into the apparatus without affecting the operation of the other components.

In relation to the problem of diffusion of reactants mentioned above, a number of designs for a small, one way valve, which would open under the pressure of fluid flow and close when the flow stopped, were built in anticipation of placing one between the mixer and the observation cell and another directly after the cell to prevent back diffusion of reacted solution. This would allow slower reactions at present disturbed by the effects of diffusion to be studied. For faster reactions, where the extra dead time introduced

FIGURE A2.1. STOPPED FLOW ASSEMBLY

A. Driving syringes
B. Front end plate
C. Three way tap assembly
D. Front mixer gasket
E. Mixer
F. Rear mixer gasket
G. Reserve syringe
H. Reserve syringe block
I. Optical observation cell
J. Cell block
K. Exit block
L. Outlet tube
M. Rear end plate

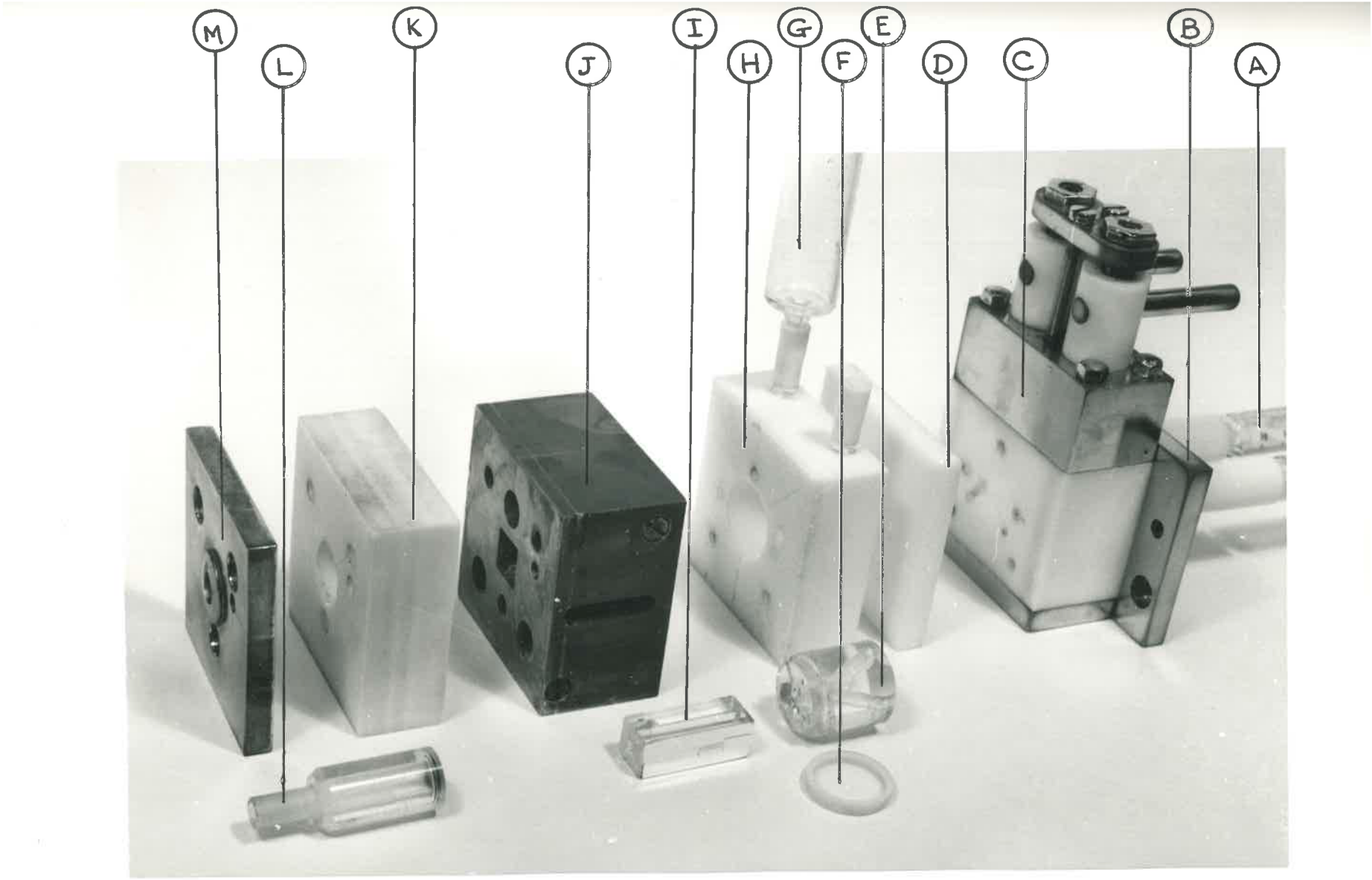
M
L
K
J
I
H
G
F
E
D
C
B
A

FIGURE A2.2. APPARATUS ASSEMBLED, THERMAL PANELS REMOVED

A. Pneumatic drive piston
B. Syringe piston trolley
C. Stopping peg
D. Trigger microswitch
E. Driving syringe pistons
F. Driving syringes
G. Three way valve assembly

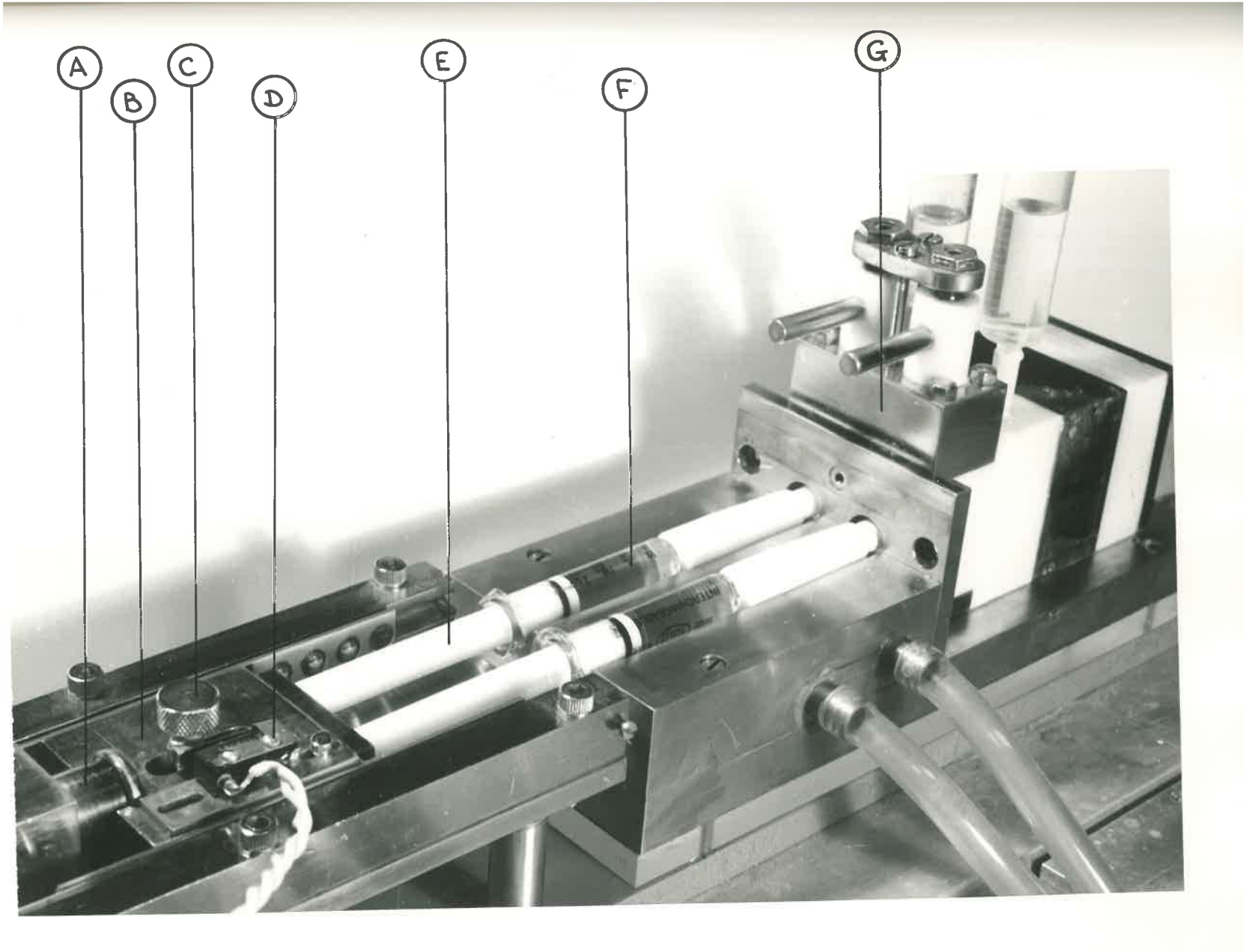
A
B
C
D
E
F
G

FIGURE A2.3. STOPPED FLOW APPARATUS AND OBSERVATION SYSTEM

A. Lamp housing
B. Light collection/monochromator input lenses
C. Monochromator
D. Monochromator exit lens system
E. Stopped flow apparatus
F. Photomultiplier housing

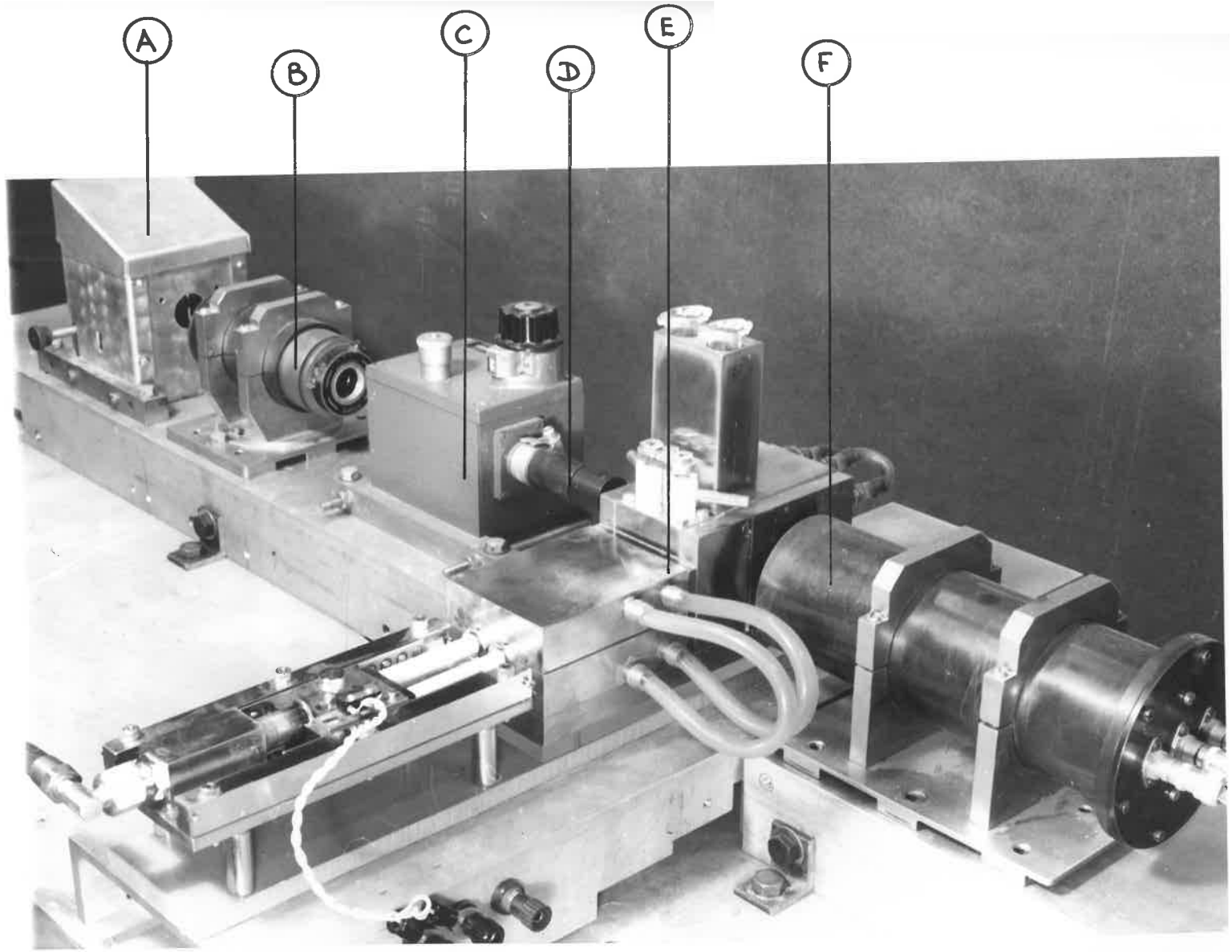
A
B
C
D
E
F

is a disadvantage and diffusion a minor problem, the valves could be removed.

The design and inclusion of different path length optical cells, including the possibility of measuring absorption by the solution along the observation tube (64Gi), of conductance (65T) or pH cells (58S) to measure the reaction parameter of interest can be undertaken without disturbing the design of the rest of the apparatus.

Wherever possible, sealing between the various sections is made between flat Teflon surfaces lapped on a surface plate. The separate modules are drawn together by long bolts running the length of the assembly. The threeway taps to the reserve syringes use a flat face seal rather than the conventional conical taps and seats used in the Mk.II apparatus; after some use the conical taps were found to settle into the seats misalligning the tap passages. In only two places, between the perspex mixer and the quartz observation cell and between the cell and the perspex exit assembly were Teflon gaskets or neoprene O-rings used to affect the seal.

Using linear V-guides and bearings, the trolley linking the syringe plungers was restrained from as much motion, other than parallel to the syringes, as possible, to avoid the possibility of injection of unequal volumes of reactants. With the driving syringes used (bore 9mm), excess movement of one piston by 15/1000" is sufficient to inject fresh solution from the mixer to the observa-

tion point; with the trolley system of the Mk.II apparatus, this degree of twist is certainly possible, although reproducibility of rate constants using the apparatus suggests that it is unlikely.

In the Mk.II apparatus the thermal panels provided mechanical support for the flow assembly, as well as circulating thermostatted water. In the Mk.III, the flow assembly was attached separately to the base of the apparatus. Because of the block design of the complete flow assembly, thermal panels could be of a simpler construction and design, while still having a high thermostatting efficiency for all parts of the apparatus, to make adaption to changes in the design or type of observation equipment more straight forward, should it be necessary.

(ii) Performance.

(a) Injection.

Driving syringes were 2ml all glass Van interchangeable types, chosen because of their necessarily similar bores. The reproducibility of injection ratios was measured by weighing the amount of water simultaneously delivered by a pair of syringes, and by measuring the optical density of solutions when a dye and water were mixed in the apparatus. These measurements suggested that injection volumes were equal and constant to within 1%, both for injection between the same and different trolley positions. For each run, 0.45ml of each reactant were injected.

Velocity profiles during injection were measured on the

Mk.II apparatus using a vane, attached to a syringe accepting spent solution from the observation cell, which partially interrupted a light beam falling on a photocell; the signal from the photocell was proportional to the vane position, i.e. the volume of expended solution, and the electrically differentiated signal proportional to the vane velocity. The flow acceleration and velocity using the pneumatic drive were reproducible to 1 - 2%, constant velocity being reached after about 30 milliseconds in a 60 millisecond push. The differentiated signal suggested a deceleration, when the trolley hit the stopping peg, from maximum velocity to zero in 1.5 milliseconds. The system used by Sturtevant and included in the Mk.III model for stopping the flow, by bringing the syringe trolley against a solid stop seems as effective as the stopping syringe used by Gibson and others (64Gi, 63D, 58S), which subject the seals within the apparatus to considerable pressure.

Corresponding measurements on the Mk.III apparatus, but using the signal from a potentiometer, the spindle of which was attached via a lever to the syringe trolley, as a measure of the trolley position gave very similar velocity profiles.

Under these conditions, velocity of fluid past the observation point just prior to stopping was 2.5 to 4 metres/second. For continuous flow studies it is desirable that the flow of liquid at the observation point should be turbulent, to ensure that the distribution of fluid velocity past the observation point is the

closest approximation possible to mass flow (53D). In stopped flow studies the systematic errors produced by deviations from mass flow, i.e. the errors in computing the average age of the sample at different distances down the observation tube from the volume flow rate, compared to the 'true' average age, which will depend on the velocity profiles, do not arise (54C). Turbulent flow, however, also ensures more efficient mixing of reactants. For water in the standard observation cell used (2mm x 2mm), the critical velocity for turbulent flow is expected to be well below 1 metre/second.

(b) Mixing.

Sturtevant (62R) has suggested that reactions with half times of a few milliseconds could be studied with his apparatus. We have tested the efficiency of mixing in the Mk.II apparatus by measuring the optical density of injected dye/water mixtures, and by measuring the conductance of perchloric acid mixtures using the conductance cell and detection system described in reference 65T; traces showed no curvature after the flow had stopped, suggesting complete mixing by the time of first observation.

The mixing chamber of the Mk.III apparatus is based on a design by Gibson (64G1), with a preliminary two jet mixer before the main eight jet mixer; it was subjected to the more stringent tests of mixing solutions of different viscosity. The efficiency of mixing solutions containing 5M NaCl with water (relative viscosity 1.9) or 1M NaCl with water (relative viscosity 1.1) was estimated from the

serious schlieren effects produced by concentration gradients in such solutions, resulting in a reduced photomultiplier signal. The mixing of 5M NaCl/water produced an apparent 'optical density' change of 0.02 during injection, which decayed to zero within 1-2 milliseconds after the flow had stopped; for 1M $NaCl/H_2O$ a change of 0.001 during the flow was observed; this can be compared with 0.02 for 5M $NaCl/H_2O$ and 0.008 for 0.6M $NaCl/H_2O$ quoted by Sturtevant (64S).

The efficiency of mixing was found to depend significantly on the flow rate (FIGURE A2.28); optimum conditions were obtained for an injection time of 60 milliseconds. This could explain the marked increase in reproducibility of kinetic results with the introduction of the pneumatic drive.

To obtain a quantitative measure of mixing efficiency, potassium permanganate solutions containing 1M NaCl and water were mixed, and 0.100M NaOH solution containing 1M NaCl and phenolphthalein indicator were mixed with 0.101M perchloric acid. For both of these systems 99.5% mixing had been achieved within 1 - 2 milliseconds after the flow had stopped. For the mixer and observation cell used, the time between the first entry of solutions to the mixer and observation was about 7 milliseconds. As about 65% of this is spent in the mixer, the chamber of the Mk.II, although slightly less efficient, is smaller in volume, and the time between first entry and observation is reduced to 4 milliseconds; because mixing is certainly not complete much before observation, the effective dead time in kinetic

All traces horizontal scale 1 millisec/cm

(a) Injection time 42 milliseconds
Flow velocity in observation tube 5.4 metres/sec.

(b) Injection time 55 milliseconds
Flow velocity in observation tube 4.1 metres/sec.

(c) Injection time 60 milliseconds
Flow velocity in observation tube 3.7 metres/sec.

(d) Injection time 70 milliseconds
Flow velocity in observation tube 3.2 metres/sec.

FIGURE A2.28. SODIUM CHLORIDE/WATER MIXING TESTS

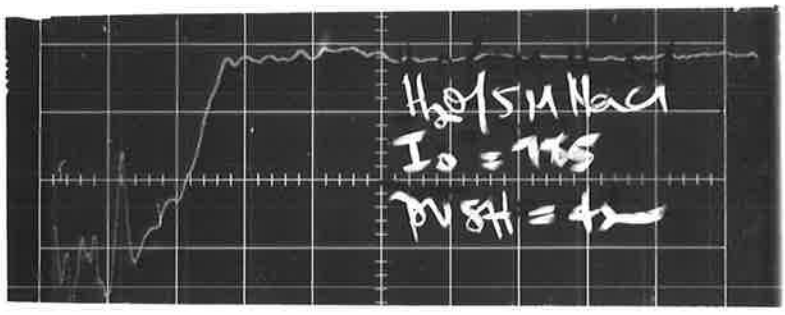
H20/5M NaCl
Io = 785
PUSH = 45

a

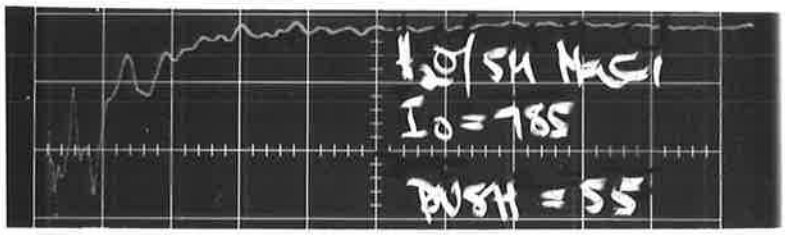
H20/5M NaCl
Io = 785
PUSH = 55

b

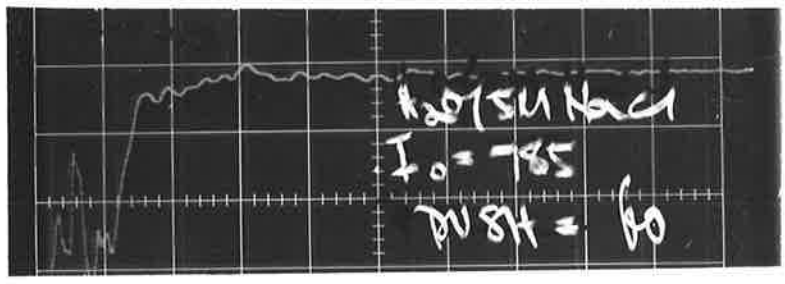
H20/5M NaCl
Io = 785
PUSH = 60

c

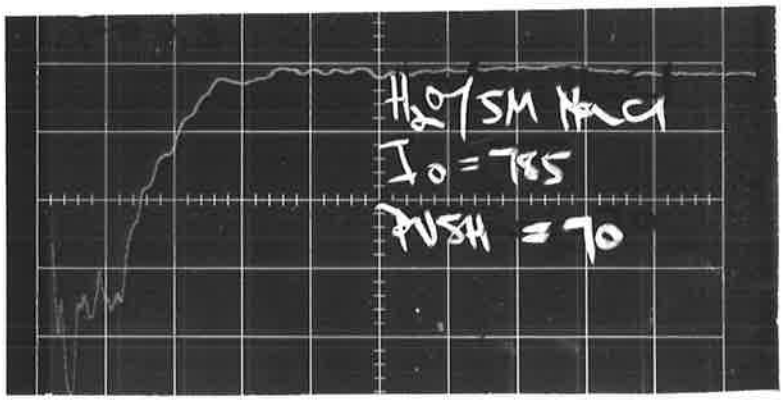
H20/5M NaCl
Io = 785
PUSH = 70

d

experiments performed on the Mk.II apparatus is probably less than this.

Although simultaneous recording of the flow rate was not performed on our Mk.II apparatus, it has been pointed out how this could be used to extrapolate to infinite flow rate (64S) and so correct for reaction taking place before first observation.

2. Spectrophotometric System.

The layout of the optical system is drawn in FIGURE A2.29. To minimise the transmission of vibration induced shock from the flow apparatus to any of the optical components when the flow was stopped, the aluminium channel on which the lamp, lens system and monochromator were mounted, that supporting the photomultiplier housing, and that on which the flow apparatus was mounted, were bolted separately to a heavy slate slab.

The photomultiplier, which was found to be the element most sensitive to vibration in the system, was supported in a two stage antivibration mount within its housing. The face of the observation cell was masked to ensure that all light reaching the photomultiplier had passed through the solution; masking was such that any slight movement of the cell due to shock in the flow apparatus was within the area of the approximately uniformly intense beam, which was significantly larger than the area of the unmasked 'window'.

Using the method described earlier to measure the decelleration of the trolley, it was found that, by sheathing the stopping peg

in 0.5mm thick p.v.c. sleeving, the stopping time was increased by only ½ millisecond, but the induced shock was considerably reduced and a slight bounce in the trolley due to flexing of the peg was entirely eliminated.

Under these conditions, noise on the photomultiplier signal due to shock induced vibration was reduced to ± 0.0003 in optical density, with a frequency of 250 c.p.s., decaying to background light/photomultiplier noise (± 0.0001) in about 70 milliseconds; these results refer to the detection system with a response time of 1 millisecond.

The individual components of the optical and detection system will now be described:

(i) Light source.

Tungsten filament lamps (Philips 13116C/04, 12V, 100W, self focussing type) and quartz/halogen filament type lamps (Philips 7023, 12V, 100W) were used; the quartz/halogen lamps, because of more efficient light output, especially in the U.V. (25% increase at 460 mμ, 100% at 350 mμ) were preferred. The lamp filament image was focussed by a silica lens system (f = 2.0) on the inlet slits of the monochromator; for most efficient location of the image, the lamp housing was fitted with vertical and horizontal positioning screws and the lamp location adjusted for maximum photomultiplier signal.

Lamp power was supplied from a constant voltage power supply,

the circuit for which is given in FIGURE A2.30; the output voltage had a stability of better than 1% for a 10% surge in mains voltage, and ripple on the output was less than 0.2%. The 24 volt negative supply line was from a transformer/full wave diode rectifier bridge/choke system operated from the mains supply.

(ii) Monochromator.

The monochromator (Hilger and Watts, f11 grating type, D292) was modified by addition of a number of baffles to reduce stray light being passed through the instrument; testing with a 4358 Å band pass filter, it was estimated that total background light passed by the monochromator was 0.2% of that at the chosen wavelength.

(iii) Observation cells.

These were 1cm square section silica with a central rectangular section observation tube (2mm x 2mm, 2mm x 1mm); the optical paths were measured with spacers and with standardised absorbance solutions as 0.196 ± 0.001mm and 0.95 ± 0.001mm.

The face of the cell was masked to ensure that all light reaching the photomultiplier passed through the reactant solution; in general, light detected by the photomultiplier, other than that which passed through the solution, was less than 0.02%.

In the Mk.II apparatus used for kinetic measurements, the cell was vertical and the monitoring beam, where it passed through the observation tube, was a focussed image of the horizontal monochromator exit slits; with the lenses used the image was half real size.

Typically, this produced a beam through the observation tube 2mm wide and 1mm high, so that the average age differential of the sample across the observation beam was less than 0.2 milliseconds for a first sample 4 milliseconds old. Under these conditions the 'slit length' error discussed by Roughton (63R) is exceedingly small.

A more subtle effect is that on the observed kinetics due to the reactant concentration profile along the monitoring light beam, as analysed by Boag (68B) for the analogous problem in flash photolysis and pulse radiolysis. For first order reactions no effect is predicted, but for second order reactions, assuming the reactant profile to be proportional to the velocity profile prior to stopping (maximum/mean velocity = 1.25 for turbulent flow (37D)), the predicted effect is less than 1%. The effect on the apparent rate constant is more sensitive to concentration variation across the monitoring light beam, but for our conditions, this is again below 1%.

(iv) Photomultiplier.

The circuit determining the dynode voltages for the photomultiplier (E.M.I. 6256S) is shown in FIGURE A2.31; the E.H.T. supplies used were an Isotope Development type 932/D or a Nuclear Enterprises type NE 5307. To maintain the recommended voltages of 160 volts for the cathode to first dynode, and at least 30 volts for the succeeding interdynode voltages, the minimum E.H.T. is 550 volts. Now the maximum anode current is limited by the necessity to have signals of less than 5 volts (generally ca 4 volts) if it is desired

to operate the oscilloscope 2A63 input amplifier in its differential mode at sensitivities higher than 0.5 volts/cm; under these conditions, the dynode chain current to anode current ratio is around 100. Lush (65Lu) has shown that the output signal should be linear to within 1% for this situation; linearity of output was verified experimentally by attenuating the incident light with standard neutral density filters (Gilford Laboratories/Kodak Ltd.).

To reduce high frequency photomultiplier noise a capacitance filter is included in the circuit; its value was changed, depending on the rate of change of the signal being followed, and, in general, was such that the response time of the photomultiplier was around 10% of the half life of the chemical change. With no such filter in the circuit, photomultiplier signal noise was 5 millivolts on a 4 volts signal, falling to 0.2 millivolts with an 11 millisecond filter; noise increased markedly with increasing E.H.T. The response time of the system was checked using a rapidly rotating sector; results agreed with those predicted from the circuitry.

(v) Backing-off source.

The reference voltage source used to balance the photomultiplier signal so that small changes in the larger photomultiplier signal could be more conveniently measured is shown in FIGURE A2.32. The reference Zener diode output was calibrated as 19.23 volts and checked several times throughout the work.

(vi) Oscilloscope.

The instrument used was a Tektronix 564 Storage Oscilloscope, with type 2A63 differential amplifier and 2B67 time base; the storage and single sweep properties of the 564 made it ideal for the study of transient phenomena.

The photomultiplier was connected to one side of the differential amplifier and the backing-off voltage to the other. The input stage of the 2A63 (1 megohm, 47pf) was used as the anode load for the photomultiplier; the instrument has a response time of 50 microseconds and a typical differential rejection ratio of 1000 to 1 at 20 c.p.s.; the calibrated variable sensitivity is accurate to within 3%.

The 2B67 could be operated at speeds between 5 seconds/cm and 1 microsecond/cm with an accuracy of 3%. The oscilloscope trace was triggered by a d.c. signal produced when a microswitch on the driving syringe trolley was automatically operated sometime during its travel.

Oscilloscope traces were photographed, using a Tektronix C12 oscilloscope camera and 4" x 5" negative film (Kodak TriX).

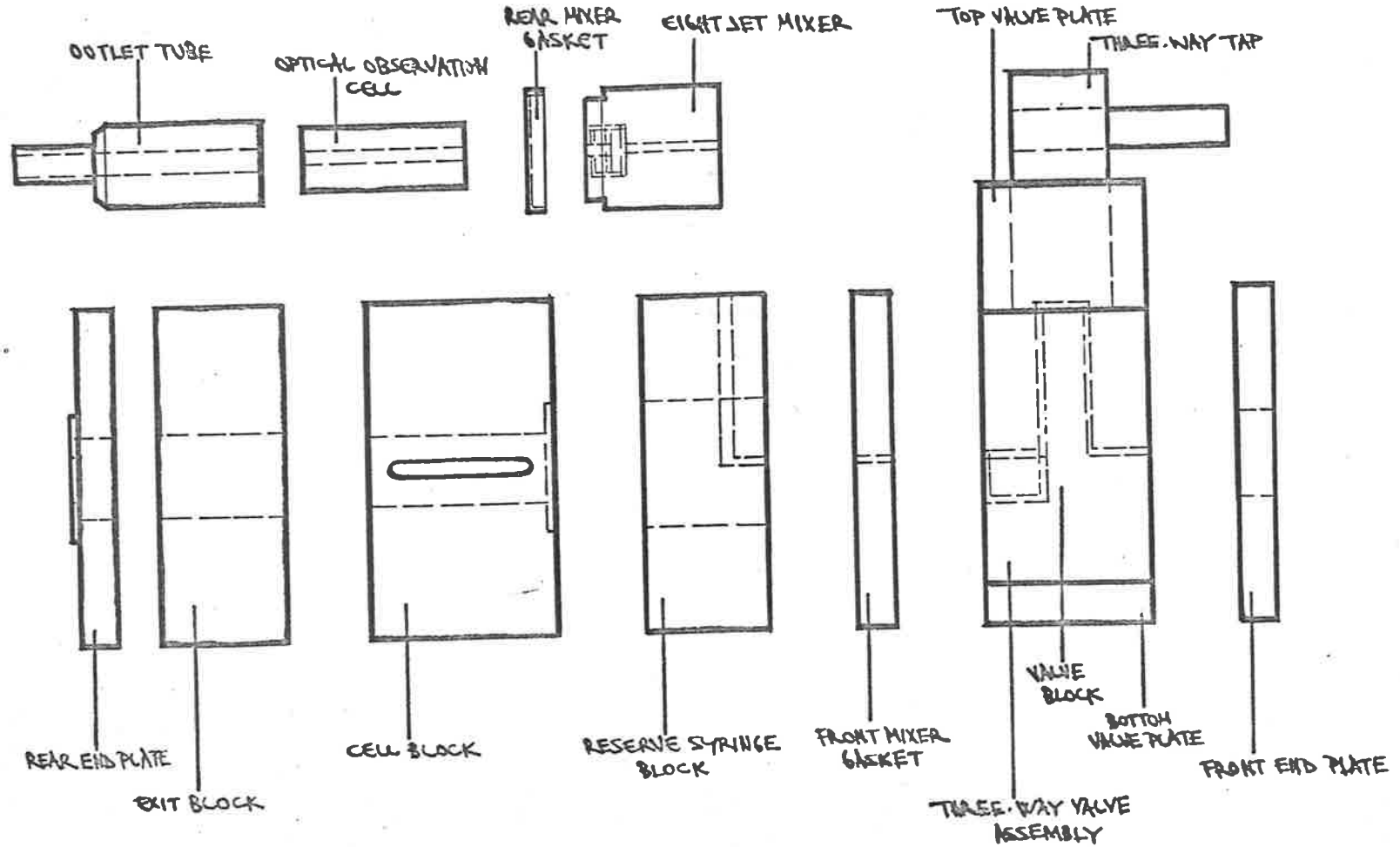

FIGURE A2.4 STOPPED FLOW ASSEMBLY.

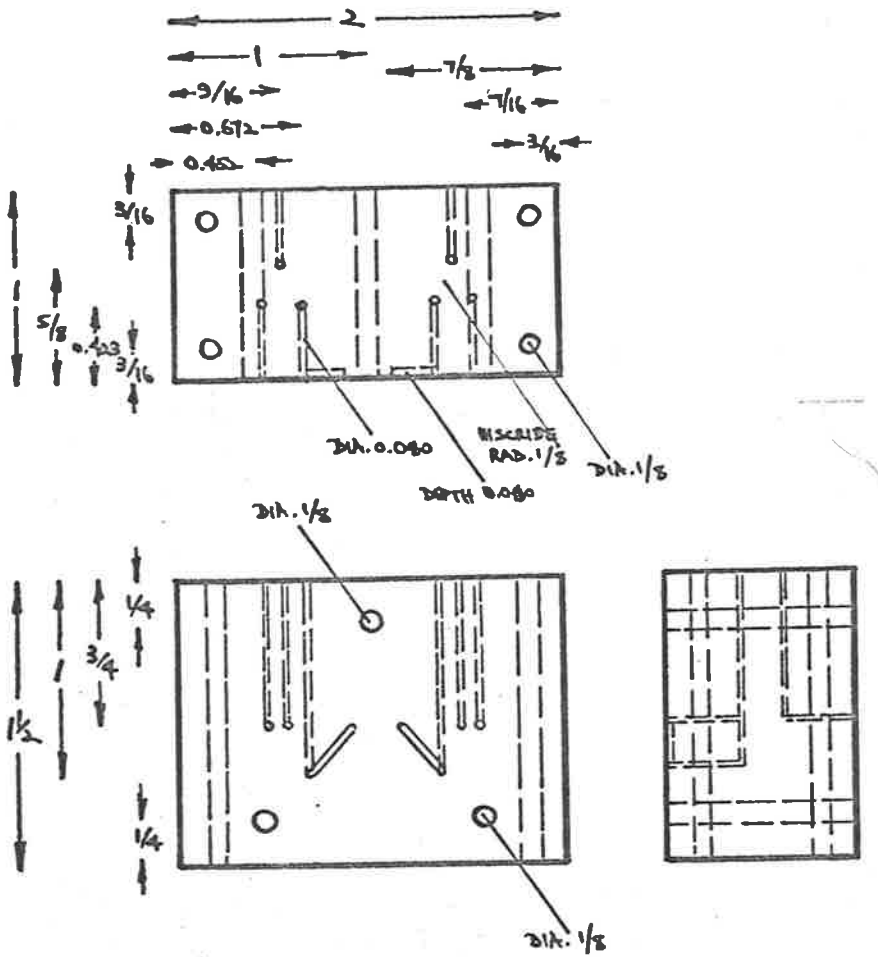

FIG. A2.5 VALVE BLOCK (TEFLON)

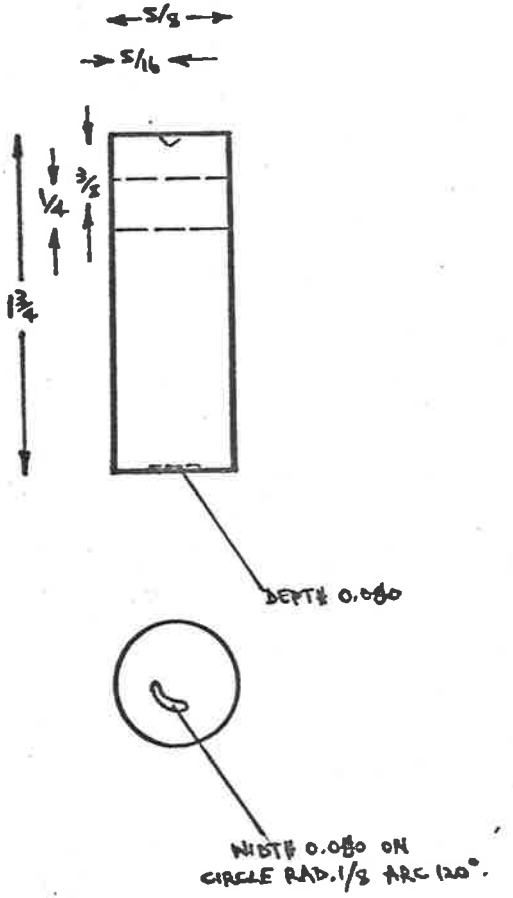

FIG. A2.6 THREE-WAY TAP (TEFLON)

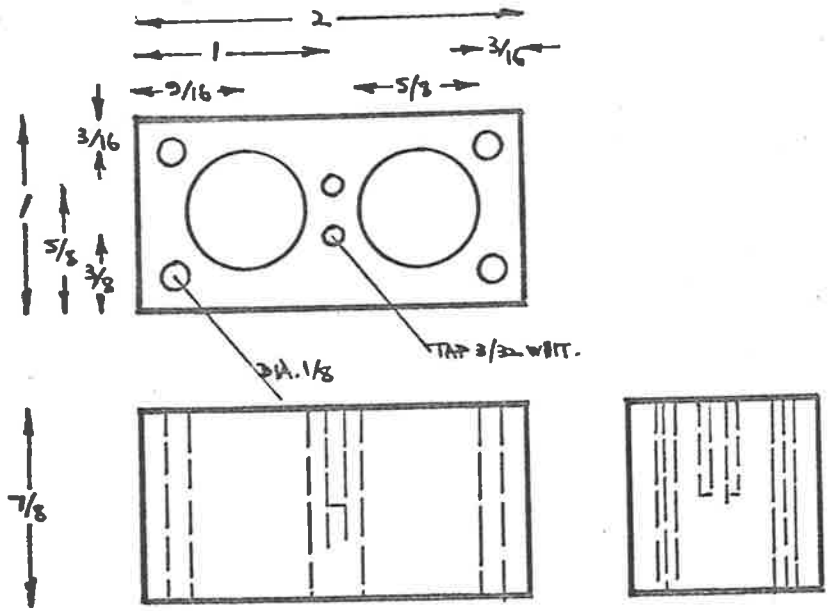

FIG. A2-.7 TOP VALVE PLATE (BRASS)

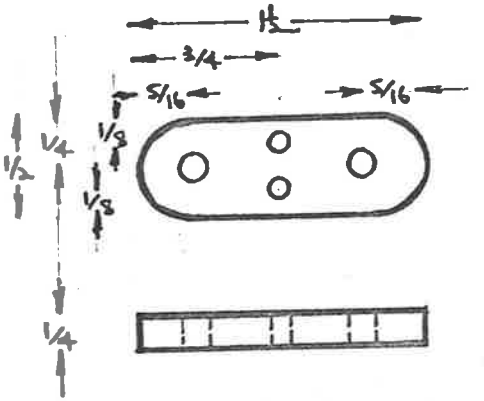

FIG. A2-.9 TAP PRESSURE PLATE (BRASS)

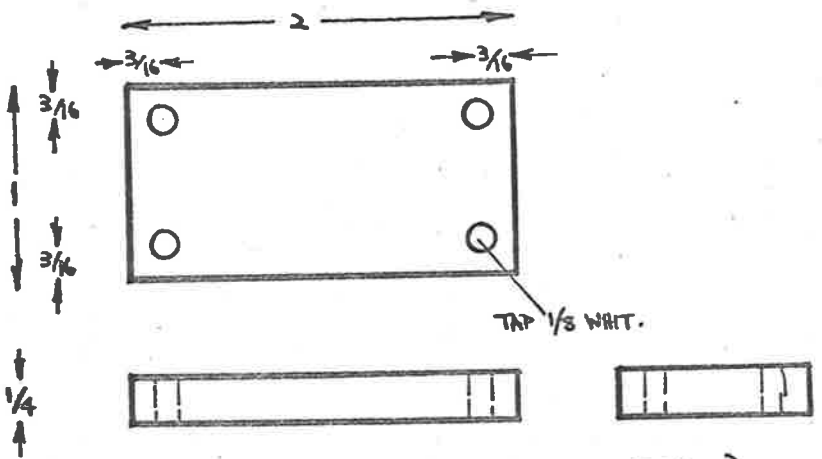

FIG. A2-.8 BOTTOM VALVE PLATE (BRASS)

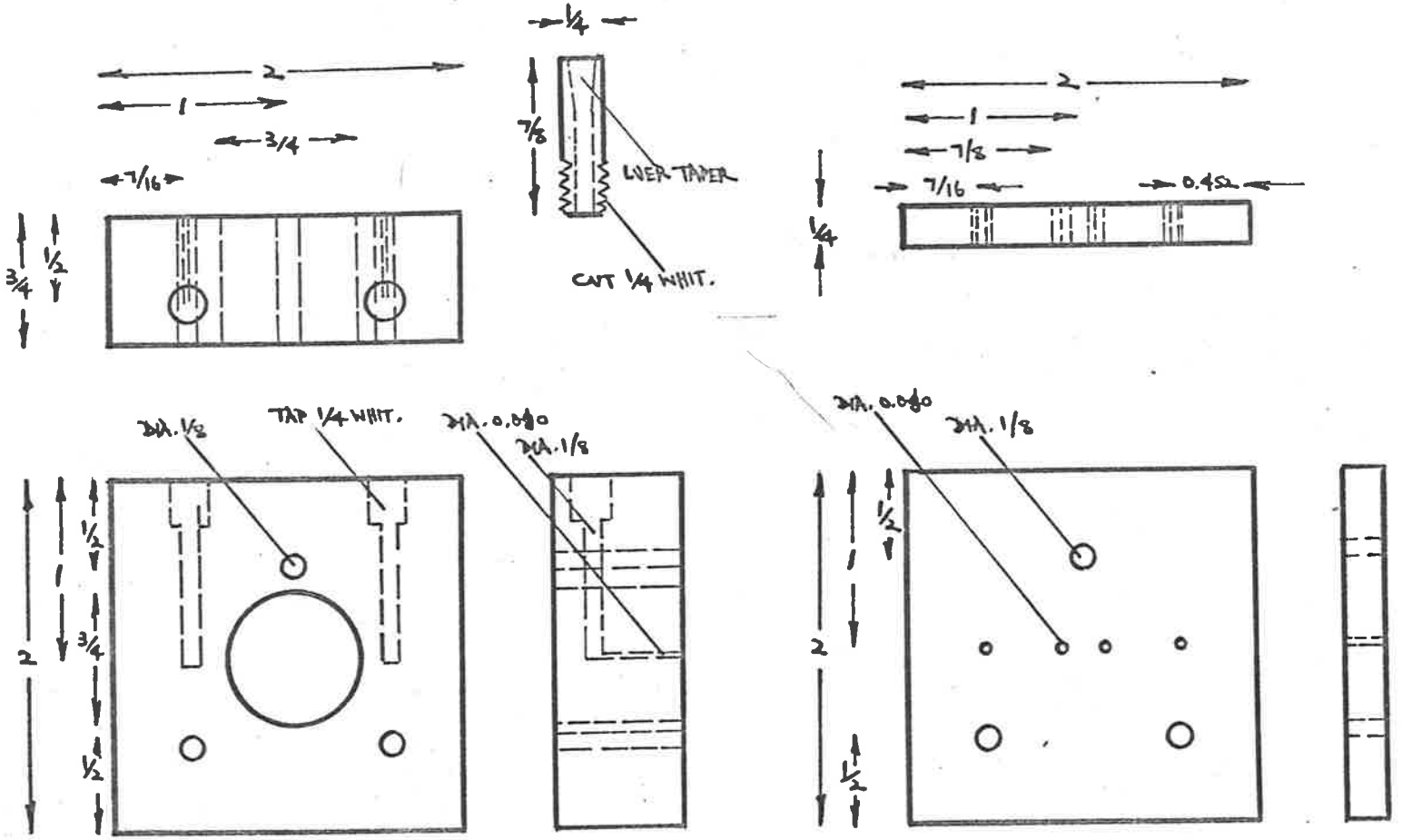

FIG. A2.10 RESERVE SYRINGE BLOCK (TEFLON)

FIG. A2.11 FRONT MIXER GASKET (TEFLON)

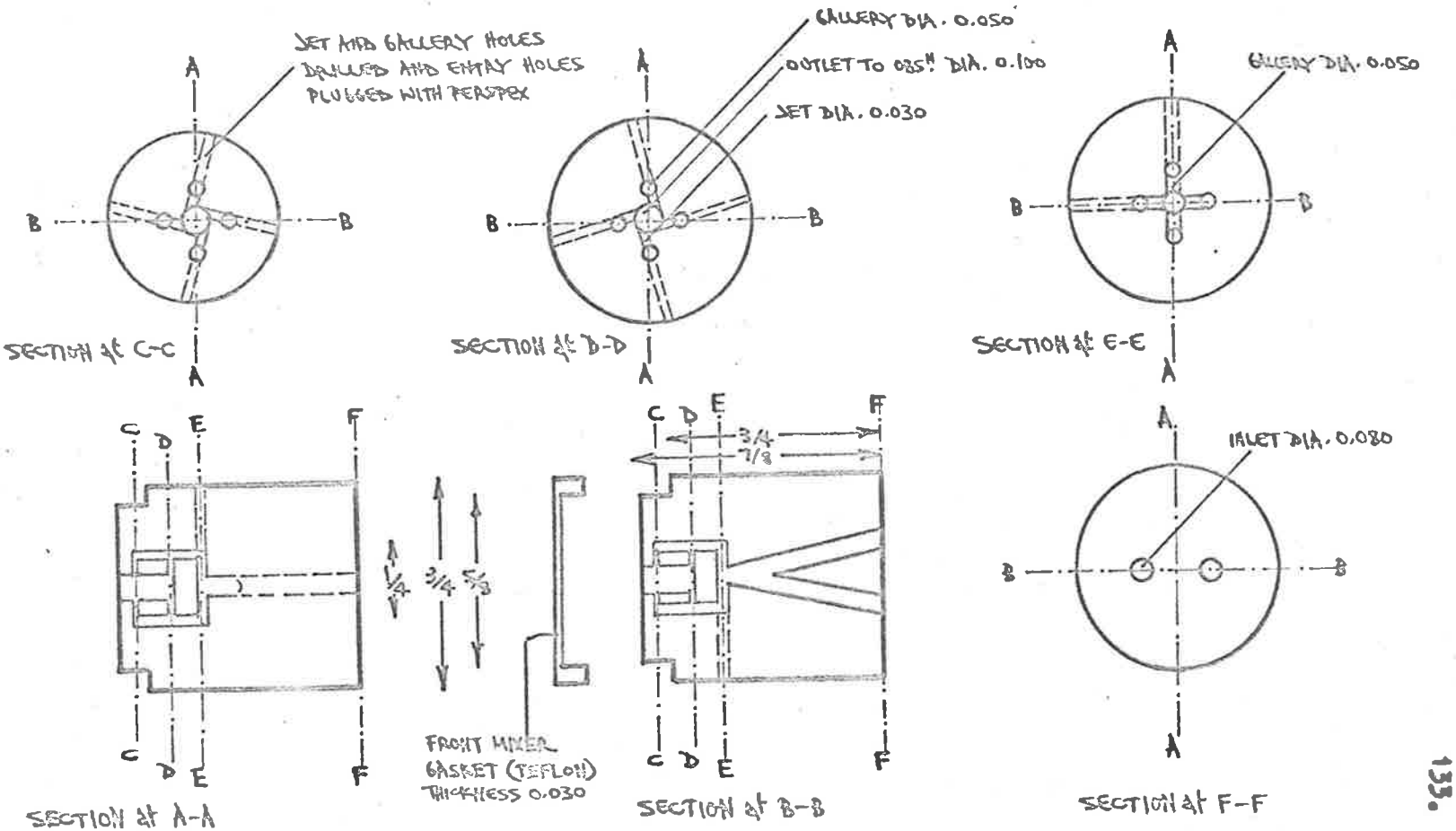

FIGURE A2-12 EIGHT JET MIXER (PERSPEX)

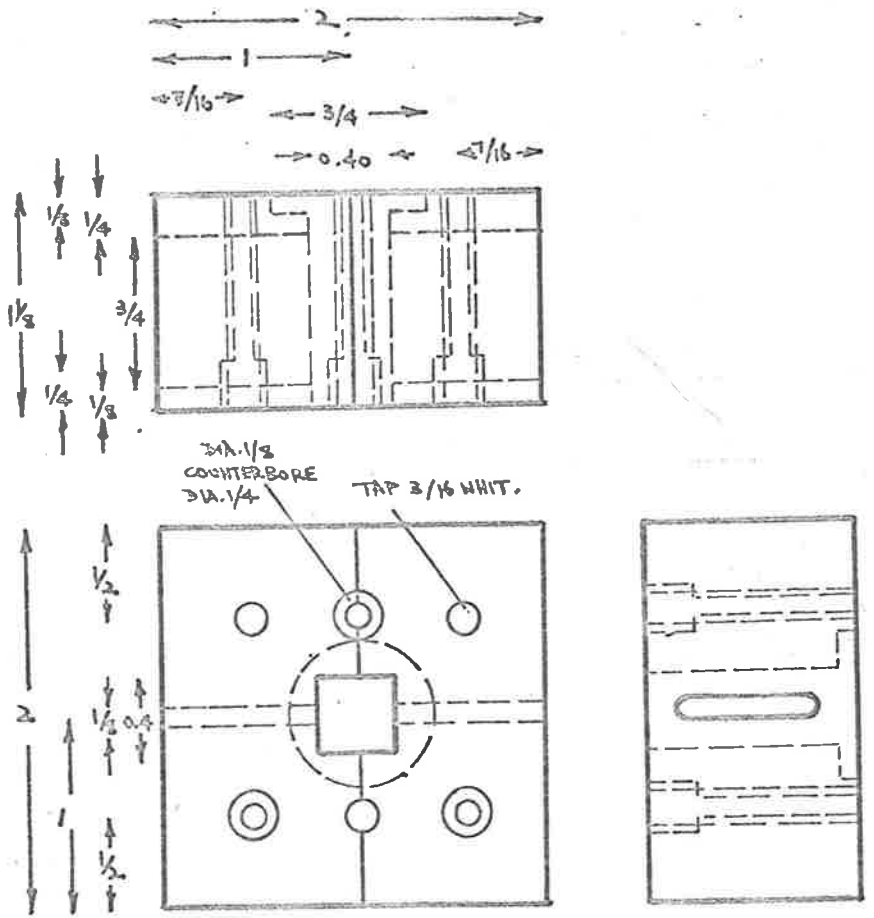

FIG. A2.13 CELL BLOCK (BRASS)

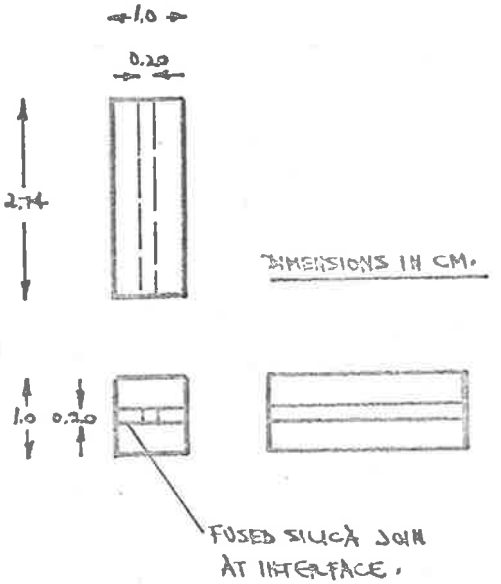

FIG. A2.14 OPTICAL CELL (SILICA).

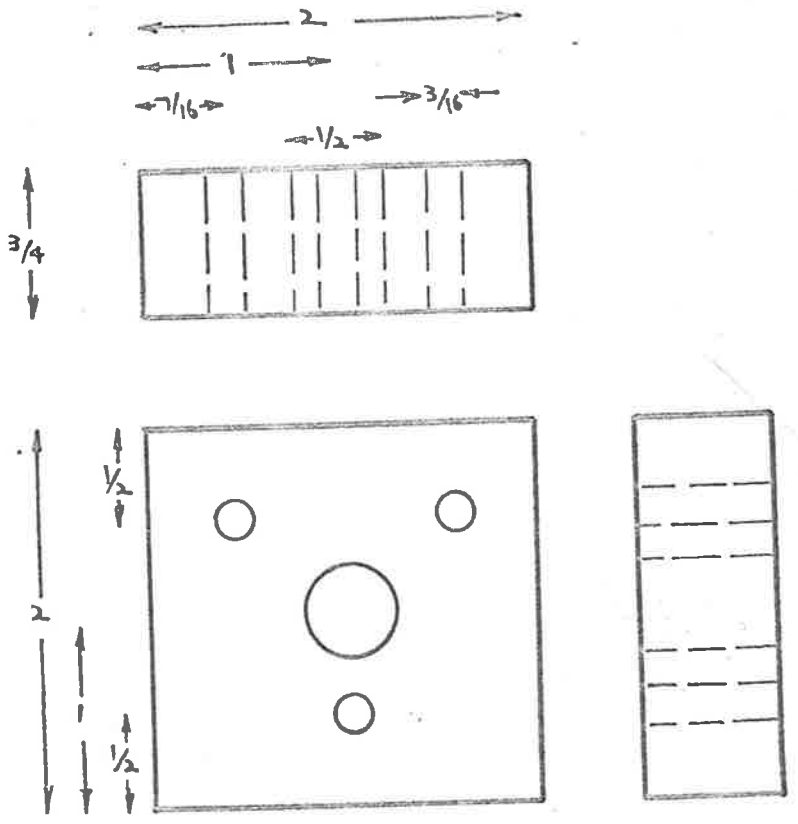

FIG. A2-.15 OUTLET BLOCK (TEFLON)

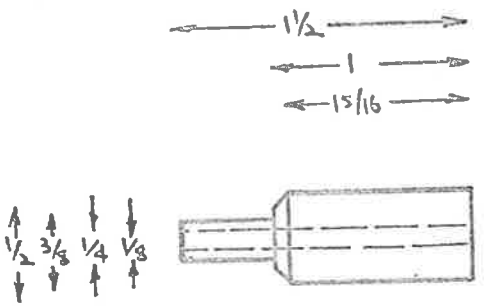

CIRCULAR VERTICAL SECTION.

FIG. A2-.16 OUTLET TUBE (PERSPEX).

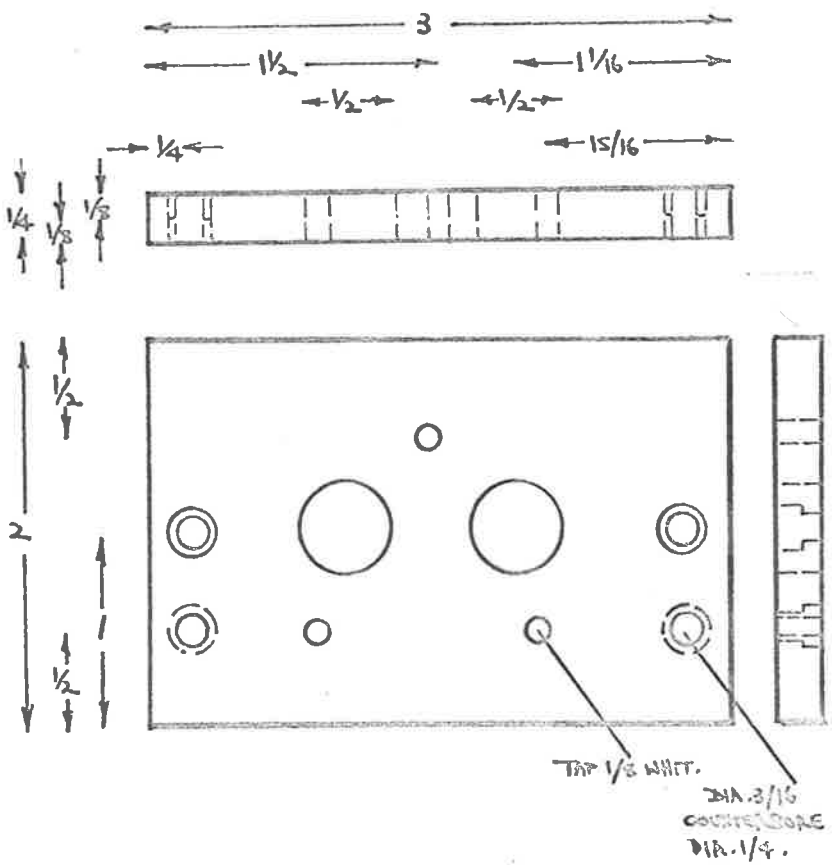

FIG. A2-.17 FRONT END PLATE (BRASS).

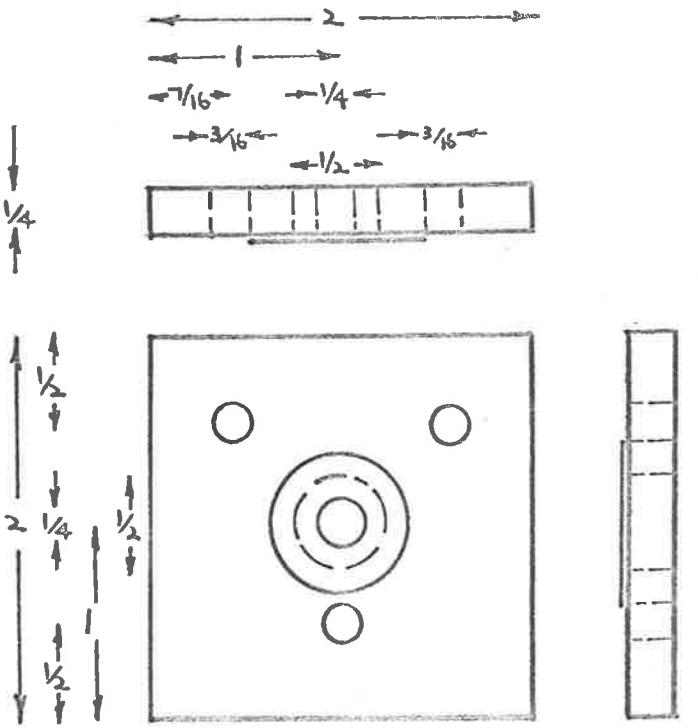

FIG. A2-.18 REAR END PLATE (BRASS).

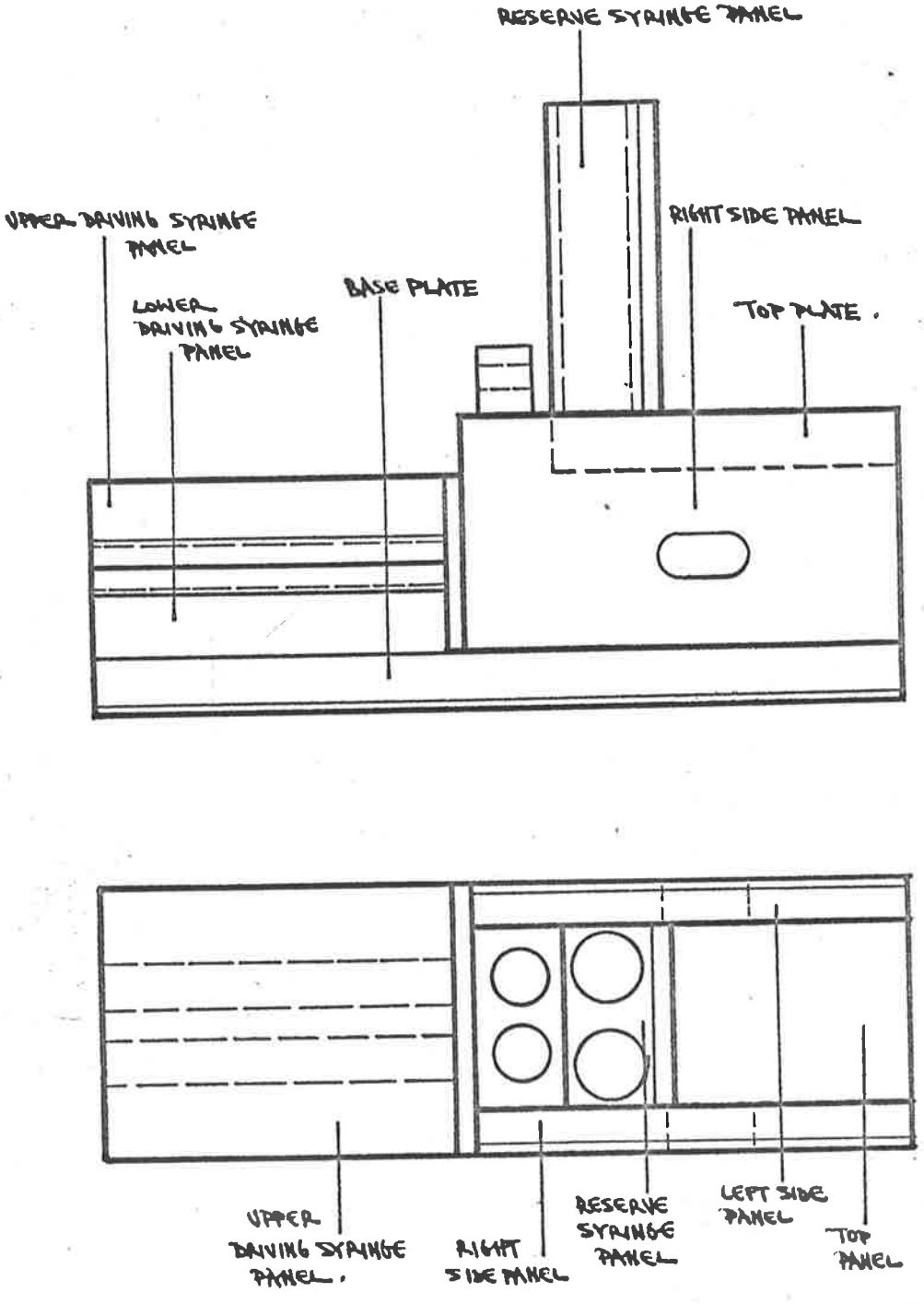

FIGURE A2.19 THERMAL PANEL ASSEMBLY.

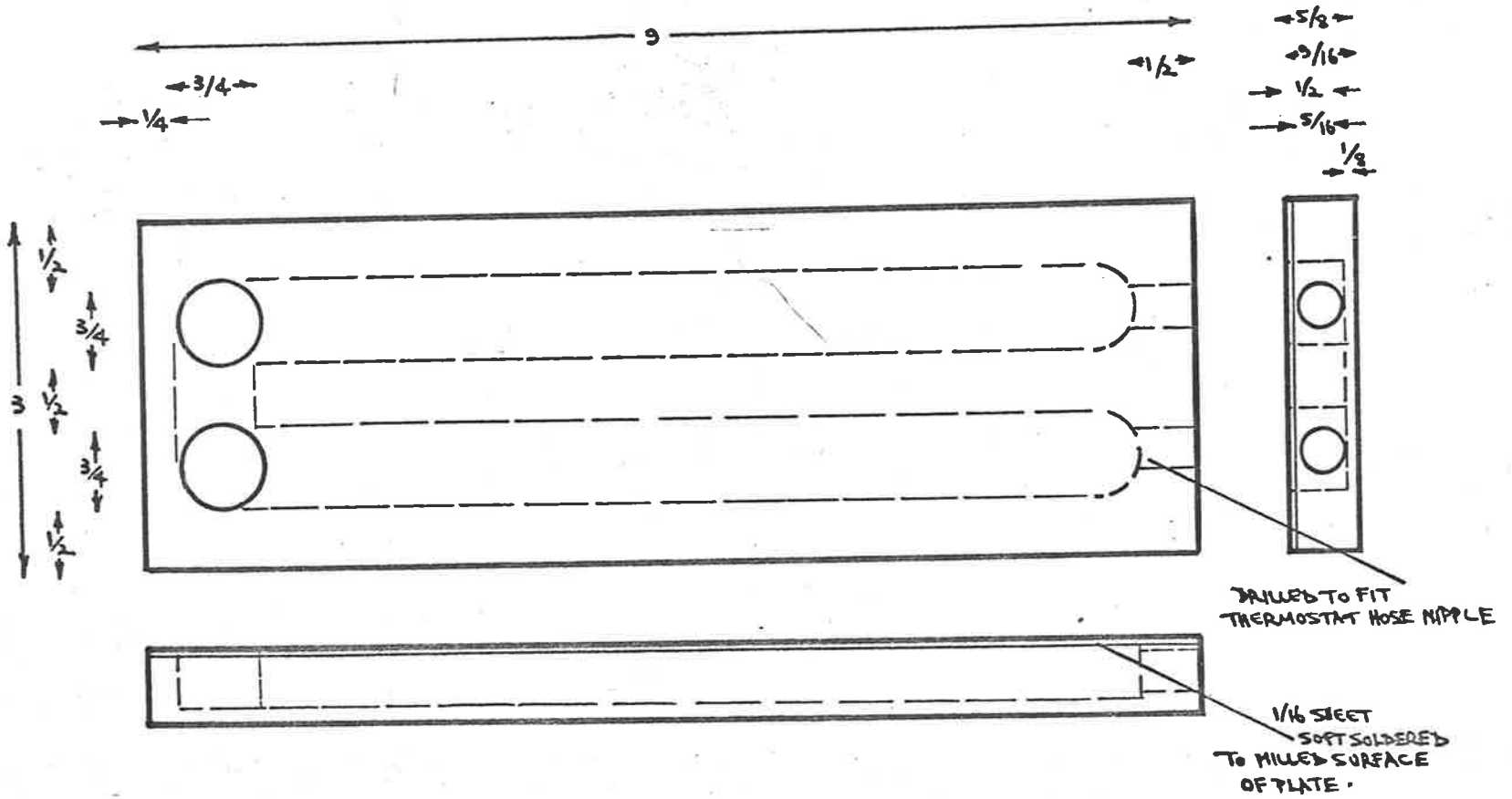

FIGURE A2.20 BASE PLATE.

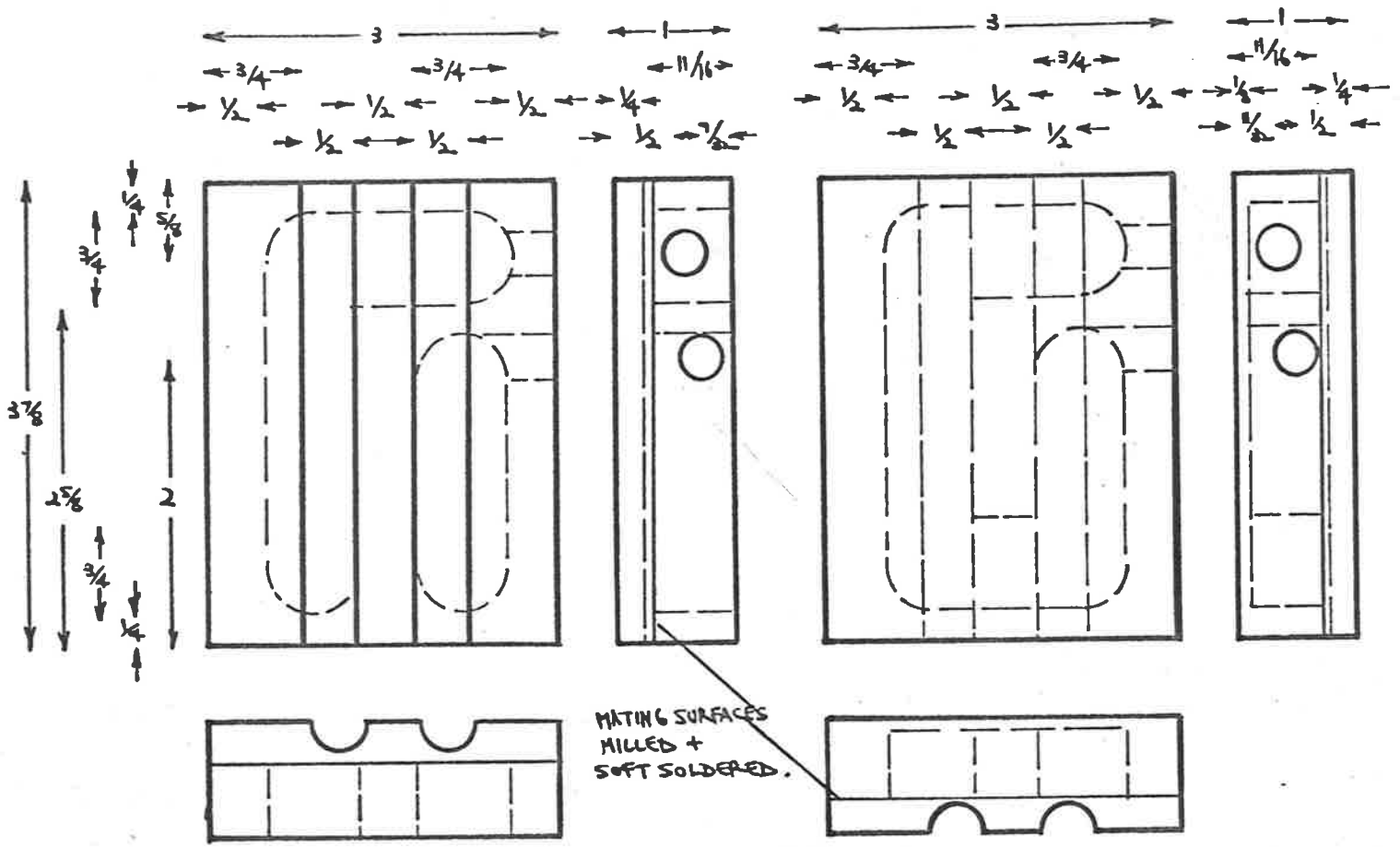

FIGURE A2.21 LOWER + UPPER DRIVING SYRINGE PANELS.

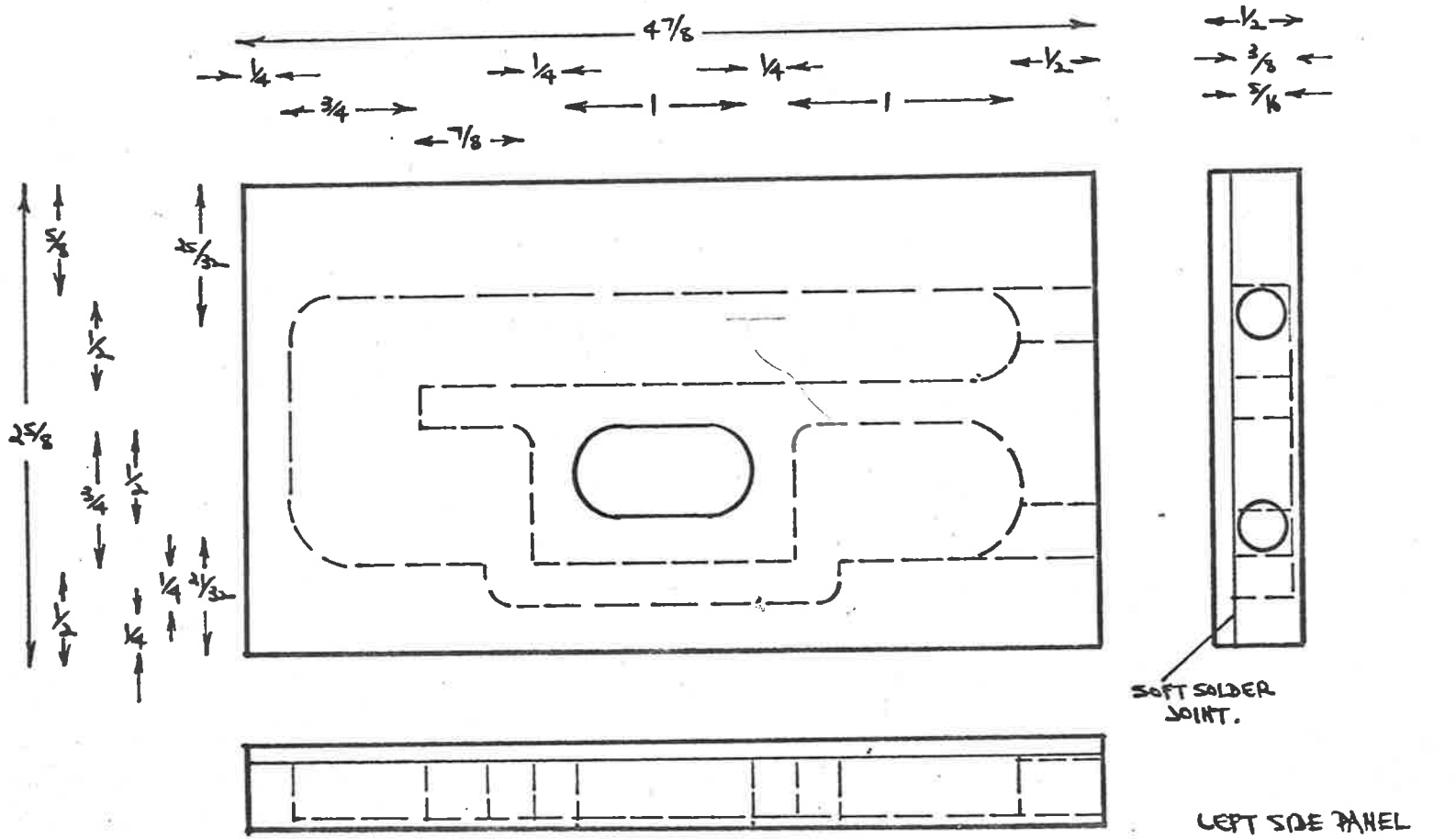

LEFT SIDE PANEL = MIRROR IMAGE.

FIGURE A2.22 RIGHT SIDE PANEL.

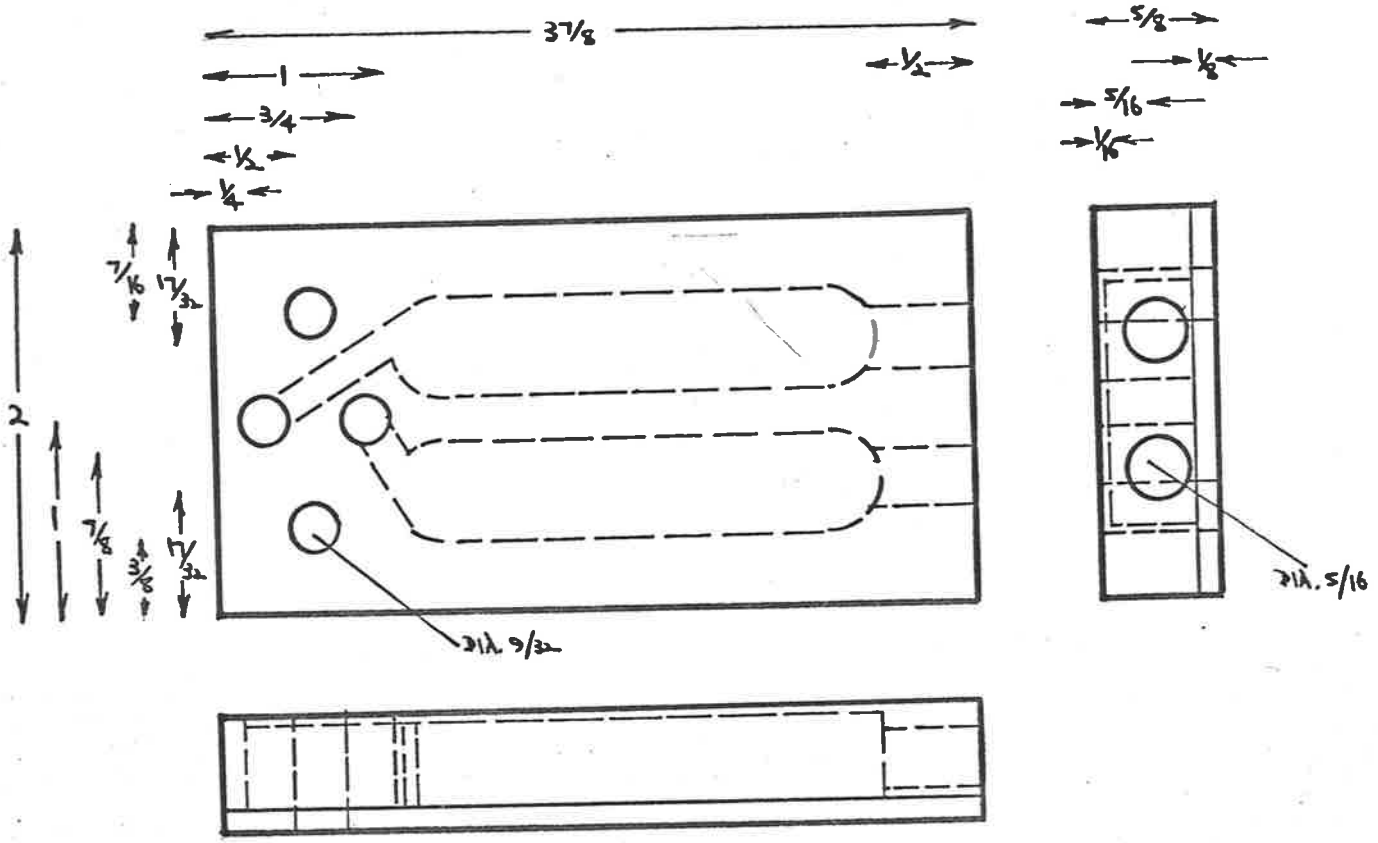

FIGURE A2.23 TOP PANEL.

PARTS A AND B ARE SILVER SOLDERED TOGETHER TO FORM THE RESERVE PANEL UNIT, THE BOTTOM FACE MILLED FLAT AND SOFT SOLDERED TO THE TOP PANEL AS SHOWN IN FIG A2.19.

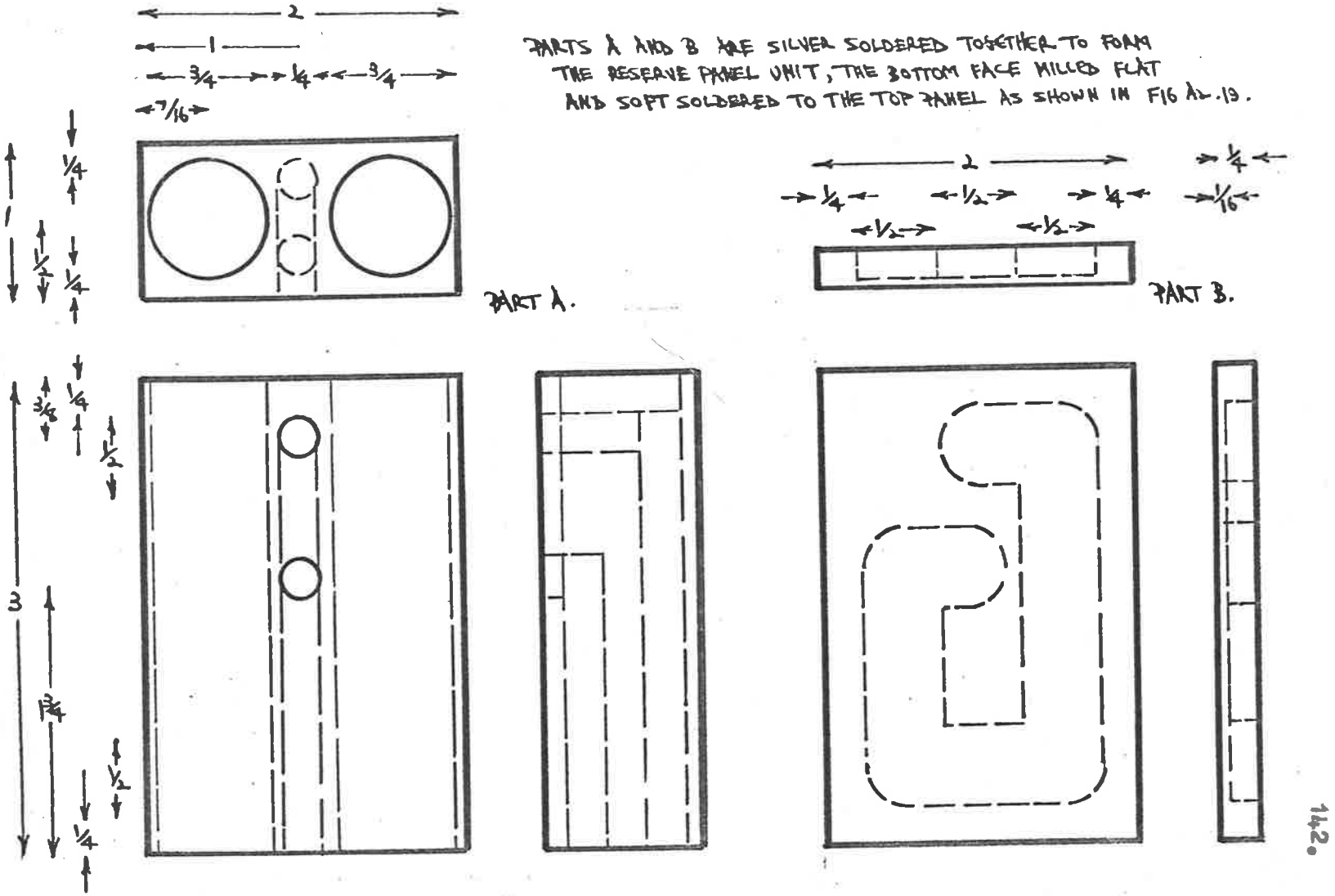

FIGURE A2.24 RESERVE SYRINGE PANEL.

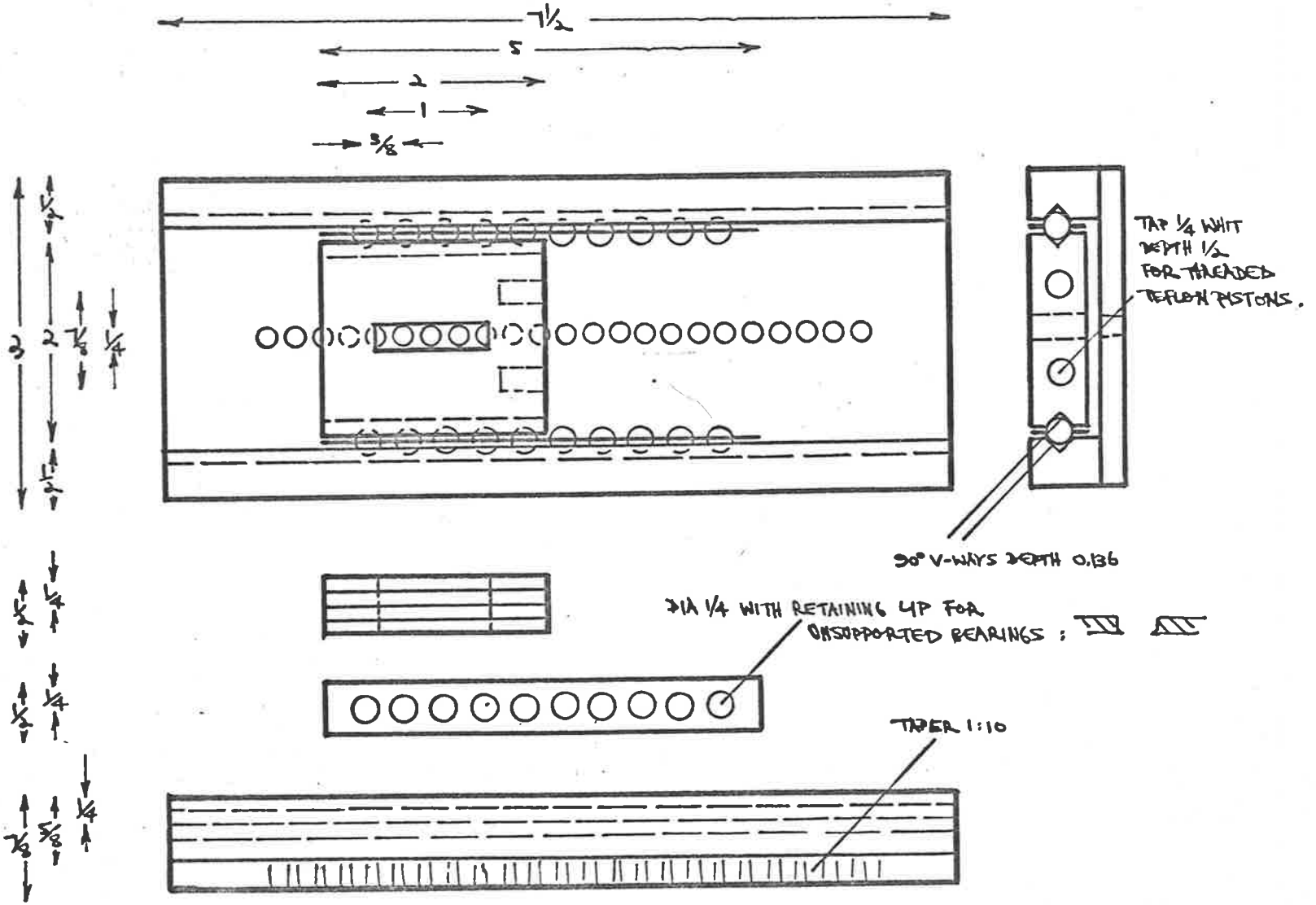

FIGURE A2.25 TROLLEY + TRACK ASSEMBLY.

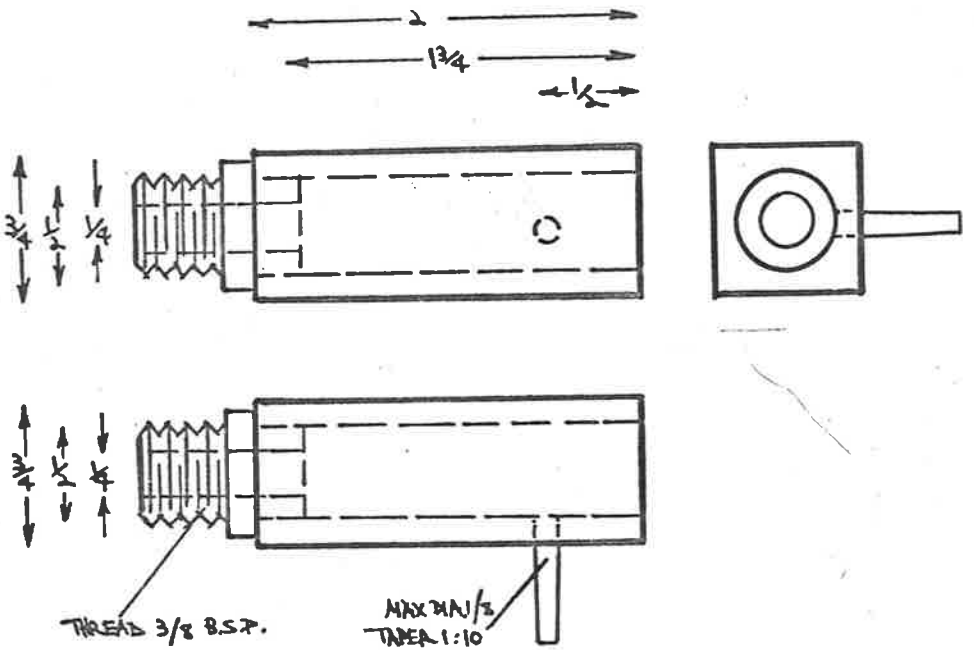

FIGURE A2.26 PNEUMATIC CYLINDER/PISTON.

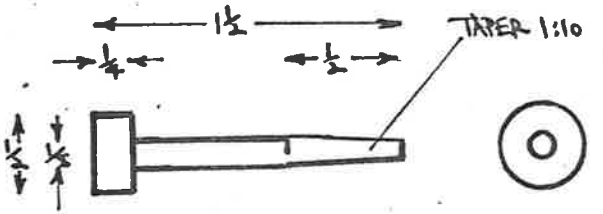

FIGURE A2.27 STOPPING PEG.

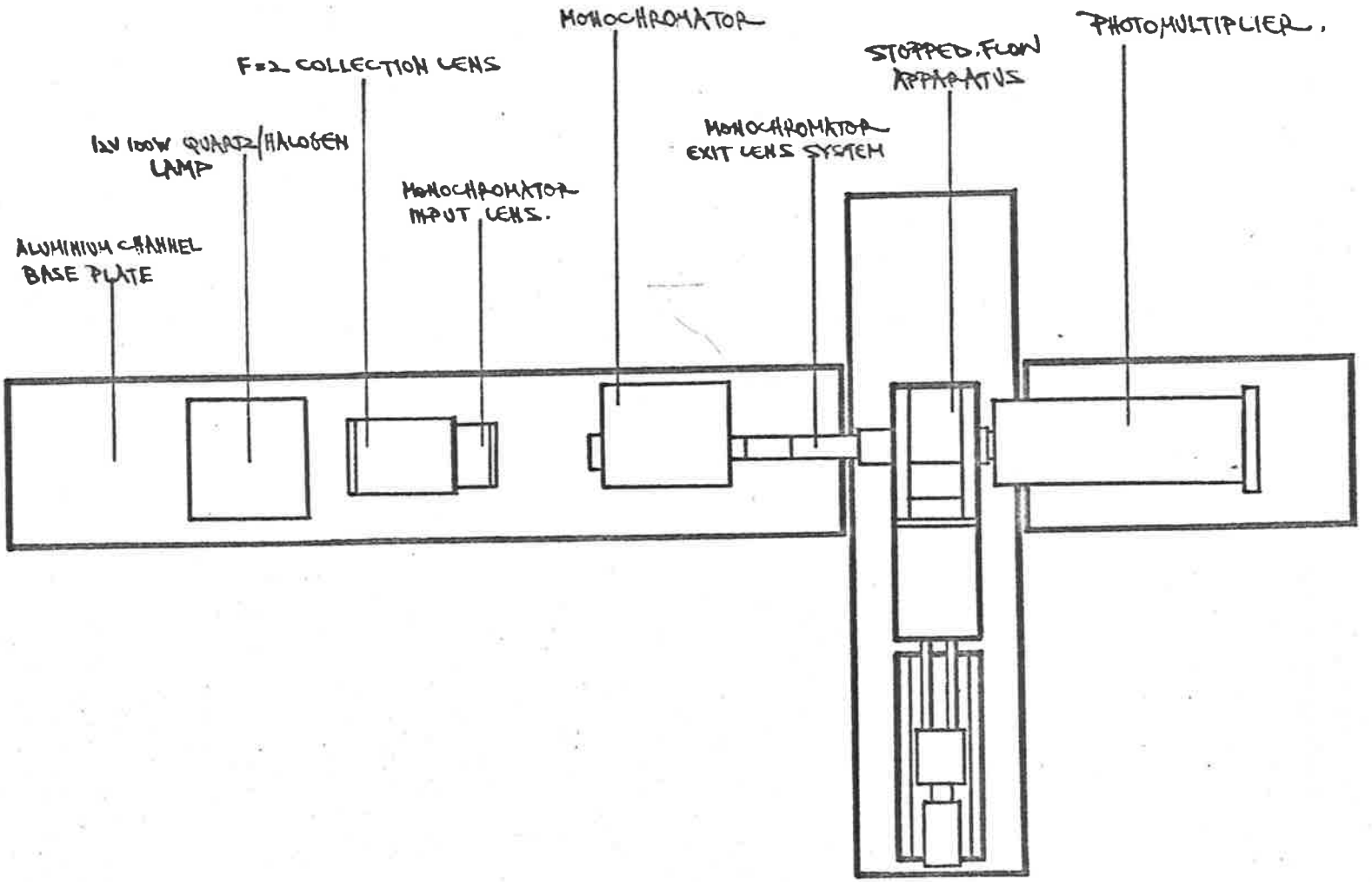

FIG. A2.29 LAYOUT OF OPTICAL DETECTION SYSTEM.

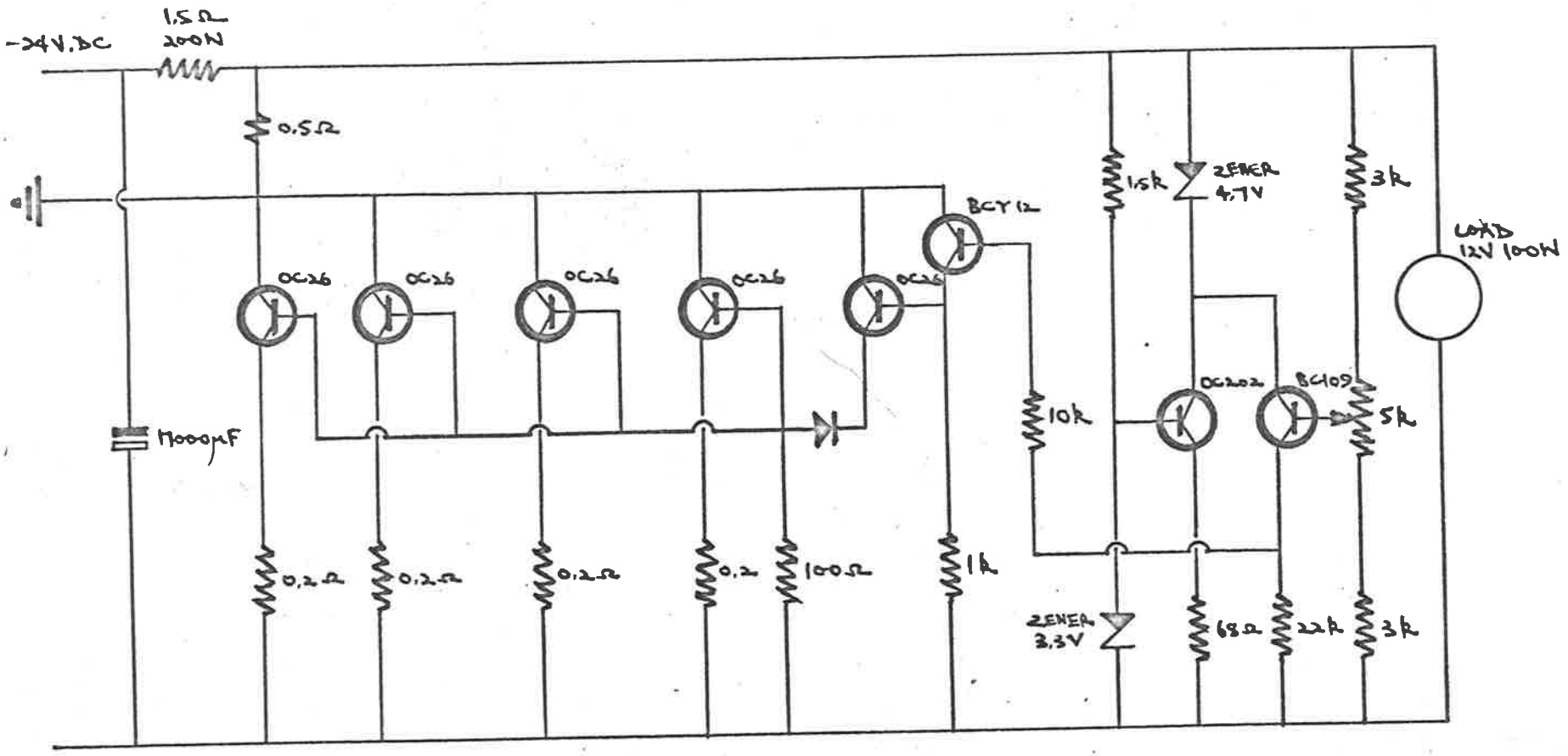

FIG. A2.30 STABILIZED D.C. LAMP POWER SUPPLY (12V/100W).

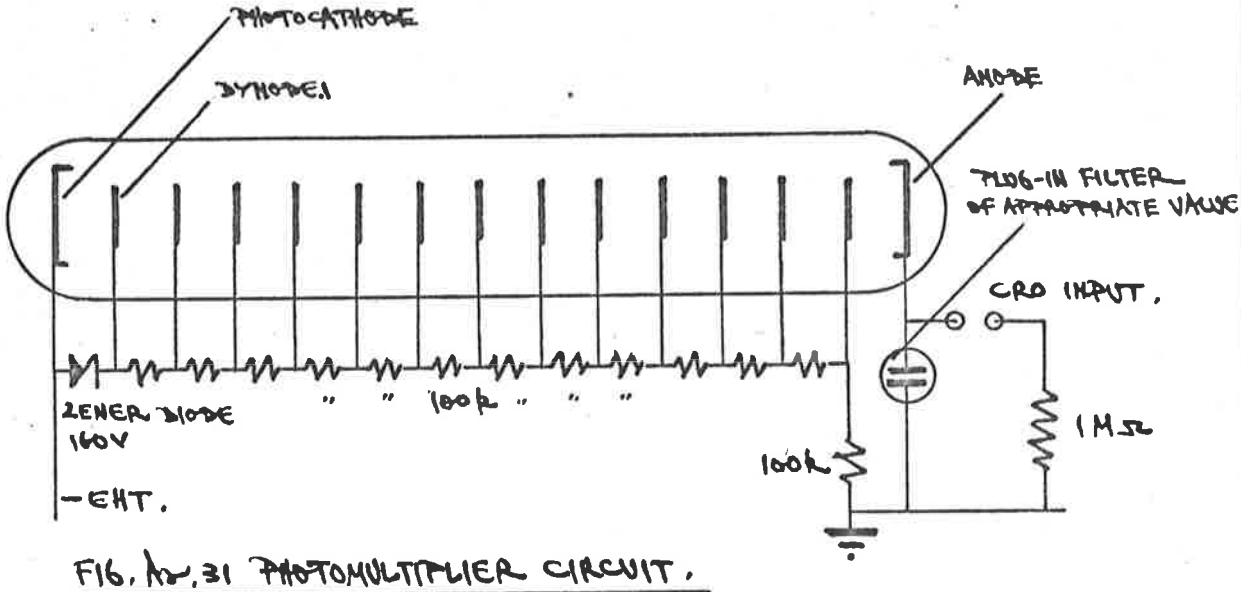

FIG. Ap. 31 PHOTOMULTIPLIER CIRCUIT.

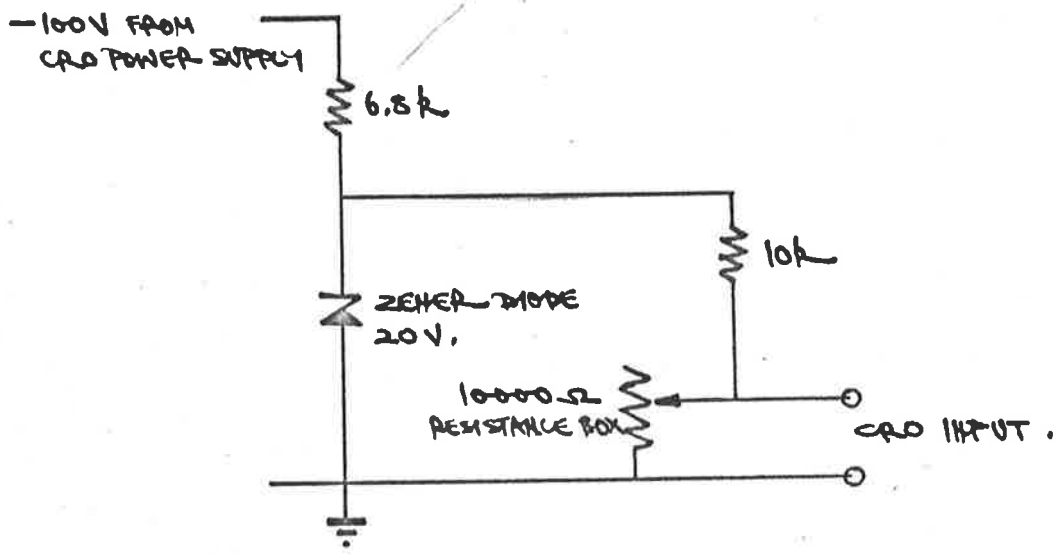

FIG. Ap. 32 BACKING-OFF SOURCE CIRCUIT.

REFERENCES

37D Dodge, R.A. and Thompson, M.J.: "Fluid Mechanics", McGraw Hill (New York) (1937)

37W Wirtz, K.: Agnew. Chem., A59, 138 (1937)

40Q Quintin, M.: Comp. Rend., 210, 625 (1940)

42R Rabinowitch, E. and Stockmayer, W.H.: J.A.C.S., 64, 335 (1942)

52H Haupt, G.: J. Opt. Soc., 42, 441 (1952)

53D Dalziel, K.: Biochem. J., 55, 79 (1953)

54C Caldin, E.F. and Trowse, F.W.: Disc. Far. Soc., 17, 133 (1954)

45R Ricca, B.: Gazz. Chim. Italia, 75, 71 (1945)

55L Lister, M.W. and Rivington, D.E.: Can. J. Chem., 33, 1603 (1955)

55Li Lister, M.W. and Rivington, D.E.: Can. J. Chem., 33, 1572 (1955)

55M Milburn, R.M. and Vosburgh, W.C.: J.A.C.S., 77, 1352 (1955)

56G Gray, P. and Waddington, J.: Proc. Roy. Soc. (Lond), A235, 106 (1956)

56S Smithson, J.R. and Litovitz, T.A.: J. Accoust. Soc. Amer., 28, 462 (1956)

57E Eigen, M.: Disc. Far. Soc., 24, 25 (1957)

57M Milburn, R.M.: J.A.C.S., 79, 537 (1957)

58B Below, J.F., Connick, R.E. and Coppel, C.P.: J.A.C.S., 80, 2961 (1958)

58F Fuoss, R.M.: J.A.C.S., 80, 5059 (1958)

58S Smithson, J.M. and Williams, R.J.P.: J. Chem. Soc., p. 457 (1958)

58Si Sirs, J.A.: Trans. Far. Soc., 54, 201 (1958)

59C C.R.C. Handbook of Chemistry and Physics, 41, 2326, 1706 (1959)

59Cn Connick, R.E. and Poulson, R.E.: J. Chem. Phys., 30, 759 (1959)

59Co Conniek, R.E. and Coppel, C.P.: J.A.C.S., 81, 6389 (1959)

59D Diebler, H. and Eigen, M.: Z. Phys. Chem., 20, 299 (1959)

59E Elshamy, H.K. and Sherif, F.G.: Egypt. J. Chem., 2, 217 (1959)

59L Laidler, K.J.: Can. J. Chem., 37, 138 (1959)

59R Robinson, R.A. and Stokes, R.H.: "Electrolyte Solutions", Butterworths (1959)

60B Brady, G.W.: J. Chem. Phys., 33, 1079 (1960)

60Bi Bigeleisen, J.: J. Chem. Phys., 32, 1583 (1960)

60D Duckworth, S.: Thesis (Leeds, 1960)

60P Pouli, D. and Smith, W.M.: Can. J. Chem., 38, 567 (1960)

61B Bunn, D., Dainton, F.S. and Duckworth, S.: Trans. Far. Soc., 57, 1131 (1961)

61C Conniek, R.E. and Stover, E.D.: J. Phys. Chem., 65, 2075 (1961)

61E Elshamy, H.K. and Sherif, F.G.: J. Chem. U.A.R., 3, 197 (1961)

61Ei Eigen, M.: "Advances in the Chemistry of Coordination Compounds", Macmillan (New York, 1961), p. 371

61M Matthies, P. and Wendt, H.: Z. Phys. Chem., 30, 137 (1961)

61V Vogel, A.I.: "A Textbook of Quantitative Inorganic Analysis", Longmans (1961)

61W Wallace, R.M. and Dukes, E.K.: J. Phys. Chem., 55, 2094 (1961)

62D Davis, G.G. and Smith, W.M.: Can. J. Chem., 40, 1836 (1962)

62G Genser, E.F.: U.S. Atomic Energy Commission Report UCRL9846 (1962)

62H Hammes, G.G. and Steinfeld, J.I.: J.A.C.S., 84, 4639 (1962)

62R Ross, P.D. and Sturtevant, J.M., J.A.C.S., 84, 4503 (1962)

62S Swift, T.J. and Conniek, R.E.: J. Chem. Phys., 37, 307 (1962)

62W Wendt, H.: Z. Elektrochem., 66, 235 (1962)

62We Wendt, H. and Strehlow, H.: Z. Elektrochem., 66, 238 (1962)

63D Duls, G. and Sutin, N.: Inorg. Chem., 2, 917 (1963)

63De De Maeyer, L. and Kustin, K.: An. Rev. Phys. Chem., 14, 5 (1963)

63E Eigen, M.: Pure and App. Chem., 6, 97 (1963)

63Ei Eigen, M. and Kustin, K.: I.C.S.U. Review, 5, 97 (1963)

63Eg Eigen, M.: Ber. Bunsenges. Phys. Chem., 67, 753 (1963)

63L Leffler, J.E. and Grunwald, E.: "Rates and Equilibria of Organic Reactions", Wiley (New York, 1963)

63R Roughton, F.J.W. and Chance, B.: "Technique of Organic Chemistry". Vol. VIII. Ed. Weissberger, Interscience (1961)

63S Seewald, D. and Sutin, N.: Inorg. Chem., 2, 643 (1963)

64B Blatt, E. and Connick, R.E.: I.C.C.C., 8, 284 (1964)

64C Caldin, E.F.: "Fast Reactions in Solution", Blackwell (1964)

64Ca Cavasino, F.P. and Eigen, M.: Ricerca. Sci. Rend., 4A, 509 (1964)

64E Eigen, M., Kruse, W., Maas, G. and De Maeyer, L.: "Progress in Reaction Kinetics", ed. Porter

64F Fukushima, S. and Reynolds, W.L.: Talanta, 11, 283 (1964)

64G Gary, R., Bates, R.G. and Robinson, R.A.: J. Phys. Chem., 68, 3806 (1964)

64Gi Gibson, Q.H. and Milnes, L.: Biochem. J., 91, 161 (1964)

64H Hammes, G.G.: Ann. Rev. Phys. Chem., 15, 13 (1964)

64N Nemethy, G. and Scheraga, H.A.: J. Chem. Phys., 41, 680 (1964)

64S Sturtevant, J.M.: "Fast Mixing and Sampling Techniques in Biochemistry". Academic Press (New York), 1964

64Si Sillen, L.G. and Martell, A.: Chem. Soc. Spec. Publ., 17 (1964)

65B Bauer, R.F. and Smith, W.M.: Can. J. Chem., 43, 2763 (1965)

65C Carter, S., Murrel, J.N. and Rosch, E.J.: J. Chem. Soc., 2048 (1965)

65Co Cennochiolli, T.J., Hamilton, E.J. and Sutin, N.: J.A.C.S., 87, 926 (1965)

65E Eigen, M. and Wilkins, R.G.: Advances in Chemistry Ser., 49, 55 (1965)

65H Holyer, R.H., Hubbard, C.D., Kettle, J.F.A. and Wilkins, R.G.: Inorg. Chem., 4, 929 (1965)

65G Geier, G.: Ber. Bunsenges. Phys. Chem., 69, 617 (1965)

65L Lus, Z. and Schulman, R.G.: J. Chem. Phys., 43, 3750 (1965)

65La Langford, C.H.: Inorg. Chem., 4, 265 (1965)

65Lu Lush, H.J.: J. Sci. Inst., 42, 597 (1965)

65M Morgan, T.D.B., Stedman, G. and Whincup, P.A.E.: J. Chem. Soc., 4813 (1965)

65T Treglean, P.A. and Laurence, G.S.: J. Sci. Inst., 42, 869 (1965)

65S Strehlow, H.: Ann. Rev. Phys. Chem., 16, 167 (1965)

66B Babiec, J.S., Langford, C.H. and Stengle, T.R.: Inorg. Chem., 5, 1362 (1966)

66L Langford, C.H. and Gray, H.B.: "Ligand Substitution Processes", Benjamin (New York), 1966

66M Moorhead, E.G. and Sutin, N.: Inorg. Chem., 5, 1366 (1966)

66R Rorabacher, D.B.: Inorg. Chem., 5, 1891 (1966)

66S Sutin, N.: Ann. Rev. Phys. Chem., 17, 119 (1966)

66Sw Swift, T.J. and Sayre, G.T.: J. Chem. phys., 44, 3567 (1966)

67A Accascina, F., Cavasino, F.P. and d'Allessandro, S.: J. Phys. Chem., 71, 2474 (1967)

67B Basolo, F. and Pearson, R.G.: "Mechanisms of Inorganic Reactions", 2nd ed., Wiley (New York), 1967

67Ba Baker, B.R., Sutin, N. and Welch, T.J.: Inorg. Chem., 6, 1948 (1967)

67Bu Burgess, J.: Chem. Soc. Ann. Reports, 64A, 365 (1967)

67C Carlyle, D.W. and Espenson, J.H.: Inorg. Chem.,

67D Duffey, N.J. and Early, J.E.: J.A.C.S., 89, 272 (1967)

67J Judkins, M.R.: U.S. Atomic Energy Commission Report UCRL17561 (1967)

67M Margerum, D.W. and Rosen, H.M.: J.A.C.S., 89, 1088 (1967)

67S Singleton, D.L. and Swinehart, J.H.: Inorg. Chem., 6, 1536 (1967)

67St Stengle, T.R. and Langford, C.H.: Coord. Chem. Reviews, 2, 349 (1967)

67Sw Swaddle, T.W.: J.A.C.S., 89, 4338 (1967)

68B Berger, R.L., Balko, B. and Chapman, H.F.: Rev. Sci. Inst., 39, 493 (1968)

68Ba Baldwin, W.G. and Stranks, D.R.: Aust. J. Chem., 21, 2161 (1968)

68Be Beck, M.T.: Coord. Chem. Reviews, 3, 91 (1968)

68C Cavasino, F.P.: J. Phys. Chem., 72, 1378 (1968)

68E Ellis, P. and Hall, P.G.: Trans. Far. Soc., 64, 1034 (1968)

68F Fiat, D. and Connick, R.E.: J.A.C.S., 90, 608 (1968)

68G Graffeo, A.J. and Bear, J.L.: J.I.N.C., 30, 1577 (1968)

68K Kunts, I.D., Gasparrow, F.P., Johnson, M.D. and Taylor, R.P.: J.A.C.S., 90, 4778 (1968)

68Kr Kruse, W. and Thusius, D.: Inorg. Chem., 7, 464 (1968)

68L Langford, C.H. and Stengle, T.R.: Ann. Rev. Phys. Chem., 19, 193 (1968)

68M Miceli, J. and Stuehr, J., J.A.C.S., 90, 6967 (1968)

68S Swaddle, T.W. and Guastalla, G.: Inorg. Chem., 7, 1915 (1968)

68W Walker, R.G. and Watkins, K.O.: Inorg. Chem., 7, 885 (1968)

69A Accascina, F., Cavasino, F.P. and Dio, E.D.: Trans. Far. Soc., 65, 489 (1969)

69C Carlyle, D.W. and Espenson, J.H.: Inorg. Chem., 8, 575 (1969)

69M McAuley, A. and Hill, J.: Quart. Rev., 23, 18 (1969)